DISSERTATION

SARS-COV-2 VIRAL RNA BIOLOGY AND ITS IMPACT ON THE INFECTED CELL

Submitted by

Noelia H. Altina

Department of Microbiology, Immunology and Pathology

Graduate Degree Program in Cellular and Molecular Biology

In partial fulfillment of the requirements

For the Degree of Doctor of Philosophy

Colorado State University

Fort Collins, Colorado

Spring, 2023

Doctoral Committee:

Advisor: Jeffrey Wilusz

Lucas Argueso
Brian Geiss
Rushika Perera
Tingting Yao

ABSTRACT

SARS-COV-2 VIRAL RNA BIOLOGY AND ITS IMPACT ON THE INFECTED CELL

The fine-tuning of the replication and transcription of RNA viruses often requires the interaction of viral RNAs with cellular RNA binding proteins. This project addresses fundamental knowledge gaps on the molecular mechanisms that underlie SARS-CoV-2 gene expression, regulation, and viral RNA-host interactions. After infection, SARS-CoV-2 generates a large set of sub-genomic mRNAs, each containing an identical ~70 base 'leader' region in their 5'UTR (from position 14 to position 75 in RefSeq NC_045512) and a 229 base region at the 3'UTR (from position 29,675 to position 29,903 in RefSeq NC_045512) generated by discontinuous transcription. The accumulation of a considerable amount of these leader/3'UTR regions during the infection represents a possible sink for cellular RNA binding proteins. We demonstrated that PTBP1, a cellular protein involved in the regulation of alternative splicing, binds to the SARS-CoV-2 leader region. SARS-CoV-2 infection critically impacted the splicing of several cellular pre-mRNAs that are normally regulated by PTBP1. Mechanistically, we suggest that SARS-CoV-2 sequesters and influences the re-localization of shuttling splicing factors like PTBP1 from the nucleus to the cytoplasm resulting in significant effects on the host cell splicing machinery leading to changes in cellular mRNA splicing patterns during SARS-CoV-2 infection.

Given the current extensive interest in epigenetic methylations of both cellular and viral RNAs, our study also explored the role of post-transcriptional RNA modifications on viral mRNAs. We demonstrated that SARS-CoV-2 can usurp the

cellular enzyme, namely PCIF1, to place the m^6A_m modification at the cap proximal position in its mRNAs. This double methylation is usually found on all host mRNAs that initiate with an adenosine residue, and thus SARS-CoV-2 likely installs this modification on its mRNAs to avoid host immune recognition. Interestingly, we also discovered that capping and m^6A_m modification are tightly regulated throughout the infection. The highest levels of these 5' end RNA modifications were observed at 12 hours post infection, correlating with the full establishment of viral gene expression in infected cells. These findings indicate that 5' end modification of SARS-CoV-2 transcripts is not simply a default process but rather undergoes unanticipated regulation throughout the infection.

Collectively, the data presented provide not only new insights into the complex interactions that SARS-CoV-2 has with the RNA biology of the cell during infection, but also identify attractive potential targets for developing novel anti-coronavirus drugs to treat future emerging coronavirus diseases.

ACKNOWLEDGEMENTS

First, I would like to thank all our collaborators who contributed to this work: Dr. Brian Geiss and his lab members at Colorado State University, Dr. Rushika Perera, and members of her lab—especially Drs. Laura St. Clair and Suad Elmegerhi—at Colorado State University for providing the viral stocks I used in my study. I would also like to thank our funding sources.

Dr. David Maranon and John Anderson provided valuable guidance, assistance, and support in the laboratory. In addition, they optimized several of the *in vitro* RNA assays I present here, for which I am deeply grateful.

I am also thankful for my graduate committee's advice and helpful suggestions. Special thanks to Dr. Carol Wilusz for her support, helpful advice, and multiple feedback on experimental approaches during my development.

I am sincerely grateful to have been a member of Dr. Jeffrey Wilusz's lab and for the opportunity to work on this project. Thank you, Dr. Wilusz, for your dedication, support, and advice and for giving me valuable opportunities.

Finally, thanks to my family and friends for years of support and encouragement.

TABLE OF CONTENTS

LIST OF FIGURES

INTRODUCTION

The *Coronaviridae* family is the largest group in the *Nidovirales* order, which also includes the *Arteriviridae* and *Roniviridae* families of viruses. The *Nidovirales* order is positive-sense single-stranded RNA enveloped viruses that share a number of common features among its members, including the transcription of multiple 3'-nested subgenomic messenger RNAs (sg mRNA), a similar genomic organization with the non-structural polyproteins encoded upstream from the structural proteins, the expression of the polyproteins utilizing a ribosomal frameshifting approach, and some interesting and unique enzymatic activities of their non-structural proteins[1]. The *Arteriviridae* and *Roniviridae* families are composed of one genus each, Arterivirus (e.g., equine arteritis virus) and Okavirus (e.g., gill-associated virus and yellow head virus), respectively. According to the ninth report of the International Committee on the Taxonomy of Viruses, the *Coronaviridae* family comprises two subfamilies: *Coronavirinae* and *Torovirinae*. The subfamily Coronavirinae includes four genera[2]: Alphacoronavirus (e.g., HCoV-229E), Betacoronavirus (e.g., HCoV-OC43 MERS, SARS), Gammacoronavirus (e.g., avian coronavirus), and Deltacoronavirus (e.g., coronavirus HKU15). Torovirus (e.g., equine torovirus, human torovirus, bovine torovirus) and Bafinivirus (e.g., white bream virus) are the two genera in the *Torovirinae* subfamily[1]. The focus of this dissertation will be on the betacoronaviruses – specifically SARS-CoV-2.

The coronavirus genome is a large 26-32 kb single-stranded, positive-sense RNA[3,4], which means that the genomic nucleic acid can be directly read by ribosomes and translated into proteins in the infected cell. Coronaviruses as a group can generally

infect a wide variety of host species, including humans, bats, mice, dogs, cats, and cows[5–8]. The first human coronavirus was isolated in 1965 from a patient with a common cold[9]. During the last 20 years, several types of coronaviruses have emerged and infected humans causing pathological problems: severe acute respiratory syndrome coronavirus or SARS-CoV in China[10], human coronavirus NL63 or HCoV-NL63 in the Netherlands[11], human coronavirus HKU1 also referred to as HCoV-HKU1 in Hong Kong[12], Middle East Respiratory Syndrome Coronavirus or MERS-CoV in a patient from Jeddah[13], and severe acute respiratory syndrome coronavirus two or SARS-CoV-2 in China in 2019[14].

SARS-CoV and MERS-CoV were likely the results of natural selection in bats before the zoonotic transmission to humans[15]. However, it is possible that instead of jumping directly from bats to humans, these viruses entered the human population by passing through one or more intermediate animal hosts[7,16,17]. For SARS, the principal intermediate animal host is thought to be civet cats[18]. In these intermediate hosts, the virus can go through several rounds of replication and acquire mutations that allow or enhance its zoonotic potential. However, in the case of SARS-CoV-2, it is currently unknown whether there are intermediate hosts[19–21]. There are still speculations about the virus's capability to jump into humans directly from bats or to evolve first within one or more intermediate animal hosts before being able to infect humans. Currently, more than 500 coronaviruses have been identified in bats in China. However, the estimates of unknown bat coronavirus diversity go up to thousands, indicating that these are probably massively under-sampled in the bat population[22]. This huge diversity of bat coronaviruses suggests that the pandemic strain of SARS-CoV-2 will not be the last

zoonotic coronavirus that emerges as highly pathogenic for the human population. Therefore, an in-depth understanding of all aspects of coronavirus biology represents an important foundation to effectively combat this emerging group of viral pathogens.

To date, SARS-CoV-2 has been hard to control from a public health perspective for two main reasons. First, the rapid community spread of the pathogen due to highly effective person-to-person viral transmission. Infected individuals spread the virus mainly via respiratory droplets and deposit infectious virions on the mucosal epithelial of the upper airway and mouth[23,24]. Second, the presence of asymptomatic and the abundance of mild cases significantly boosts the transmission in the community. The symptomatology of the disease caused by SARS-CoV-2, COVID-19, is highly variable spanning the gamut from minor cold symptoms to fever, dry cough, fatigue, loss of smell (anosmia), reduced sense of taste (dysgeusia), loss of appetite, among others like headache, sore throat, diarrhea, etc.[25,26]. COVID-19 symptoms can be severe; the elderly population can rapidly progress to hypoxia and respiratory distress leading to the hospitalization of the patients, requiring oxygen and ventilator support[27]. Severe cases of COVID-19 were observed in children developing a multisystem inflammatory disease similar to Kawasaki disease[28]. In some cases of COVID-19, the virus causes damage to endothelial cells of the blood vessel, leading to coagulopathy, strokes, potential kidney, and neurological problems[29]. Finally, long COVID with extended impacts on a variety of organ systems can occur in up to 10% of SARS-CoV-2 infected patients[30]. The ultimate goal of this dissertation was to gain additional insight into host cell-SARS-CoV-2 interactions at the molecular level that may contribute to viral growth and pathogenesis.

General

Coronavirus virions are pleomorphic particles with a helical nucleocapsid composed of an ~30Kb (+) RNA genome coated by nucleocapsid (N) protein wrapped in a lipid envelope derived from the host cell[31]. Three integral membrane viral proteins, envelope (E), membrane (M), and spike (S), decorate the lipid envelope of coronaviruses. The S protein is the most prominent, conferring coronaviruses its name because of the crown-like appearance of the virion surface under two-dimensional transmission electron microscopy[32]. In addition, the spike protein is responsible for engaging two cellular receptors: angiotensin-converting enzyme 2 (ACE2), which is highly expressed in the epithelia of the lung and small intestine[33,34], and the protease TMPRSS2 which is responsible for the proteolytic cleavage and activation of spike protein leading to viral-host membrane fusion and consequently entry process[35–39]. The virus enters the cell largely by endocytosis[40]. The viral RNA gets into the cytoplasm and hijacks the cellular machinery to translate the key viral polyprotein that generates the replication-transcription complex (RTC). The RTC produces large amounts of mRNAs to translate into proteins, and double-membrane vesicles (DMVs) eventually develop during the infection to surround these virus production factories. SARS-CoV-2 encodes 16 non-structural proteins (named nsps 1-16), among which are the RNA-dependent RNA polymerase (nsp-12), an RNA helicase (nsp13), and several other components necessary for virus replication[41,42]. Seven additional accessory proteins are also made whose function in viral replication or packaging remains to be conclusively demonstrated[43,44]. The assembly of new virions includes RNA coated by the nucleocapsid (N) protein wrapped by a lipid envelope containing the membrane (M),

envelope (E), and spike (S) proteins. When the virus is released, it can infect cells from the lower airway (type II pneumocytes) and cells from the gastrointestinal tract (enterocytes)[45,46].

Furthermore, after entering the cell, SARS-CoV-2 utilizes the cell's machinery not only to selectively translate its RNA[47] - but also likely interfaces and impacts other aspects of the RNA biology of the cell. These include effects on generalized host cell splicing[48], in part by nsp16 interacting with host cell U1/U2 RNAs[31], nsp14 altering cellular GTP levels[49], and a general influence on host cell RNA-binding proteins[50]. SARS-CoV-2 infection also influences the level of m^6A epigenetic marks on host cell RNAs[51,52]. The aims of my dissertation were to expand on these observations of the interface of SARS-CoV-2 RNA on cellular RNA biology and gain novel insights into these interactions and their implications for viral infections.

SARS-CoV-2 genome organization, replication, and gene expression

The SARS-CoV-2 genome possesses about 14 open reading frames (ORFs) that encode 27 proteins with diverse functional roles in virus replication and packaging[3,4,53]. The production of many individual proteins from a single mRNA is possible because coronaviruses evolved to express their non-coding ORFs as a polyprotein that is eventually cleaved later into many single proteins[54]. Interestingly, this protease activity is the target for one of the two currently approved COVID-19 therapeutics (Paxlovid or nirmatrelvir and ritonavir)[55]. The viral nsps are encoded in two overlapping ORFs, ORF1a, and ORF1b, which extend over about two-thirds of the viral RNA genome. The nsps generated by these ORFs are involved in the proteolytic processing of the

polyprotein, viral genome replication, and the synthesis of sub-genomic mRNAs. The ORF1a/1ab is translated from the 5'-end by cap-dependent translation to produce nsps 1-11 as a polyprotein if the stop codon is recognized or nsps 1-16 as a polyprotein if the stop codon is bypassed by recognition of a conserved Programmed FrameShift (PFS) element[56]. Nsps 1-11 encoded in the ORF1a are involved in the blockage of the initial immune response, and several act as key cofactors for replication and transcription. The nsps encoded in the portion 1b of the ORF 1ab represent the components for the replication and transcription complex, e.g., the RNA-dependent RNA polymerase (RdRp) (nsp12), helicase (nsp13), and other enzymes/factors necessary for RNA modification which are vital for viral replication. Structural and accessory proteins are translated directly from additional subgenomic mRNAs (sg mRNAs) that are generated by discontinuous transcription, a unique feature of coronaviruses[57]. The synthesis of sg mRNAs starts at the 3'-end of viral genomic RNA with the viral RNA-dependent RNA polymerase "jumping" on the template when encountering transcription regulatory sequences (i.e., TRS-B) along the genomic RNA body. These "jumping" events could be mediated by long-distance RNA–RNA interaction due to the interaction with the TRS-L motif located at the 5' end (aka the leader region) of the genomic RNA. Thus, this polymerase jumping after transcribing the TRS-L to the TRS-B upstream of each structural ORF in the 3' half of the genome results in a deletion of the viral genomic sequences between the leader region and the start of the downstream ORF in individual sg mRNA template strands. This event is important for the studies presented in this dissertation because this process of discontinuous transcription results in the same leader sequence present at the 5' end of each and every SARS-CoV-2 mRNA.

Therefore, huge amounts of this ~70 bases viral leader sequence are produced during a SARS-CoV-2 infection.

The mRNAs of SARS-CoV-2 have a 265 nts long 5'UTR (from position 1 to 265 in RefSeq NC_045512), which can promote effective translation and help to protect the transcript from degradation by cellular RNA decay enzymes. The 5'UTR of these mRNAs can be further divided into the 5' leader sequence of 72 nts, the TRS-L, ACG AAC, and other cis-elements that regulate translation, sgRNA synthesis, and packaging of viral RNAs[58]. In addition, the SARS-CoV-2 5'UTR has a predicted secondary structure comprised of five stem loops[56] and a four-way junction near the ORF1a start codon[58]. On the opposite end, the viral 3'UTR is 229 nts and includes the binding site for the RTC for the initiation of the negative-sense RNA transcription, a conserved sequence 5'-GGAAGAGC-3' of unknown function, a ~55 nt conserved pseudoknot, a non-essential hyper-variable region, and a 3'UTR polyadenylation signal[56,59–61]. The coronavirus genomic and subgenomic RNA structures, like most cellular mRNAs, contain a 5' end methylated cap structure and a polyadenylated tail at the 3' end.

Once viral infection is fully established in the host cell, the replication and transcription processes occur inside DMVs, an intricate, interconnected double membrane structure derived from the endoplasmic reticulum. Thus, the virus likely produces and protects its RNA and gene expression from host antiviral mechanisms via this compartmentalization. DMVs can also help the virus efficiently concentrate the necessary factors to replicate and transcribe the viral genome. Since SARS-CoV-2 is a positive sense RNA virus, ORF 1a and 1b are directly translated from its genomic RNA upon uncoating. ORF 1b is at the -1 reading frame with ORF 1a; therefore, a -1

ribosomal frameshift is necessary for the expression of ORF 1b[62]. The generated polyproteins are cleaved into 16 nsps by a viral papain-like protease (nsp3) and a 3-chymotrypsin-like protease (nsp5). All structural and accessory proteins are translated from the newly synthesized sgRNA and contain the 5' leader sequence from the viral 5' end RNA. An overview of coronaviral gene expression is presented in Figure 1.

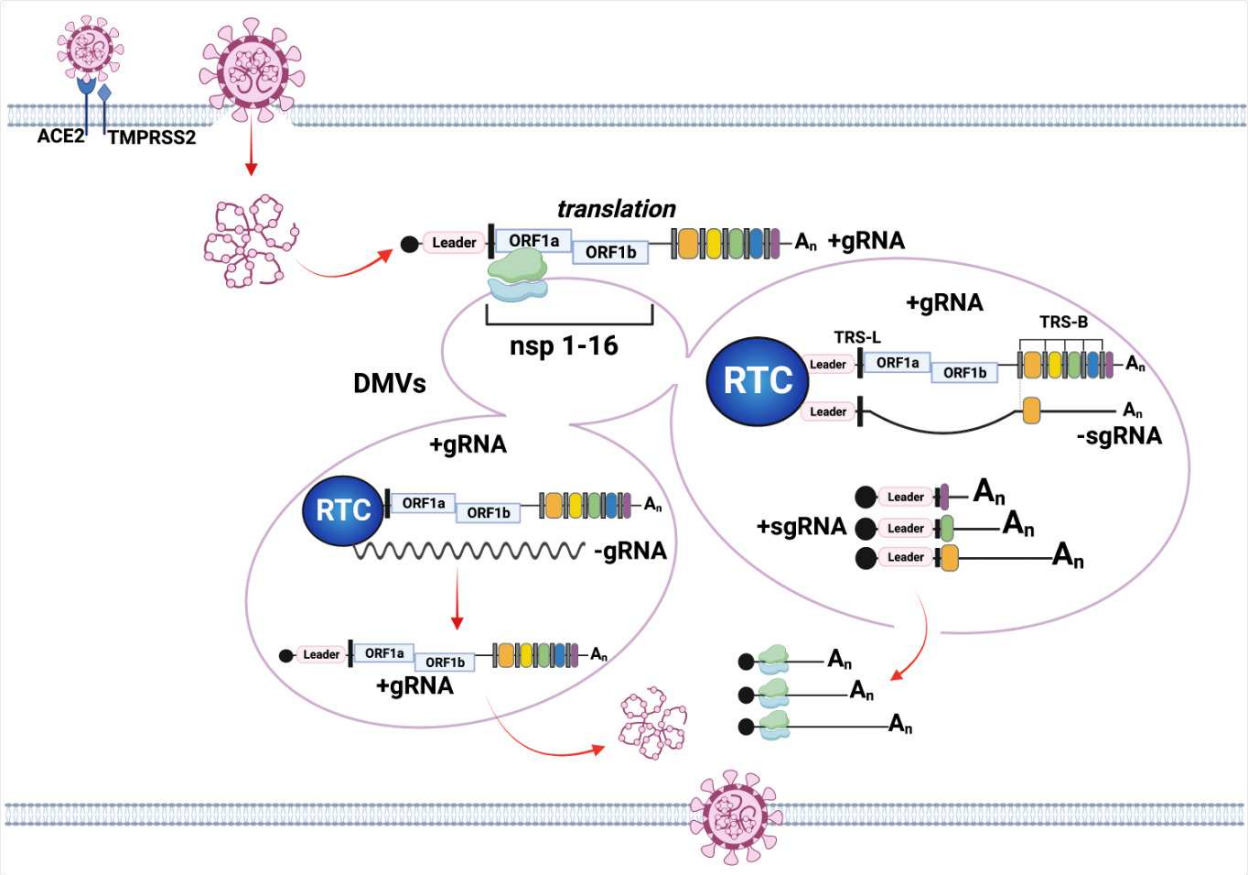

Figure 1. SARS-CoV-2 replication and transcription. *The scheme shows the main steps of coronavirus entry and gene expression. First, the viral positive-sense genomic RNA (+gRNA) is translated into non-structural proteins (nsps) 1-16 from ORF1a and ORF1b. Then, double-membrane vesicles (DMVs) eventually form at later times post-infection and serve as major sites for the replication-transcription complex (RTC) to copy the +gRNA by continuous transcription, generating a full-length negative-sense genomic RNA (-gRNA) intermediate. The RTC also generates negative-sense subgenomic RNA (-sg RNA) by discontinuous transcription and uses these as templates to produce positive-sense subgenomic RNAs (+sgRNAs). Finally, the +sgRNAs will be translated into structural and accessory proteins necessary for coating the full-length +gRNA and assembly of the new virions. This figure was created using BioRender.com.*

Immune Interactions

The mammalian innate immune system is designed to detect and block viral infections at all stages of the virus life cycle[63,64]. A major component of the innate immune system is the interferon type I (IFN type-1) pathway. IFN type-1 is part of the intracellular virus surveillance system, which generates and amplifies signals that stimulate a generalized antiviral response upon infection[65,66]. A major clinical determinant of COVID-19 severity is a delay in IFN-1 signaling. Interestingly, many critical genes stimulated by IFN (ISGs) are spliced; therefore, maintaining accurate and efficient mRNA splicing is crucial for a robust IFN response. Viruses can modify the host cell environment in multiple ways to try to avoid cellular antiviral responses. One of these mechanisms is by disrupting cellular splicing[67]. Thus, inhibition of mRNA splicing can reduce the host cells' innate immune response to viral recognition. Furthermore, increased intron retention has been observed upon SARS-CoV-2 infection[31]. Thus, the interplay between SARS-CoV-2 infection and the cellular splicing machinery appears to be a key part of the viral molecular arms race to counter cellular defenses. Examining one part of this interplay, SARS-CoV-2 binding and usurping of an important cellular RNA binding protein involved in regulating alternative splicing, is the goal of the first half of this dissertation.

RNA-Protein Interactions

The interaction between mRNA and proteins is both extensive and of vital importance in the regulation of gene expression. There are almost 2,000 different proteins in mammalian cells that are capable of interacting with RNAs and regulating

aspects of the post-transcriptional control of gene expression in cells[68]. RNA-binding proteins (RBPs) can bind to single- or double-stranded RNA facilitating the formation of ribonucleoprotein complexes[68]. Dysregulated RBP expression and functions contribute significantly to the underlying pathology of many diseases, such as cancer, genetic diseases (i.e., myotonic dystrophy and familial amyotrophic lateral sclerosis), and – importantly for this dissertation, viral infections[69–72].

Heterogeneous nuclear ribonucleoproteins (hnRNPs) are RBPs; some members of this protein group can travel from the nucleus to the cytoplasm and regulate mRNA translation and degradation[73,74]. Polypyrimidine Tract Binding Protein 1 (PTBP1) is a member of this hnRNP family of RBPs[75,76]. The structure of the PTBP1 monomer has four RNA recognition motifs (RRMs), a nuclear export signal (NES), and a nuclear localization signal (NLS). Both of these nuclear import/export signals are located in the N terminal portion of the 529 amino acid protein, with the RRMs roughly evenly spaced between residues 60 to the C terminal region of the protein. Importantly, PTBP1 is essential in regulating pre-mRNA alternative splicing (AS) and was first discovered as a factor that could bind to conserved polypyrimidine tracts found near the 3′ splice site of introns[77]. PTBP1 largely functions in splicing; however, not by competing with the core splicing machinery at these constitutive elements, but rather functions on numerous intron/exon sites by interacting with splicing enhancer or suppressor elements and regulating exon inclusion/skipping. PTBP1 is a versatile protein that also plays a role in the polyadenylation[78], cytoplasmic export[79], and stability[80] of select transcripts.

Viral RNA carries the information for its replication, protein production, and viral spread; however, viruses largely rely on cellular machinery to accomplish these tasks.

Viral RNAs often interact with RBPs from the host cell, which can exert proviral functions like efficient translation (e.g., PTB strongly binds EMCV IRES)[81], generate RNA modifications[82], and/or establish RNA localization[83]. On the other hand, host RBPs could also have antiviral functions, for example promoting 'non-self' recognition and targeting viral RNAs for inhibitory actions[84]. Therefore, the interaction of viral RNA with host RBPs plays a vital role in many viral infections and could be major factors in determining cellular susceptibility to viral infection, viral replication efficiency, tissue tropism, and infection pathology[85].

Cellular RBPs likely play a role in coronavirus infections. There is evidence revealing that coronavirus RNA interacts with a variety of human RBPs, including PTBP1, other heterogeneous nuclear ribonucleoprotein family proteins (hnRNPA1 and Q), serine/arginine-rich splicing factor 7 (SRSF7), and transformer two alpha homolog (TRA2A)[6,86–89]. The focus of the first part of my research was to explore the impact of SARS-CoV-2 leader RNA interactions with PTBP1 on the RNA biology of the infected cell.

Alternative Splicing (AS)

The biogenesis of functional eukaryotic mRNA involves removing intervening non-coding sequences (introns) by pre-mRNA splicing. The pre-mRNA has two classes of cis-acting sequences that direct and regulate mRNA splicing. The first class is splicing signals necessary to assemble the ribonucleoprotein complex known as spliceosome on the pre-mRNA. These constitutive splicing elements are composed of the 5' splice site (5'SS), a branch-point site, and a 3' splice site (3'SS)[90]. The second

class of elements is splicing regulatory elements (SREs) involved in recruiting trans-acting factors to regulate the process[91]. SREs are divided into four groups: exonic sequences that act as splicing enhancers referred to as ESEs, exonic sequences that act as splicing silencers or ESSs, intronic sequences that enhance splicing or ISEs, and intronic sequences that act as splicing silencers or ISSs. There are two main families of trans-acting factors that regulate alternative splicing through these elements: Ser/Arg-rich (SR) proteins – which usually bind to splicing enhancer elements[92] and heterogeneous nuclear ribonucleoprotein (hnRNP) proteins that usually bind to suppressor elements[93].

Alternative splicing can occur in diverse patterns generating different protein isoforms that can determine very distinct cell fates. For example, failure in proper splicing regulation can lead to problems such as exon skipping (which can result in truncated protein products), intron retention (which can cause aberrant translation of intronic regions and often introduce premature termination codons/activate RNA decay), altered levels of protein isoforms (which can alter downstream cell processes depending on the gene)[94].

Spliceosomes are large RNA-protein (RNPs) complexes that direct the pre-mRNA splicing process and are comprised of five small nuclear RNAs (snRNAs) (U1, U2, U4, U5, and U6) and >200 protein factors (e.g., U2AF65 and U2AF35)[95,96]. In the first step of this process, the spliceosomal factors U1 and U2 associate with specific signals at the 5’SS and branchpoint in the pre-mRNA in an ordered fashion driven by ATP hydrolysis. Conformational rearrangements during this and subsequent steps generate the optimal conformations for efficient and accurate pre-mRNA splicing[96]. U1

snRNP binds to the 5'SS motif, and splicing factor SF1 binds to the branch-point sequence upstream of 3'SS—forming the E' complex, committing the pre-mRNA region to the splicing pathway. Next, the U2AF65 splicing factor binds SF1 and recognizes a conserved polypyrimidine tract upstream of the 3' SS generating the early (E) complex. The U2 snRNP then base pairs with the branch-point motif replacing SF1 and forms the ATP-dependent (A) complex. The A complex recruits the U4, U5, and U6 snRNPs to generate the pre-catalytic spliceosome or complex B. Complex B gets activated for enzymatic activity after a series of conformational changes by which the U1 and U4 snRNPs are released. Ultimately, the activated spliceosome (complex B) turns into the C1 complex in a second conformational change. The splicing process continues with two transesterification reactions. In the first transesterification 'branching step,' the spliceosome attacks the phosphodiester bond at the 5'-end of the intron and generates a 2'-5' bond with a bulged adenosine residue at the branch site generating an intron-lariat and a free 5' exon. In the second transesterification reaction, exon-exon ligation occurs where the 3' hydroxyl of the 5'- exon attacks the phosphodiester bond at the 5'-end of the 3'-exon resulting in the intron removal and exon ligation to generate a functional and mature protein-coding mRNA[95–97]. Curiously, occasionally backsplicing can also occur where the 5' exon instead attacks an upstream 3' SS – generating circular RNAs[98].

Clearly, coordinating the gymnastics of splice recognition is a complex process, particularly given the limited size and complexity of the elements that determine splice site choice. Strong splice sites – those with high similarity to established consensus sequences – can result in constitutive splicing with slight variation in exon/intron

inclusion or site selection[99]. On the other hand, it is very common for splice sites to diverge far from the consensus sequence, resulting in weaker splice sites that rely on auxiliary elements to determine splice site choice and selection[100].

Alternative splicing is a vital process in biology, expanding eukaryotic proteome diversity and complexity by producing multiple proteins from one pre-mRNA substrate. Numerous protein isoforms resulting from AS are involved in the biological evolution of humans[101] and play a role in defining individual phenotypes in cell differentiation, aging, and sexual dimorphism[102,103]. As noted above, RBPs regulate splice site recognition in pre-mRNAs by binding cis-regulatory elements to enhance or suppress the recruitment of spliceosome subunits[104]. The rules for how RBPs will behave when they interact with splicing elements, however, can be complex as well. When hnRNPs bind exonic motifs, they act as splicing suppressors; inversely, when hnRNPs bind intronic motifs, they sometimes act as splicing enhancers[105]. hnRNPs bind to cis-acting exonic and intronic splicing silencers (ESS and ISS), preventing the recruitment of U1 and U2 to the splice site[106,107]. On the other hand, exonic and intronic splicing enhancers (ESE and ISE) are binding sites for serine-arginine repeat (SR) splicing activator proteins[108,109]. Dysregulation of RBPs in splicing is often associated with different pathological stages in the disease. The normal interactions between mRNAs and RBPs can be disrupted by at least three innate mechanisms in cells, 1) disruption of splicing elements, 2) toxic mutant mRNA transcripts, and 3) mutations in the spliceosome and splicing factors[110,111]. This dissertation will explore how viral RNAs that invade the cell can also disrupt the homeostasis of cellular RBP-mRNA interactions by focusing on SARS-CoV-2 infections.

Viral infections can sometimes cause global changes in mRNA splicing in infected cells. By hijacking/disrupting cellular splicing pathways, viruses can create conditions in the cell that favor their replication and/or help evade antiviral responses. The nsp16 protein of the SARS-CoV-2 virus, for example, was shown to bind to the mRNA recognition domains of the U1 and U2 snRNA host splicing factors and create significant disruptions in the constitutive splicing process in the host mRNA[31]. NS5 protein of dengue virus[112], NS1 protein of influenza virus[113], and Vpr protein of HIV-1[114] also interact with the cellular spliceosome complex and reduce overall mRNA splicing in infected cells. However, some can be more subtle in how they affect cellular splicing during infection. Our laboratory, for example, demonstrated that an abundant non-coding viral RNA (sfRNA) generated by the Zika virus during infection can disrupt splicing accuracy only at select exons of certain genes by sequestering the alternative splicing factor SF3B1[115]. It is a key goal of this dissertation to determine if SARS-CoV-2 can also target and affect the activity of an alternative splicing factor – in this case, PTBP1 – by potentially sequestering it on abundant viral RNAs.

An Overview of mRNA Capping

All eukaryotic mRNAs have an evolutionarily conserved structure added co-transcriptionally to the 5'-end of the first nucleotide of the nascent RNA, known as an N7 methylguanosine cap (m^7G cap). This modification is also referred to in the literature as a 'cap 0' structure. The capping process is the first modification that nascent RNA transcripts undergo in a co-transcriptional manner shortly after transcription initiation by RNA polymerase II[116,117]. The process of capping requires three distinct enzymatic

steps: an RNA triphosphatase (TPase), a guanylyltransferase (GTase), and a guanine-N7-methyltransferase (MTase).

Briefly, Cap 0 is generated by successive enzymatic reactions while RNA polymerase II stalls shortly after initiating transcription on a promoter: 1) the γ-phosphate of the 5' triphosphate on a nascent pre-mRNA is removed by the RNA triphosphatase (TPase), generating a diphosphate 5'-end; 2) the guanylyltransferase (GTase) transfers a 5'-phosphoguanosine (GMP) group from GTP to the diphosphate 5'-end generating a 5'-5' triphosphate bond between the first RNA base and the capping base; and 3) the guanine-N^7 methyltransferase enzyme (MTase) places a methyl group from S-adenosylmethionine (SAM) on the N7 amine of the guanosine. Cap 0 can be further modified by a m^7G-specific 2'-O MTase, which catalyzes the addition of a methyl at the 2'-O position of the ribose group on the +1 ribonucleotide of the mRNA, generating a cap 1 structure[118,119]. Interestingly, the 2'-O methylation of the +1 nucleotide is a signature of a 'self-RNA' and is used by the cellular innate immune machinery to differentiate self (methylated) vs. non-self (unmethylated) foreign RNA[120,121]. Cap 1 can be further modified by additional methylations, including the methylation at the 2'-O position of the ribose of the +2 transcribed nucleotide, forming cap 2 structures.

In eukaryotes, the cap structure has numerous fundamental functions, including protection against 5'-3' exonuclease degradation, recruitment of protein factors like pre-mRNA processing factors, and nuclear export factors[122]. In addition – and perhaps most notably - the cap structure is involved in the cap-dependent initiation of mRNA translation via recognition by eukaryote initiation factor 4E (eIF4E)[123].

Perhaps not surprisingly, given the ongoing molecular arms race of host-pathogen interactions, through viral-host co-evolution, many viruses have evolved ways to generate 5'-capped RNAs – and to make them appear as 'self-like' as possible via additional methylations to allow efficient viral protein synthesis and avoid the host cell innate immune response. There are three conventional strategies by which viruses add a cap to their RNAs. One viral mRNA capping strategy is simply borrowing the capping machinery from their host cell. Due to the subcellular localization and association of cellular capping enzymes with the C-terminal domain of the large subunit of RNA polymerase II, this strategy requires a nuclear presence of the virus as well as the use of RNA polymerase II to generate viral transcripts. Many DNA viruses and retroviruses use this strategy[124]. Another strategy used by some RNA viruses to cap their transcripts is called 'cap snatching.' In this strategy, viruses steal the cap structure from the host RNA pol II transcripts to prime viral RNA synthesis. Members of the *Orthomyxoviridae*, *Arenaviridae,* and *Bunyaviridae* are great examples of this strategy[125]. The final strategy used by many viruses is to simply encode their own capping machinery, a strategy generally favored by RNA viruses that replicate in the cytoplasm. For example, flaviviruses (positive single-stranded RNA viruses) like the Dengue virus and Zika virus, also Paramyxoviruses (negative single-stranded RNA viruses) possess GTase and MTase activities in their RNA-dependent RNA polymerase (RdRp)[126]. Interestingly, SARS-CoV-2 encodes its own capping enzymes in three separate proteins -nsp13 (TPase), nsp12 (GTase), and nsp14-nsp16 (MTase) to add a cap to its RNAs via an unconventional enzymatic mechanism that may be targetable by therapeutics[127].

While mRNA capping is generally assumed to be the default process for mRNAs following transcription, there is evidence in the literature that capping may be a regulatable process. There is clear evidence, for example, that non-capped Sindbis virus genomic plus sense RNAs play an integral role in the efficient production of new virions and viral pathogenesis[128,129]. In addition, rotavirus RNA particles contain a substantial amount of uncapped RNA[130]. A goal of this project was to examine the potential regulation of mRNA capping of SARS-CoV-2 transcripts throughout infection to determine if the virus perhaps is potentially using its genomic and subgenomic RNAs as uncapped non-coding transcripts to impact cell biology as well as for translation to generate viral proteins.

The Cellular Innate Immune Response to Viral RNAs

How does the cell respond when SARS-CoV-2 RNAs enter and start to amplify in its cytoplasm? Usually, single-stranded RNA derived from genomic, sub-genomic, or replicative intermediates of SARS-CoV-2 are sensed by RIG-I-like receptors (RLRs), which include MDA5, RIG-I, and LGP2[131]. RIG-I and MDA5 are the most studied RLRs and are critical regulators of the IFN pathway. The presence of viral RNA induces post-translational modifications and activation of RIG-I and MDA5, leading to translocation of the complex to mitochondria, where it interacts with the adaptor protein mitochondrial antiviral signaling (MAVS)[132]. This complex formation activates Tumor Necrosis Factor receptor-associated factor 3 or TRAF3, TANK-binding kinase1 or TBK1, and IκB kinase or IKK to induce phosphorylation of IRF3[133]. IRF3 phosphorylation facilitates nuclear translocation to promote the transcription of genes that encode type I and III IFNs.

Production and release of IFNs trigger a downstream signaling cascade through IFN receptors in an autocrine and paracrine manner producing hundreds of interferon-stimulated genes (ISGs) with numerous antiviral functions[134]. For example, the ISG Ly6E prevents SARS-CoV-2 entry[135], members of the IFIT family (IFIT1, IFIT3, and IFIT5) inhibit viral replication[136], and BST2 blocks the release of new viral particles in cell lines that ectopically or stably express these ISGs[137]. Interestingly, patients with circulating autoantibodies against type-I IFN have reduced IFN responses after SARS-CoV-2 infection[138] and present an increased risk of severe COVID-19 and death. Fine-tuning a type I IFN response is crucial because the over-activation and under-activation of IFN signaling can be harmful to the host[139].

The mechanism used by SARS-CoV-2 to evade innate immune responses is becoming clearer but is still not fully elucidated. Studies in patients with severe COVID-19 showed reduced levels in the blood of IFNs type I and III[140]. SARS-CoV-2 infections reduce the IFNs production post-transcriptionally by stopping the release of mRNA from transcription sites, promoting transcript degradation in the nucleus[141]. Several proteins encoded by SARS-CoV-2, such as papain-like protease (PLpro), can inhibit and disrupt the RIG-I-like receptor and MDA-5 pathways and, consequently, IFN induction. MDA-5, specifically, is activated by presence of RNA viruses in the cell via the addition of ISG15 to the receptor in a process called ISGylation[142]. PLpro inhibits MDA5 activation by de-ISGylation[143]. In addition, other proteins, such as ORF9b, ORF3b, ORF6, N, and M, can inhibit the expression of IFN-β and proinflammatory cytokines by interfering with RIG-I and MDA5 pathways[144–148]. SARS-CoV-2 virus also hampers the immune response by attacking translation; for instance, nsp1 and nsp14 inhibit host translation by association

with the ribosomes, preventing gene expression from the IFN signaling pathway[149,150]. For instance, nsp1 binds directly to the 18S rRNA (within the 40S sub-unit), restricting host mRNA entrance and effectively blocking their translation. However, mRNA containing the coronavirus leader sequence can modulate nsp1 binding allowing viral RNA translation[151]. Finally, the MAVS antiviral pathway is usually activated by the detection of RNA viral genomes in the cytoplasm, resulting in an aggregation of MAVS protein[152]. However, SARS-CoV-2 uses N protein to obstruct the aggregation of the MAVS protein by viral RNA leading to blocking the induction of the IFN pathway[153]. The physical interaction between the N and MAVS proteins thus provides another layer of disruption affecting the activation of the innate immune response.

The m^{6}A Modification: Not Just Another RNA Modification

Numerous aspects of gene expression can be regulated not only by RNA sequence alterations but also by RNA epigenetic modifications such as methylations[154]. These modifications add complexity to the information in the RNA, influencing its structure and interaction with other molecules. These subtle structural changes can diversify RNA functions leading to significant changes in cellular metabolism by affecting RNA stability, splicing, and translational efficiency[155,156].

The most abundant mRNA modification in eukaryotes, from yeast to mammals, is the methylation of adenosine at position N6, generating N^6-methyladenosine (m^{6}A). At least 25% of mRNAs contain one m^{6}A[157,158]. Even though m^{6}A was first discovered in 1974[159,160], the field of m^{6}A modification was reborn and began to rapidly accelerate in 2012 due to the application of m^{6}A-specific antibody-based immunoprecipitation[161]

coupled with high-throughput sequencing[162]. The early high throughput studies performed a decade ago indicated that m^{6}A modifications were enriched in three places on a transcript - within atypically long internal exons, in proximity to stop codons, and in the 3' UTR[157,158]. Later studies expanded this list to include other areas of the transcript associated with m^{6}A modification, including intron-exon junctions[163]. This expansion of the investigations led to numerous data indicating a pivotal role of m^{6}A in regulating various aspects of RNA metabolism, including RNA structure, localization, splicing, stability, and translation[164–167].

Work in the field has also led to debates regarding whether or not RNA methylation events are truly dynamic[163,168,169]. All the requisite enzymatic activities required for dynamic RNA epigenetic modification are, however, clearly present in the cell. These factors are 1) 'writers,' m^{6}A methyltransferases (MTases); 2) 'erasers,' m^{6}A demethylases; and 3) 'readers,' m^{6}A binding proteins that recognize and regulate the modification determining the cellular effects.

Mutations in the enzymes related to m^{6}A modification are linked to diverse human diseases (e.g., cancer, cardiovascular diseases, metabolic diseases, and neurological disorders). The methyltransferase-Like protein 3-14 (METTL3-METTL14) MTases complex catalyzes the methylation on the N6 position of the adenine to form m^{6}A within sites in the mRNA at a specific consensus sequence motif - DRACH (D=G, A, or U, R=G or A, and H= U, C, or A)[162,170–173]. METTL3 is the catalytic subunit of the MTase complex, while METTL14 contains an RNA-binding domain that activates and enhances METTL3 activity[174]. Regulatory factors, like Wilms tumor one associated protein (WTAP), interact with and stabilize the METTL3-METTL14 complex. WTAP

does not possess MTase activity, but it is required for the localization of the METTL3-METTL14 complex at nuclear regions enriched with pre-mRNA processing factors[175]. Other regulatory factors can also be found in the methylation complex. VIRMA, KIAA1429, and RBM15, for example, recruit the catalytic complex METTL3-METTL14-WTAP to specific m^{6}A methylation target sites[176,177]. Another example of a regulatory factor is ZC3H13, which in a similar fashion also guides the MTase complex to methylation target sites[178]. Recent studies identified additional MTases, such as MTTL5, MTTL16, and ZCCHC4, which catalyze the m^{6}A methylation on non-coding RNAs[179]. MTTL16, for example, used to be considered a methyltransferase that solely targets ribosomal RNA, but now it is recognized to also modify specific snRNAs, lncRNAs, and mRNAs[180].

The m^{6}A modification can be removed from the mRNA by the 'erasers.' Fat mass and obesity-associated protein (FTO) and α-ketoglutarate-dependent dioxygenase alkB homolog 5 (ALKBH5) proteins possess clear RNA demethylase activity. This finding provided the first insights into the reversible character of m^{6}A post-transcriptional modification of mRNAs. FTO m^{6}A demethylase was first described for its activity on N^3-methylthymidine of single-stranded DNA[181] and N^3-methyluridine of single-stranded RNA[182]. Later, Jia et al. (2011) demonstrated that FTO can remove m^{6}A from both DNA and RNA *in vivo*, and, importantly, its inhibition leads to increased levels of total m^{6}A of polyadenylated RNAs[183]. In humans, FTO is associated with levels of body mass and obesity, and it is expressed in all adult and fetal tissues, with higher expression in the brain[181]

The second identified m^{6}A demethylase, ALKBH5, removes m^{6}A from single-stranded RNA in a sequence context dependent fashion[184]. ALKBH5 localizes in the nucleus, and its depletion causes the intranuclear reduction of polyadenylated RNA levels. This reduction in the levels of polyadenylated RNA indicates that ALKBH5 may have a role in regulating the nuclear export of mRNA[184]. ALKBH5 is a very important factor for a number of biological processes. It is involved, for example, in cardiomyocyte fate determination[185], cancer[186,187], and neuronal synaptic plasticity[188]. Additionally, it has been demonstrated that ALKBH5 has a role in the immune response during viral infections. After infection, the nuclear protein DEAD-box 46 (DDX46) recruits ALKBH5 to remove m^{6}A modifications from antiviral transcripts, sequestering them into the nucleus. This prevents their translation with the consequent inhibition of type I interferon production[189].

Deciphering the impact of the m^{6}A modification of RNAs in diverse post-transcriptional processes depends on nuclear and cytoplasmic ‘reader’ proteins that specifically recognize m^{6}A-decorated mRNAs[190]. The YT521-B homology (YTH) family proteins were the first described m^{6}A-readers. YTH proteins recognize m^{6}A through an RNA-binding YTH domain[191] and have a critical role in regulating m^{6}A-modified mRNAs. The YTH family of proteins has five members in humans. The only nuclear member of this family is YTHDC1. This factor is involved in transcription[192], mRNA splicing[193], and mediates nuclear export[165]. YTHDC1 forms granular structures called YT bodies in the nucleus, near mRNA speckles, that interact with splicing factors like SRSF3, SAM68, and SC35[194,195]. YTHDC1 has been implicated in the regulation of mRNA splicing by recruiting splicing factors to favor exon inclusion and blocking splicing factors that

promote exon skipping[196]. Four other members in the YTH reader family are in the cytoplasm: YTHDF1, YTHDF2, YTHDF3, and YTHDC2[197–200]. These cytoplasmic readers are involved in mRNA translation and degradation. YTH-domain family 2 (YTHDF2) was the first described m^6A reader in regulating m^6A RNA stability in the cytoplasm[197] and has a significant impact on cell biology and disease[201].

In addition to m^6A, there are at least 170 other modifications that can be found on cellular RNAs[202]. Work in the second half of this dissertation will focus on one of these – m^6A_m located on the cap proximal nucleotide of some eukaryotic transcripts[203]. This relatively abundant RNA modification is a double methylation of the cap 1 structure[204] on mRNAs that initiate with an adenosine residue. The first transcribed nucleotides adjacent to the m^7G cap are usually methylated at the 2'-hydroxyl position of the ribose. Furthermore, if the first transcribed nucleotide is adenine (A), the 2'-O-methyladenosine (A_m) can undergo a second methylation at the N6 position to generate N^6, 2'-O-dimethyladenosine (m^6A_m). This double methylation is found in ~30% of the first transcribed nucleotides of cellular mRNAs; therefore, m^6A_m is a major modification of a large subset of the cellular transcriptome[205].

Recently, PCIF1 was identified as the methyltransferase responsible of adding a methyl group on A_m to generate m^6A_m next to the m^7G cap[204,206–209]. Interestingly, the FTO demethylase can remove the N^6 methylation from the m^6A_m moiety, reducing the stability of m^6A_m-containing mRNAs in vivo[210]. The potential m^6A_m modification of viral RNAs – in particular SARS-CoV-2 – is a key focus of this project.

The m^6A modification has also been identified in the transcripts of viruses, such as influenza virus, simian virus 40, avian sarcoma virus, and adenovirus. However, the

role of m^6A in viral life cycle regulation is still unclear[192,211–214]. Recent studies have greatly expanded this list and showed, for example, that m^6A modifications are present in 12 positions over ZIKV viral RNA regulating viral gene expression and influencing viral replication[215–217]. Viral infections have also been shown to affect m^6A modification patterns of cellular RNAs[218]. However, the distribution, function, and regulatory mechanism of m^6A in coronaviruses, including SARS-CoV-2, were unknown when we initiated this project.

The genome of SARS-CoV-2, like other coronaviruses, mimics a eukaryotic mRNA with a 5'-terminal cap structure and a 3' polyadenylated tail[51,219]. The cap structure and methylation of the adjacent ribose at the 2'-hydroxyl position to form 2'-O-methyladenosine (A_m) stabilizes the coronavirus RNA by helping the virus avoid cellular innate antiviral effectors like interferon-induced protein with tetratricopeptide repeat 1 protein (IFIT1), which recognize viral mRNAs that lack this 2'-O methylation, activating a strong interferon response[51,120,220]. Whether or not the initial 5' adenosine of coronavirus transcripts contains additional methylation to form m^6A_m is a key knowledge gap in the field that will be addressed in this dissertation.

In summary, the goal of this dissertation is to address two important areas of virus interactions with the RNA biology of the cell in the context of SARS-CoV-2 infections. First, we investigated whether the abundant leader RNA that is found at the 5' end of every positive sense viral transcript can interact with the cellular PTBP1 splicing factor. Furthermore, we tested the hypothesis that this interaction sequesters PTBP1, preventing it from performing its normal function in the cell of regulating alternative splicing of target genes. Second, we tested the hypothesis that SARS-CoV-2

specifically modifies the 5' termini of its transcripts with an m^6A_m modification via usurping cellular enzymes (since a similar enzymatic activity has not been identified in the viral genome). Furthermore, we assessed whether this modification is regulated during viral infection and investigate its functional role in efficient viral replication.

Collectively, these studies provide new insights into the interface between SARS-CoV-2 and the RNA biology of the infected cell, demonstrating new molecular mechanisms that can contribute to viral replication and pathogenesis.

RATIONALE

In this project, we investigated two aspects of the molecular mechanism by which non-coding SARS-CoV-2 RNA sequences may impact key aspects of virus-host interactions. Previously our lab demonstrated that non-coding regions of flavivirus and alphavirus RNAs significantly affect different cellular processes like polyadenylation[115], stability[115,221–225], and splicing[115,223] of RNAs by binding and usurping the functions of cellular RNA binding proteins. Thus, we wished to explore whether coronaviruses – specifically SARS-CoV-2, may also interact with the cell by binding and usurping the functions of cellular RNA binding proteins. We focused on the SARS-CoV-2 leader RNA as a likely sink for cellular RNA binding proteins, given its abundance and presence on every plus sense RNA made by the virus.

Next, we wanted to explore the potential that coronaviruses mRNAs might be capped in a regulated fashion. The premise for this hypothesis was that another positive sense RNA virus family that generates a subgenomic RNA – alphaviruses – does not uniformally cap all of its transcripts; the relative levels of[127,222] capped vs. uncapped alphavirus RNA affects the dynamic of virion production[129]. Uncapped RNAs could, for example, function as long non-coding RNAs during infection and have very different impacts on the cell from their capped and translated counterparts. Thus, we explored the nature and extent of 5'end capping of coronavirus RNAs during a time course of infection.

Finally, the methylation of the first transcribed nucleotide adjacent to the mRNA cap is an important modification for effective virus infections[226]. Methylation at the 2'-O of the ribose of the 5' proximal nucleotide is used by cells in differentiating the mRNAs

that are self versus non-self[227]. Cellular IFIT1-based surveillance[120] routinely scan capped mRNAs for 2'-O-methylation to suggest that they are cellular rather than invading transcripts. The absence of 2'-O-methylation activates the cellular interferon response[220,227,228]. Coronaviruses can methylate the 2'-O position because they encode a 2'-O-methylase, nsp16, avoiding the cellular surveillance system[120]. Interestingly, there is another cap-proximal methylation on the mRNAs that also could have a role in self versus non-self-recognition. All cellular mRNAs that initiate with adenosine have this residue also modified with methylation at the N6 position of the adenosine. This methylation is performed by the nuclear PCIF1 enzyme, generating an m^6A_m moiety[207,229]. Interestingly, all the mRNAs of all coronaviruses initiate with an A residue and have the 2'-O-methyl ribose modification; however, it is unknown if they contain a methyl at the N6 position of the adenosine. To date, there has been not virally encoded m^6A modifying enzyme identified that is able to perform this modification on the first adenosine. We hypothesize; therefore, the SARS-CoV-2 mRNAs likely contain this m^6A_m modification at its 5' terminal adenosine base by usurping the cellular enzyme PCIF1 to add it. This study was the first of its kind to our knowledge to examine this additional 5' end modification as well as determine its potential impact on viral mRNAs.

HYPOTHESES

Our research tested the following hypotheses:

- The abundant and conserved 5’ UTR of SARS-CoV-2 can impact cellular RNA biology by binding and sequestering cellular RNA binding proteins in the cytoplasm, thus impairing their function in cellular RNA processes.

- The ratio of uncapped to capped SARS-CoV-2 mRNA is regulated and thus may vary during infection to provide adjustments for optimal host-viral interactions and gene expression.

- As part of the molecular arms race between pathogens and cells, SARS-CoV-2 has likely uncovered a way to usurp the cellular machinery to place an m^6A_m modification at the 5’ base of its mRNAs to escape a key RNA surveillance pathway and establish a highly productive infection.

MATERIALS AND METHODS

Cell lines and culture conditions

HeLa, HeLa PCIF1 KO, human embryonic kidney 293T (hereon referred as 293T) (ATCC, CLR-3216), and 293T PCIF1 KO cell lines were cultivated in Dulbecco's Modified Eagle's Medium (DMEM, Corning, 50-003-PC) supplemented with 10% fetal bovine serum (FBS, Sigma, F2442), 2mM L-glutamine (Gibco, 25030-081), 100 U/mL penicillin and 100 mg/mL streptomycin (Cytiva, CV30010) using 75cm^2 cell culture flasks (T-75 flask, CELLSTAR^R, Greiner Bio-One, 658175) coated with poly-D-lysine hydrobromide (Sigma-Aldrich, P6407). HeLa-PCIF KO and 293T PCIF1 KO cell lines were generated using the CRISPR/Cas9 system and generously provided by Dr. Eric Greer's laboratory at Harvard Medical School.

The African green monkey (*Cercopithecus aethiops*) kidney cell line (Vero E6, ATCC CRL-1586) was cultivated in DMEM, supplemented with 10% FBS, 2mM L-glutamine, 100 U/mL penicillin and 100 mg/mL streptomycin, using uncoated T-75 cell culture flasks.

The human lung epithelial cell line Calu3 (ATCC, HTB-55) was maintained in DMEM, supplemented with 15% v/v non-heat inactivated FBS, 2mM non-essential amino acids, 2mM L-glutamine, and 25mM HEPES buffer (Sigma-Aldrich, 83264).

All cells were maintained at 37^{0}C, 5% CO_2 in a humidified atmosphere as monolayer cultures and split when they reached 80%-90% of confluency by washing twice with 1X phosphate buffered saline (PBS, Cytiva, SH30256.01) and incubating with

0.25% trypsin (1X) solution (Cytiva, SH30042.01) at 37^0C for 3-5 minutes. Cells were re-plated at an ~1/10 dilution for passaging.

Virus sample propagation and infections

Severe acute respiratory syndrome coronavirus 2, isolate Wuhan-Hu-1 (SARS-CoV-2, accession number NC_045512) and Zika virus, PRVABC59 strain (ZIKV, accession number KX377337) were courteously provided by Dr. Perera at Colorado State University. The ZIKV stock was propagated in our BSL-2 laboratory while SARS-CoV-2 was maintained—and all infections were performed—under BSL-3 conditions.

For ZIKV viral propagation, we seeded $7x10^6$ Vero cells in a T-175 flask (CELLSTAR^R, Greiner Bio-One, 660160) 24 hours before infection. ZIKV stocks were thawed inside the hood, the 1X PBS and infection media (DMEM supplemented with 2% FBS and 25mM HEPES) also were pre-warmed at 37^0C using a water bath. The necessary volume of viral inoculum for the desired multiplicity of infection (MOI) (e.g., 0.01 for virus propagation) was calculated using the equation:

$$\mathrm{MOI} = \frac{(\mathrm{PFU/ml})(\mathrm{volume\ of\ inoculum})}{\mathrm{number\ of\ cells}}$$

The calculated volume of ZIKV stock was transferred to a 15ml conical tube (Corning,430791) and brought up to a final working volume of 10ml using pre-warmed infection media. Growth media was removed and discarded from the plated Vero cells and cultures were washed twice with 10ml pre-warmed 1X PBS prior to adding the ZIKV inoculum. Cultures were incubated at 37^0C and 5% CO_2 for 2 hours with gentle rocking

every 15 minutes to ensure an even spread of the viral inoculum over the Vero cells monolayer. After the 2 hour adsorption period, the inoculum media was removed and replaced with 35ml of infection media. The cells were incubated for 96 hours at 37^0C and 5% CO_2. ZIKV was harvested by transferring the media to a 50ml conical tube (Corning, 430829) and centrifuging at 180xg relative centrifugal force (rcf) at 4^0C for 10 minutes. An aliquot of 200µl was used for viral titer determination using a plaque titration assay. The remaining supernatant was aliquoted in 15ml tubes and stored at -80^0C until further use.

The SARS-CoV-2 stock was propagated at CSU BSL3 facility using Dr. Perera's Lab protocols. Briefly, in a standard BSL-2 laboratory, $1x10^7$cells were plated one day prior to infection in T-175 flasks (CELLSTAR^R, Greiner Bio-One, 660160) in culture media for the chosen cell type. One flask serves as a mock-infected control and the other for infection. The flasks were maintained in a humidified incubator at 37^0C with 5% CO_2. The flasks were transferred into BSL-3 room, a SARS-CoV-2 stock was thawed at 37^0C, and the volume of virus needed to infect at the desired multiplicity of infection (MOI = 0.01) was determined as described above. The volume of virus calculated was raised up to 20ml with infection medium. The culture media was removed from T-175 flasks and replaced with 20ml of fresh infection medium for mock-infected flask. The culture media was replaced with 20ml of infection medium containing virus the flask for infection. The flasks were incubated for 48–72 hours at 37^0C monitoring daily for evidence of cytopathic effect (CPE). We routinely used the mock-infected flask as a control for any non-specific subtle CPE that might be observed to ensure quality control at every step of inoculum production. The virus was harvested by collecting the cell

culture supernatant into two 15ml conical tubes and centirfuging at 450xg rcf for 5 minutes at 4^0C to clarify supernatants and pellet cell debris. Next, the supernatants were combined into a single tube and gently mixed using a serological pipette to ensure homogeneity across aliquots of the stock. Finally, the supernatant was separated in aliquots of 1ml in O-ring tubes and stored at -80^0C.

The concentration of viral stocks was determined by plaque titration on Vero cells. Briefly, 10-fold dilutions of viral stock in infection media were generated and 450µl of each dilution was added to a monolayer of 150,000 Vero cells/well seeded on 12-well plates (Greiner Bio-One, 665180) according to the scheme presented in figure 2.

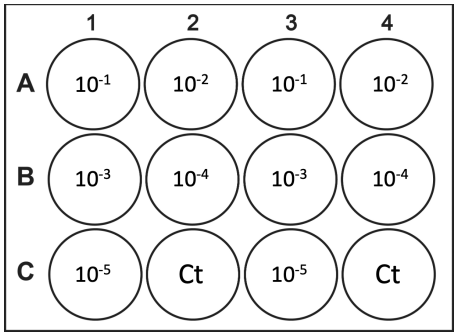

Figure 2. Plating scheme to determine viral titers. *Titers were determined by plaque assay applying 10-fold serial dilution—10^{-1}-10^{-5}—of viral stock on 12-wells plates seeded with Vero cells using the pattern shown.*

The plates were incubated for 2 hours for ZIKV and 1 hour for SARS-CoV-2 at 37^0C and 5%CO_2 to allow viral adsorption, then the media in each well was removed and replaced by infection media containing 2% agarose (Bio-Rad, 1613102EDU) in 1X PBS. The plates were incubated for 96 hours at 37^0C and 5%CO_2. The cells were then fixed to the plate and virus inactivated by adding 4% v/v of formaldehyde in 1X PBS and incubating for 20 minutes at room temperature inside the hood. The fixative was

discarded, and the agarose media was removed before staining with 1ml of crystal violet stain (working solution 0.5% crystal violet in 20% ethanol) added to each well. The stained plates were incubated at room temperature for 20 minutes and the wells were rinsed repeatedly with tap water multiple times until washes become clear. The plaques were visualized by eye, counted, and the viral stock concentration was determined by applying the equation below:

$$\text{Pfu/ml} = \frac{\text{Avg. \# of plaques}}{\text{D x V}}$$

D=dilution V=volume of diluted virus added to the plate

All SARS-CoV-2 infections were performed at the CSU Foothills campus BSL3 facility following approved biosafety protocols. ZIKV infections were performed in a similar fashion under BSL2 conditions. Sub-confluent cells (e.g., Calu3, Vero, HeLa, and HeLa- PCIF1 KO cells) were infected at an MOI of 3 with SARS-CoV-2 virus for 48 hours or mock infected. Viruses were incubated with the cells for one hour followed by a gentle wash of the monolayer with 10ml of pre-warmed 1X PBS to remove residual viral particles. The wash was discarded, and 10ml of fresh pre-warmed infection media was added to the flask. After 48 hours (or at the indicated times), media supernatant as well as the cells were collected in 1ml of TRIzol® Reagent (Ambion, by Life Technologies, 15596018) and transferred into 1.5ml microfuge tubes for total RNA extraction.

Protein-RNA binding predictions, crosslinking, and immunoprecipitation

Mapping binding sites for RNA-binding protein PTBP1

Potential PTBP1 RNA binding sites on the SARS-CoV-2 leader sequence were predicted using the free web server RBPmap version 1.2 (http://rbpmap.technion.ac.il/). RBPmap uses the algorithm based on Weighted-Rank (WR) approach to map the protein binding sites on the RNA sequence[230]. Briefly, the PTBP1 RNA consensus binding motif and the SARS-CoV-2 leader sequence were entered as input to be mapped using the BLAST utility. RBPmap software calculated the match score for predicted PTBP1 binding motifs per each site in the leader sequence in an overlapping tiling fashion. Then, all the match scores bellow a significant threshold (P-value<0.005) were filtered out and the propensity of suboptimal motifs (default P-value<0.01) to cluster around the significant motif was calculated by a WR score. Finally, the sites falling into non-conserved regions were filtered out by the application of a conservation-based filter. This generated a summary of the predicted binding sites in the leader RNA sequence for our protein of interest.

SARS-CoV-2 leader RNA production and radiolabeling

To assess whether the SARS-CoV-2 leader sequence can bind host RNA binding proteins, we designed gene-blocks to be synthesized by Integrated DNA Technologies (IDT). The gBlock constructs contained 75 nucleotides (nts) of the SARS-CoV-2 5' mRNA leader sequence with an SP6 promoter sequence at the 5'-end of the construct. A DNA template to generate a similarly sized control RNA was generated by cutting pGEM-4 plasmid at position 2629 with Nhe I-HF restriction enzyme (New England Biolabs, R3131S) and at position 61 with Hind III restriction enzyme (New

England Biolabs, R0104S) to obtain the 65 nucleotides long fragment along with the SP6 promoter at the 5'-end (see Table 1):

Table 1: Overview of DNA templates to generate radiolabeled SARS-CoV-2 leader and control RNAs. The upper case bolded G represents the start site of transcription.

	SP6 promoter (20nts)	Sequence
pGEM-4	atttaggtgacactata**G**aa	tacacggaattcgagctcggtacccggggatcctctagagtcgacctgcaggcatgca
SARS-CoV-2	atttaggtgacactata**G**aa	attaaaggtttataccttcccaggtaacaaaccaaccaactttcgatctcttgtagatctgttct ctaaacgaac

The RNAs were generated and radiolabeled by *in vitro* transcription in the presence of [α32P]-UTP (Perking Elmer, BLU007X250UC) as previously described[231]. Briefly, *in vitro* transcribed RNAs were prepared using SP6 RNA polymerase (Thermo Scientific, EP0131) and internally labeled with [α32P] UTP. DNA templates in RNase-free water were incubated with 500mM cap analog (7MeGpppG), rNTP mix (500mM ATP, 500mM CTP, 50mM GTP, 50mM UTP), 45 mCi [α32P]-UTP (800 Ci/mmol), 20 units of RiboLock RNase inhibitor (Thermo Scientific, EO0381), 20 units of SP6 RNA polymerase (Thermo Scientific, EP0131), and transcription buffer (40mM Tris-HCl at pH 7.6, 6mM $MgCl_2$, 2mM spermidine, 10mM DTT) for 1 hour at 37^0C in a total volume of 10 µL. The reaction was stopped by the addition of 90µL of RNase-free ddH_2O and 100 µL of phenol:cholorform:isoamyl alcohol (25:24:1). After ethanol precipitation in 2 M ammonium acetate, the transcripts were centrifuged, and the pellets washed with 70% ethanol. The pellets were resuspended in RNA loading buffer (7M urea, 25mM Tris-HCl at pH 7.6, 1mM EDTA at pH 8.0, 0.05% bromophenol blue, 0.05% xylene cyanol), denatured at 90^0C for 30 seconds, and loaded onto a 5% polyacrylamide denaturing gel

with 7 M urea. Following electrophoresis, transcripts were visualized by autoradiography, and the appropriate bands were excised and incubated in 400 µl of HSCB buffer (0.4M NaCl, 25mM Tris-HCl at pH 7.6, 0.1% SDS) with 40 µg of proteinase K (Sigma) at 25^0C overnight. Eluted RNAs were extracted with an equal volume of phenol:chloroform:isopropyl alcohol (25:24:1), ethanol precipitated, and centrifuged. The pellet was washed with 70% ethanol and resuspended in RNase-free ddH_2O.

Preparation of HeLa cytoplasmic extracts

Aliquots of cytoplasmic HeLa cell extract were obtained as described at Sokoloski, et al.[232]. Briefly, large-scale preparations of cytoplasmic extract were produced from several liters of healthy and actively growing HeLa spinner cells at a density of approximately $1x10^6$ cells/ml. HeLa cells were harvested by centrifugation at 300xg rcf for 5 minutes at 4^0C and the pelleted cells were washed with ice-cold 1X PBS until a clear colorless supernatant was obtained. The cell pellet was gently resuspended in chilled Buffer A (10mM HEPES, pH 7.9, 1.5mM $MgCl_2$, 10mM KCl, and 1mM DTT) for 10 minutes for osmotic swelling. Next, the swollen cell suspension was transferred to a pre-chilled dounce and ten strokes were used to break the cell membrane. The cell lysate was transferred to a pre-chilled 50ml centrifuge tube and centrifuged at 850xg rcf for 10 minutes to clear the extract from intact nuclei. The cytoplasmic extract was removed and clarified by adding cold buffer B (300mM HEPES, pH 7.9, 30mM $MgCl_2$, 1.4M KCl) and centrifugating at 100,000xg rcf for one hour at 4^0C. Finally, the the cytoplasmic extract was adjusted to 10% glycerol, mixed, and separated in aliquots to be stored at -80^0C.

Protein-RNA crosslinking, and immunoprecipitation

Radiolabeled SARS-CoV-2 leader and pGEM-4 RNA sequences were incubated with HeLa cytoplasmic extracts for 10 minutes. Samples were transferred to a microplate placed on ice and RNA-protein complexes were covalently crosslinked using 0.5J of UV light in a UV Stratalinker 2400 (Stratagene). The crosslinked samples were transferred to a 1.5ml microfuge tube and treated with RNase A (Millipore Sigma, 10109142001), leaving only a small radioactive RNA oligomer crosslinked to proteins. PTBP protein-RNA complexes were then specifically immunoprecipitated by incubation with PTBP1 monoclonal antibody (Invitrogen, 32-4800) or a control normal mouse IgG polyclonal antibody (Millipore, 12-371) for 1 hour at 4^0C on a rotating platform. Note that the PTBP1 antibody was validated by immunoprecipitation and western blotting prior to use (Fig. 2B). Samples were incubated with pre-washed Protein G magnetic beads (New England BioLabs, S1430) by rotating for 1 hour at 4^0C. The beads were washed with 500µl of LS-RIPA (Low Stringency-Radioimmunoprecipitation Assay) buffer (50mM Tris-Cl pH 7.5, 0.5% w/v sodium deoxycholate, 1% v/v NP-40, 0.05% w/v sodium dodecyl sulfate (SDS), 150mM sodium chloride, 1mM EDTA). Finally, all samples, including a separate fraction representing 10% of the input material, were incubated with 6X Laemmli SDS sample buffer (Thermo Scientific, J61337.AD) for 5 minutes at 100^0C and electrophoresed on a 10% SDS polyacrylamide gel. The position of crosslinked proteins on the gel was analyzed by phosphorimaging.

RNA Splicing Analyses

RNA isolation and reverse transcription

TRIzol® reagent samples collected as described above were processed by the addition of 200 µl of chloroform followed by vortexing and centrifugation at 16,100xg rcf and 4^0C for 10 minutes. The upper aqueous phase of each tube was transferred to 1.5ml microfuge tubes containing 2µl of glycogen (Thermo Fisher, R0561). Isopropanol (500 µl) was added, mixed by inversion and the samples were centrifuged at 16,100xg rcf, 4^0C for 30 minutes. Supernatants were discarded, the pellets were washed with 150µl of ice-cold 70% ethanol, then re-centrifuged at 16,100xg rcf, 4^0C for 10 minutes. Pellets were air-dried for ~5 minutes prior to resuspension in 160µl of RNAse-free water. The resuspended pellets were treated with 20µl DNase I buffer and 20µl of RNase free DNase I (Thermo Scientific, EN0521), and incubated at 37^0C for 30 minutes. The RNA was extracted by adding 200µl of phenol:chloroform:isopropyl alcohol (25:24:1) and centrifugation for 15 minutes at 16,100xg rcf and 4^0C. The top aqueous layer containing RNA was transferred to a 1.5ml microfuge tube. 2µl of glycogen, 66µl of 10M of ammonium acetate, and 500µl of 100% ethanol were added, and tubes were incubated at -80^0C followed by centrifugation at 16,100xg rcf, 4^0C for 30 minutes. The supernatants were discarded, the pellets were washed with 150µl of 70% ethanol, and centrifuged at 16,100xg rcf, 4^0C for 10 minutes. Pellets were air-dried and resuspended in 30µl of RNAse-free water. RNA concentrations were measured using a NanoDrop 2000c spectrophotometer (Thermo Scientific).

Cloning and Sequencing

Calu3 cells were seeded on 6-well plates at 150,000 cells per well and mock infected or SARS-CoV-2 infected at an MOI=3 on the next day. Cells were collected 48 hours post infection (hpi) in TRIzol® and RNA was extracted as described above. The RNA was converted into cDNA by reverse transcription PCR (RT-PCR) using reverse transcriptase (ImProm-II; Promega, A3800) and random hexamer primers from IDT. After conversion, a high fidelity PCR procedure was used to amplify the cDNA using the exon-specific primers listed in Table 2 for each gene as well as Q5® High-Fidelity DNA polymerase (New England BioLabs, M0491). The amplification product was gel purified and cloned using an NEB® PCR cloning kit (E1202S). Next, the pMiniT plasmids, containing the cloned PCR products, were isolated by mini-preps (Zymo Research, ZR Plasmid Miniprep™-Classic, D4016) and sent for Sanger sequencing to AZENTA (https://www.genewiz.com). Finally, the sequencing results were aligned using SnapGene 6 (https://www.snapgene.com).

Table 2: Primers used for gene/exon-specific cloning

Target	GenBank accession #	Organism/Virus	Forward	Reverse
FMNL2	ENSG00000157827	Homo sapiens	GCAAGAAGCTCTGATGAGCA	TGGGCAGTTTCATTCACGCA
TPM1	ENSG00000140416	Homo sapiens	GCAGAGGATAAGTACTCGCAGA	AGTCTGATCCAGCATCTGATGC
ACTN4	ENSG00000130402	Homo sapiens	AGTTCAAGGCCTGCCTCATCA	TACAGAGTGGAGGAATGGGACT
TEAD3	ENST00000338863	Homo sapiens	TAAACTGAGGACGGGGAAGACT	TGAAGGGCTTTGTCCTTGGAGA
SARS-CoV-2	NC_045512	SARS-CoV-2 leader	ACCTTCCCAGGTAACAAACCAACC	ACTAAGCATGCAGCCGAGTGACA

Cytoplasmic-nuclear separation and protein extraction

Two sets of HeLa cells were plated for 12, 24, and 48 hpi collection times. One of the sets was mock-infected and the other set was SARS-CoV-2 infected (MOI=3). At the indicated collection time the cells were harvested with 0.25% trypsin (1X) solution and pelleted by centrifuging at 850xg rcf for 5 minutes. The pellets were washed with 1X PBS and $2x10^6$ cells were transferred to a 1.5ml microfuge tube and pelleted by centrifugation at 850xg rcf for 3 minutes. The NE-PER^{TM} nuclear and cytoplasmic extraction kit (Thermo Scientific, 78833) was used for the separation and preparation of cytoplasmic and nuclear fractions/extracts following the manufacturer's protocol. Briefly, after cells were pelleted, the supernatants were discarded, 200µl of ice-cold cytoplasmic extraction reagent I (CER I) was added to each pellet, vortexed and incubated on ice for 10 minutes. Then, 11µl of ice-cold cytoplasmic extraction reagent II (CER II) was added to each tube, vortexed, incubated on ice for 1 minute, and centrifuged for 5 minutes at 16,100xg rcf. The supernatants containing the cytoplasmic extract were transferred to pre-chilled 1.5ml microfuge tubes and kept on ice until transfer from BSL3 facility to a BSL2 lab. The remaining pellets were resuspended with 100µl of ice-cold nuclear extraction reagent (NER), vortexed, incubated on ice for 40 minutes with vortexing every 10 minutes, and centrifuged for 10 minutes at 16,100xg rcf to lyse the nuclei. The supernatants, containing the nuclear extract, were transferred to pre-chilled 1.5ml microfuge tubes, and kept on ice until transfer from the BSL3 facility to BSL2. The extracts were either used immediately or stored at -80^0C until use.

PTBP1 knockdown

To knockdown the expression of PTBP1 we used siRNAs and the jetPRIME^{R} transfection reagent (Polyplus, 101000046). Briefly, the day before transfection, HeLa and 293T cell lines were individually plated on poly-D-lysine hydrobromide coated 6-well plates (Greiner Bio-One, 657165) in concentrations of 125,000 cells/ml. The following day 50nM of siRNA (Millipore Sigma, NM_002819) was diluted in 200µl of jetPRIME^{R} buffer, and 4µl of jetPRIME^{R} reagent was added to the mix. After 10 minutes at room temperature, the transfection mixture was added to the media of the plates with the seeded cells. The transfection step was repeated once more 24 hours later (to ensure efficient knockdown) and incubated for 48 hours at 37^{0}C.

Protein extraction

Semi-confluent cells in 6-well plates were washed with 1ml of pre-warmed 1X PBS, harvested by adding 500µl of 0.25% trypsin (1X) solution, and incubated at 37^{0}C for 3-5 minutes until cells detached from the bottom of the flask. Trypsin was inactivated by adding an equal volume of pre-warmed culture media and the cell clumps were disaggregated by gently pipetting up and down several times with a 10ml pipet. Samples were collected in a 15ml conical tube and centrifuged at 175xg rcf for 10 minutes. Pelleted cells were resuspended with 1ml of 1X PBS, transferred to a 1.5ml microfuge tube, and centrifuged for 5 minutes at 16,100xg rcf at 4^{0}C in a microcentrifuge. Cell pellets were resuspended in 750µl of ice-cold LS-RIPA buffer supplemented with one caplet of protease inhibitor (cOmplete^{TM}, Mini, EDTA-free protease inhibitor cocktail, Roche, 11836170001) per 10ml of LS-RIPA buffer and 0.1 M

PMSF or phenylmethylsulfonyl fluoride (20µl per 10ml of LS-RIPA buffer). The suspension was sonicated on ice by applying 5 rounds of a 10 second pulse / 2 minutes rest, at power 6 (Fisher Scientific, Sonic Dismembrator, Model 100). After sonication, the samples were centrifuged at 16,100xg rcf in a microcentrifuge for 10 minutes at 4^0C. The supernatant was transferred to a new 1.5ml microcentrifuge tube and the total protein concentration was determined by a bicinchoninic acid (BCA) assay (Pierce™ BCA protein Assay Kit, Thermo Scientific™, 23225) following the manufacturer's instructions. Briefly, 200µl of BCA mix was added to each tube containing 10 µl of total protein (or a standard) and the tubes were incubated at 60^0C for 5 minutes. A standard curve and total protein concentrations were determined by loading 2µl of each sample in a NanoDrop 2000c spectrophotometer (Thermo Scientific) and comparing the values obtained in the test samples to the values obtained for known protein standards.

Western blots

In a typical experiment, a sample volume containing 20µg of total protein per lane was mixed with an equal volume of 2X Laemmli sample buffer (Bio-Rad, 161-0737) and denatured at 100^0C for 5 minutes. Samples were loaded on a 10% polyacrylamide gel along with a molecular weight marker (Thermo Scientific, PageRuler prestained protein ladder, 26616). Proteins that were separated by SDS-PAGE were then transferred to nitrocellulose membranes (Immobilon®-P transfer membrane, IPVH00010) using a Trans-Blot SD Semi-Dry Transfer cell apparatus (Bio-Rad). Membranes were blocked with 5% low-fat milk in 1X TBST (10mM Tris-Cl pH 8.0, 150mM NaCl, 1% Tween-20) by incubation with rotation for 1 hour at room temperature. The blocking solution was

replaced with a dilution of the indicated primary antibody (see Table 3) in 1X TBST and incubated overnight at 4^0C with rotation. Membranes were washed three times with 1X TBST and incubated with the appropriate secondary HRP-conjugated antibody for 1 hour at room temperature. SuperSignal™ West Pico PLUS chemiluminescent substrate (Thermo Scientific, 34580) was used for visualization with Azure Sapphire biomolecular imager (azure biosystems) and Sapphire Azure biosystems software.

Table 3: Antibodies used in this study

Primary antibody	Information	Dilution	Secondary antibody	Information	Dilution
Normal Mouse IgG	Millipore, 12-371	1:10,000			1:10,000
PTBP1	Invitrogen, 32-4800	1:10,000	Goat anti mouse IgG-HRP	Abcam, ab97023	1:10,000
GAPDH	Millipore, MAB374	1:20,000	Goat anti mouse IgG-HRP	Abcam, ab97023	1:10,000
A/C Lamin	Thermo Fisher, MA535284	1:10,000	Mouse anti rabbit IgG-HRP	Santa Cruz, SC-2357	1:10,000
β-Tubulin	Cell Signaling Technology, 2146	1:5,000	Mouse anti rabbit IgG-HRP	Santa Cruz, SC-2357	1:10,000
m^7G	MBL, RN016M	1:10,000			1:10,000
m^6A	Millipore, MABE1006	1: 10,000	Goat anti mouse IgG-HRP	Abcam, ab97023	1:10,000
PCIF1	Bethyl Laboratories, A304-711A	1:5,000	Mouse anti rabbit IgG-HRP	Santa Cruz, SC-2357	

Plaque assay

Vero cells were seeded at $1.5x10^5$ cells per well in 12-well plates (Greiner Bio-One, 665180), using DMEM supplemented with 10% FBS, 100 U/mL penicillin and 100 mg/mL streptomycin. Cultures were incubated at 37^0C in a humidified atmosphere with 5% CO_2 for 24 hours before infection. Serially diluted virus was allowed to adsorption onto confluent cell monolayers (ZIKV for 2 hours; SARS-CoV-2 for 1 hour). Following

adsorption, media was aspirated, and the infected monolayers were covered with an overlay media containing agarose at 0.5% final concentration to prevent uncontrolled viral spreading due to mechanical or convectional flow of the liquid media during viral propagation. Plates were incubated for 96 hours (ZIKV) or 48 hours (SARS-CoV-2) and followed our standard plaque assay protocol outlined above using crystal violet, For SARS-CoV-2 infected plates, all steps were performed in BSL3 setup.

Fragmentation and double pulldown for m^{6}A assays

Fragmentation

Using small tubes designed to be used in polymerase chain reaction, known as PCR tubes, 18µl of 1µg/µl RNA per reaction were mixed with 2µl of 10X RNA fragmentation buffer (NEBNext Magnesium RNA fragmentation kit, NEB, E6150S) and incubated for 3 minutes at 94^{0}C. The tubes were placed on ice, 2µl of stop solution were added and then the tubes were placed at -80^{0}C. After fragmentation, the tubes were centrifugated and the RNA was ethanol precipitated and resuspended in 18µl of RNAse-free water. Samples were stored at -80^{0}C until use.

Pull-down 1: RNA cap-pulldown

Five µg of fragmented RNA was mixed with 230µl LS-RIPA buffer, 3µl RiboLock, and 5µg of anti-cap (anti-m^{7}G) antibody (MBL, Medical & Biological Laboratories) or anti-normal mouse IgG (Millipore) antibody. The mixture was incubated for 2 hours at 4^{0}C with rotation. Twenty-five µl of protein G magnetic beads were pre-washed with 250µl LS-RIPA buffer (supplemented with protease inhibitor), separated using a magnetic stand, resuspended with 25µl of supplemented LS-RIPA buffer, and added to

the sample tubes. The mix, sample-antibody-magnetic beads was incubated for 1 hour at 4^0C, with rotation. Protein G beads were separated with a magnetic stand and the supernatants were collected. The magnetic beads were washed 3 times with 600µl LS-RIPA buffer and once with 600µl of 1X PBST (1X PBS, %0.1 Tween®20 detergent). The magnetic beads were then resuspended in 100µl of TEDS (10mM Tris-Cl, 1mM EDTA, %1 Sodium cholate, %0.1 NP-40) buffer containing 1mM DTT and incubated for 45 minutes at 70^0C to release the captured RNA from the beads. After incubation, 300µl of TRIzol® and 80µl chloroform were added, samples were vortexed, and centrifuged at 16,100xg rcf, 4^0C for 15 minutes in a microcentrifuge. The aqueous upper layer was transferred to 1.5ml centrifuge tube containing 1.5µl glycogen and 350µl isopropanol and pelleted in a microcentrifuge at 16,100xg rcf for 30 minutes at 4^0C. The pelleted RNA fragments were rinsed with 150µl of 70% ethanol and centrifuged at 16,100xg rcf, 4^0C for 15 minutes in a microcentrifuge. Supernatants were discarded and the pellets were air dried and resuspended in 10µl of water. One µl was used for reverse transcription and ddPCR to quantify SARS-CoV2 capped fragments recovered.

Pull-down 2: Capped-RNA: m^{6}A-pulldown

To proceed with the second pulldown, the previously resuspended cap antibody immunoprecipitated pellets were mixed with 230µl of supplemented LS-RIPA buffer, 3µl of RiboLock, and 2µg of anti-m^{6}A antibody (Millipore) followed by 2 hours incubation with rotation at 4^0C. Protein G magnetic beads were washed and added to the reaction as described above for the first pulldown. The protein G beads were separated from the mixture with a magnetic stand, supernatants were collected, and the beads were

washed 3 times with 600µl LS-RIPA buffer. The beads were resuspended in 100µl of TEDS with 1mM DTT, incubated for 45 minutes at 70^0C, and then transferred to 1.5ml microfuge tubes containing 300µl of TRIzol®. To isolate the RNA, 80µl of chloroform were added, vortexed and centrifuged at 16,100xg rcf, 4^0C for 15 minutes in a microcentrifuge. The upper layers were transferred to 1.5ml microfuge tubes containing 2µl glycogen, 99µl of 10M ammonium acetate, and 750µl of 100% ethanol. The samples were incubated for 5 minutes at -80^0C and centrifuged at 16,100xg rcf 4^0C for 30 minutes. The supernatants were discarded, and the pellets were washed with 150µl of 70% ethanol. After centrifugation at 16,100xg rcf for 5 minutes, the supernatants were discarded, and the pellets were air-dried. Finally, the pellets were resuspended in 5µl TE (10mM Tris-Cl, 1mM EDTA, pH 8.0) buffer, we used these RNAs to perform reverse transcription and ddPCR.

Semi-quantitative PCR

All reactions were assembled by mixing the reaction components (see table 4) in a tube on ice.

Table 4: Semi-quantitative PCR components

Component	Volume per reaction (µl)	Final concentration
5X Q5 reaction buffer	5	1X
10mM dNTPs	0.5	200 µM
Forward primer	1.25	0.5 µM
Reverse primer	1.25	0.5 µM
DNA template	1	25 ng
Q5 High-fidelity DNA polymerase	0.25	0.02U/µl
RNase/DNase-free water	15.75	-
Total volume	25	-

Mix the components by tapping the tubes and give a quick spin to collect all the liquid to the bottom of the tubes. Transfer the PCR tubes to the thermocycler and procede to run the PCR protocol as follow:

Table 5: semi-quantitative PCR cycling conditions.

Cycling step	Temperature (°C)	Time
Denaturation	98	30 sec.
30 cycles	98	10 sec.
	55	10 sec.
	72	30 sec.
Final extension	72	2min.
Hold	4	infinite

Agarose gels

Some PCR products were evaluated by agarose gel electrophoresis in a semi-quantitative fashion. The DNA samples were prepared by mixing 25µl of each PCR product with 5µl of 6X TriTrack DNA loading dye (Thermo Scientific, R1161) and loaded onto 1% agarose gels in 1X TAE buffer (40mMTris-acetate, 1mM EDTA) to resolve the samples. GeneRuler 1kb Plus DNA ladder (Thermo Scientific, SM1333) was used as a size marker. Gels were imaged using Gel Doc™ EZ Imager (Bio-Rad) and Image Lab software.

Digital droplet PCR (ddPCR) analyses

All kit components were warmed to room temperature, homogenized by vortexing, and clarified by a quick spin in a microcentrifuge. We used 1µl and 4µl from the first and second pulldown (as described above in the cap/m^{6}A pulldown strategy) respectively. The reaction mixes were prepared according to Table 6. For droplet generation, 20µl of each reaction mix were loaded per well of a DG8™ cartridge for the QX200™/QX100™ droplet generator (Bio-Rad, 1864008) followed by the addition of 70µl of QX200 droplet generation oil for EvaGreen® (Bio-Rad, 1864005 or 006) into the wells. Cartridges were placed into the automated droplet generator. After droplet generation, plates containing ddPCR droplets were removed, sealed using the PX1 PRC plate sealer, and subjected to thermal cycling following the conditions showed in Table 7. The QX200 droplet reader was used to read the droplets.

Table 6: Digital Droplet PCR Components

Component	Volume per reaction (µl)	Final concentration
2X QX200™ ddPCR™ EvaGreen® Supermix	10	1X
Forward primer	1	125 nM
Reverse primer	1	125 nM
DNA template	1	2.5 ng
RNase/DNase-free water	7	-
Total volume	20	-

Table 7: Digital Droplet PCR cycling conditions

Cycling step	Temperature (^{0}C)	Time	Ramp rate	Number of cycles
Enzyme activation	95	5 min.	2^{0}C/sec.	1
Denaturation	95	30 sec.		40
Annealing/extension	60	1 min.		40
Signal stabilization	4	5 min.		1
	90	5 min.		1
Hold	4	infinite		1

RESULTS

SARS-CoV-2 leader RNA can interact with the cellular alternative RNA splicing factor PTBP1

Polypyrimidine tract-binding protein 1 (PTBP1) is an important splicing factor that is expressed in most human cell types[233]. While previous studies showed that the leader RNA, a ~75 base region at the 5' end, from various betacoronaviruses can interact with PTBP1[88], it is unknown if SARS-CoV-2 leader RNA is able to interact with the cellular splicing factor. We hypothesize that in addition to perhaps using PTBP1 to directly promote viral replication, the binding and sequestration of the factor by abundant SARS-CoV-2 RNAs (or other betacoronavirus RNAs) could also interfere with the normal function of the PTBP1 protein in splicing. This could represent a novel molecular mechanism that contributes to pathogenesis. Therefore, we decided to explore whether the abundant SARS-CoV-2 leader RNA could indeed interact with the cellular PTBP1 protein.

Using the RBPmap web server we bioinformatically investigated whether the PTBP1 RNA consensus binding motif, CUCUCU, was present in the leader RNA of SARS-CoV-2. As shown in Figure 3A, SARS-CoV-2 leader RNA possesses two motifs with five-out-of-six matches to the consensus PTBP1 binding sequence. To definitively demonstrate that PTBP1 could indeed bind to these motifs, we first validated a PTBP1 antibody for immunoprecipitation assays. As shown in Figure 3B, anti-PTBP1 antibody (α-PTBP1) effectively and specifically immunoprecipitated PTBP1 from HeLa total cell extracts compared to a control IgG antibody. Finally, we performed a UV crosslinking

assay combined with α-PTBP1 immunoprecipitation to directly demonstrate a specific interaction between the SARS-CoV-2 leader RNA and PTBP1 protein. We incubated radiolabeled leader RNA and a similarly sized control RNA derived from the pGEM4 polylinker with HeLa cytoplasmic extracts followed by irradiation with UV light to covalently cross-linked closely associated proteins to the RNA. Following RNAse A treatment to leave only small radioactive RNA oligomers attached to cross-linked proteins, we analyzed the samples on a 10% SDS polyacrylamide gel before or after immunoprecipitation using α-PTBP1 or control IgG antibodies. As seen in Figure 3C, while the control RNA failed to cross-link to PTBP1, the SARS-CoV-2 leader RNA specifically cross-linked to a ~55-57 kD band that was immunoprecipitated with anti-PTBP1 antibodies. Therefore, we conclude that the SARS-CoV-2 leader RNA is indeed capable of interacting with the cellular PTBP1 protein. These findings suggest that SARS-CoV-2 infection in general might have a large impact on PTBP1-regulated RNA splicing and possibly other PTBP1-regulated processes in infected cells.

Alternative splicing is a process during gene expression that allows for the selection of different combinations of splice sites within a pre-mRNA producing multiple protein isoforms from a single gene[234]. PTBP1 has been shown to regulate the alternative splicing of many mRNAs[235–237]. In this study, we focused on the analysis of the alternative splicing of four PTBP1-regulated genes during SARS-CoV-2 infection due their possible contributions to the biology of infection.

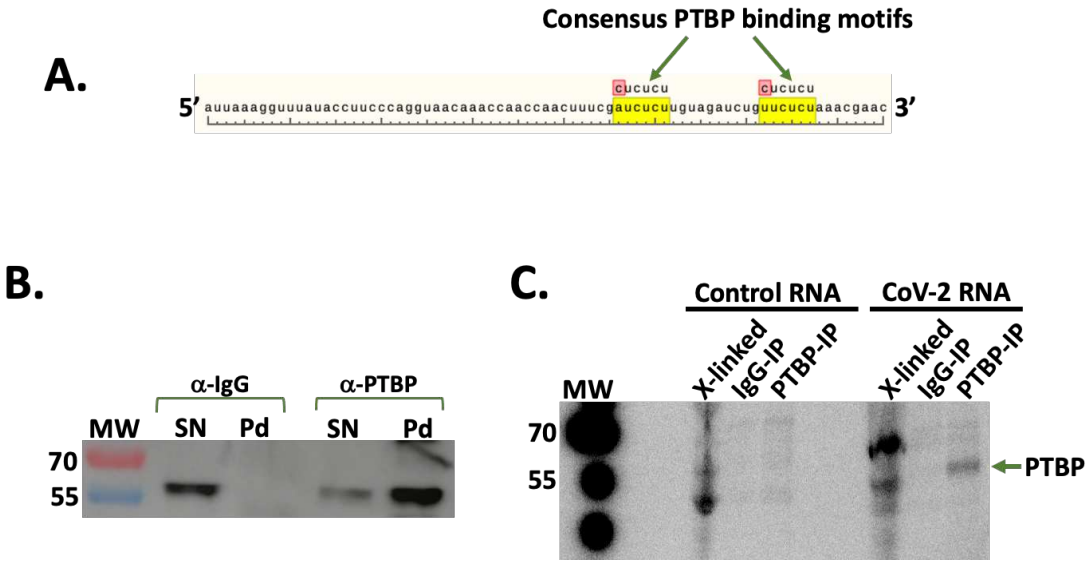

Figure 3. The SARS-CoV-2 leader RNA can interact with the cellular PTBP1 protein. *Panel A: The RBPmap software program (http://rbpmap.technion.ac.il/) indicates that the SARS-CoV-2 leader RNA contains two near-consensus CUCUCU PTBP1 binding motifs. Panel B: total cellular protein extracts from HeLa cells were incubated with anti-IgG antibody (α-IgG) or anti-PTBP1 antibody (α-PTBP1). Western blot shows the detection of PTBP1 in cellular extracts after specific PTBP1 immunoprecipitation using α-PTBP1 in the immunoprecipitated (IP) fraction/lanes, while the IP fraction/lanes from unspecific immunoprecipitation using α-IgG did not show PTBP1 presence.SN lanes indicate the supernatant of the immunoprecipitation reactions and the numbers on the left indicate the molecular weight (MW) of marker proteins in kD. Panel C: A control RNA derived from the pGEM4 polylinker (Control RNA lanes) and the SARS-CoV-2 RNA (CoV-2 RNA lanes) were incubated with HeLa cytoplasmic extract, and bound proteins were cross-linked to the RNAs using UV light. RNA-protein complexes were treated with RNAse A to leave a short cross-linked radiolabeled RNA oligomer. Then, the samples were electrophoresed on a 10% SDS gel either before (X-linked lanes) or after immunoprecipitation using control IgG antibodies (IgG-IP lanes) or PTBP1-specific antibodies (PTBP1-IP lanes). The green arrow indicates the ~55-57kD PTBP1 cross-linked protein. Molecular weight markers (in kD) are labeled for the MW lane on the left.*

PTBP1-regulated gene FMNL2 is mis-spliced during SARS-CoV-2 infection

FMNL2 (Formin Like 2) protein is required for the regulation of actin filament dynamics, the organization of the cytoskeleton, and the regulation of cell morphology[238,239]. Recently, it was demonstrated that SARS-CoV-2 infection causes alterations in the actin cytoskeleton leading to changes in cellular shape and the formation of longer protrusions in cells[240–242]. The modification of the host cell's actin

cytoskeleton is a conserved mechanism observed in coronavirus and other virus infections, suggesting its importance for infection efficiency[240,243,244]. Importantly for this project, alternative splicing of the FMNL2 mRNA has been shown to be regulated by PTBP1[245].

To determine if the FMNL2 mRNA demonstrates dysregulated splicing during SARS-CoV-2 infection, we generated PCR primers pairs to span a region of the FMNL2 pre-mRNA (exons 21-27) whose splicing is regulated by PTBP1. This portion of the mRNA obtained from uninfected or SARS-CoV-2-infected Calu3 cells was amplified using RT-PCR. As shown in Figure 4A, we detected slight alterations in the migration pattern of the ~720bp PCR product of the FMNL2 targeted region as well as the appearance of a large ~1,500bp product, which were consistent with possible alternative splicing. To investigate whether there was indeed dysregulated alternative splicing in this region during SARS-CoV-2 infection, we sequenced RT-PCR products from two independent uninfected or 6 independent SARS-CoV-2 infected Calu3 cultures. As seen in Figure 4B, we identified retention of a portion of the intron between exons 26 and 27 in all FMNL2 mRNAs from infected cells, which was never observed in uninfected samples. Curiously, the observed band of ~1500 bp in RT-PCR amplified products from infected cells in Figure 4A does not represent an alternative spliced product but rather represents the non-specific amplification of a portion of the SARS-CoV-2 S (Spike) gene. Why this region of the viral RNA was consistently amplified in our experiments is unclear as there is no significant homology noted to our FMNL2 primers. In summary, our results indicate that infection with SARS-CoV-2 affects cellular

splicing by causing the activation of cryptic intronic splice sites, resulting in partial intron retention in the PTBP1-regulated FMNL2 mRNA.

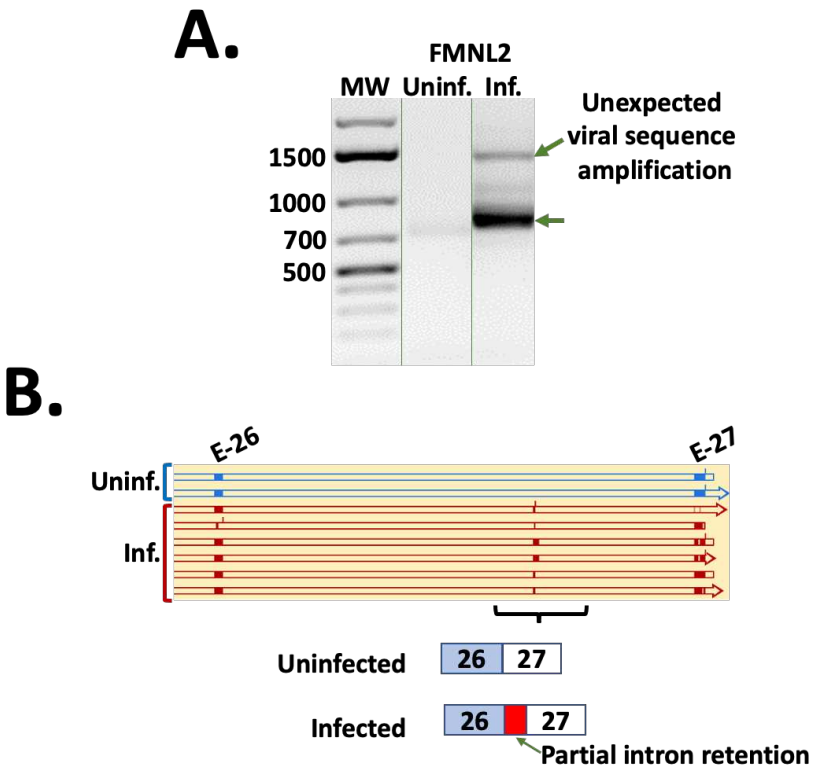

Figure 4. SARS-CoV-2 infection dysregulates the splicing of the PTBP1-regulated FMNL2 pre-mRNA. *Panel A. Calu3 cells were mock-infected (Uninf. lanes) or infected for 48 hrs with SARS-CoV-2 (Inf. lanes). Total RNA was obtained and analyzed by RT-PCR using primers specific for exons 21 and 27. The green arrows indicate the mis-spliced band of interest (lower arrow) or a non-specifically amplified piece of SARS-CoV-2 viral RNA (upper arrow). Molecular weight markers (MW lane) are shown on the left. Panel B. The ~750bp PCR product amplified from uninfected or infected cells was extracted from agarose gels and analyzed by Sanger sequencing. Results diagram the consistent retention of a partial intron segment between exons 26 and 27in SARS-CoV-2-infected cells.*

TPM1, another PTBP1-regulated gene, is also mis-spliced during SARS-CoV-2 infection

To determine whether the dysregulation of the PTBP1 regulated FMNL2 mRNA was an isolated event, we extended our observation of SARS-CoV-2-induced mis-splicing to another PTBP1-regulated cellular mRNA: TPM1 (Tropomyosin1). TPM1 encodes an actin-binding protein that plays a role regulating the contractile system of striated and smooth muscles and the cytoskeleton coordination of non-muscle cells[246]. As noted above for FMNL2, cytoskeletal rearrangements may play a key role in many viral infections. Furthermore, altered TPM1 expression/splicing may be important because myocardial and vascular injuries related to SARS-CoV-2 infections are the principal cause of acute cardiac injury associated with COVID-19[30]. To analyze the splicing pattern of a PTBP1-regulated region of the TPM1 pre-mRNA in infected and uninfected Calu3 cells by RT-PCR, we generated TPM1-specific forward and reverse PCR primers spanning exons 2-8. As shown in Figure 5A, we observed that there was a slight increase in size of the ~670 bp PCR product using total RNA from SARS-CoV-2 infected cells as compared to the product amplified from uninfected cells, as well as the appearance of a novel, infection-specific ~1,500 bp product. PCR products were cloned and sequenced to provide a detailed analysis of SARS-CoV-2-induced dysregulated splicing in this region. As diagrammed in Figure 5B, infecting cells with SARS-CoV-2 (8 independent samples) resulted in the reproducible loss of exon 6 in the TPM1 mRNA and the inclusion of a portion of the intron between exons 6 and 7 due to the activation of cryptic splice sites never seen with total RNA from uninfected cells (4 independent samples shown). This novel inserted region represents exon 6b which is occasionally observed in the alternative splicing of the TPM1 pre-mRNA in other tissues (https://omim.org/entry/191010). We also observed non-specific amplification by the

primers of another ~1,500 base portion of the SARS-CoV-2 genomic RNA like what we observed with FMNL2 in Figure 4. This time, however, the unexplainable amplified product was from the N (nucleocapsid) gene (and once again no sequence similarity to the primers used was noted). These data, along with the similar observation we made with the FMNL2 primers noted in Figure 4A, suggest some promiscuity of regions of the coronaviral genome for nucleic acid interactions and possibly recombination. However, most importantly, we conclude from our data that infection with SARS-CoV-2 affects exon skipping and intron inclusion in the PTBP1-regulated portions of the TPM1 pre-mRNA.

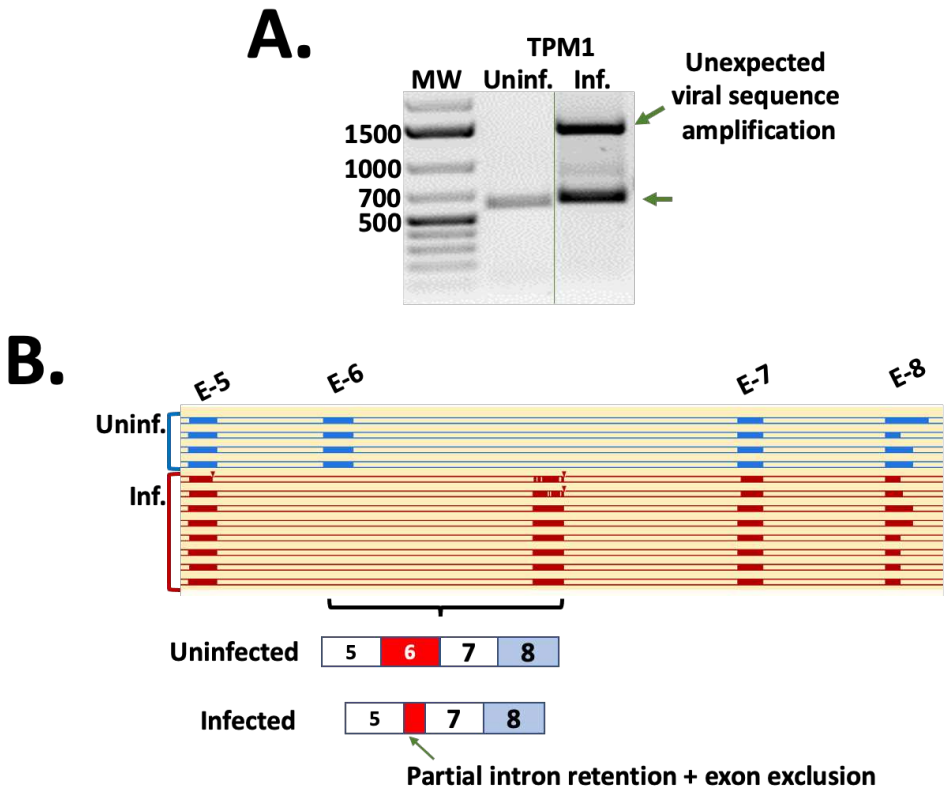

Figure 5. SARS-CoV-2 infection dysregulates the splicing of the PTBP1-regulated TPM1 pre-mRNA. *Panel A. Calu3 cells were mock-infected (Uninf. Lanes) or infected for 48 hrs with SARS-CoV-2 (Inf. Lanes). Total RNA was obtained and analyzed by RT-PCR using primers specific for exons 2 and 8. The green arrows indicate the mis-spliced band of interest (lower*

arrow) or a non-specifically amplified piece of SARS-CoV-2 viral RNA (upper arrow). Molecular weight markers (MW lane) are shown on the left. Panel B. The ~750bp PCR product amplified from uninfected or infected cells was extracted from the agarose gel and analyzed by Sanger sequencing. Results diagram the retention of a partial intron segment between exons 6 and 7 and the exclusion of exon 6 in infected cells.

ACTN4 and TEAD3 PTBP1-regulated gene, shown altered splicing patterns during SARS-CoV-2 infection

To further generalize the effect of SARS-CoV-2 infection on the splicing of PTBP1-regulated pre-mRNAs, we analyzed the splicing patterns of PTBP1-regulated the cellular ACTN4 and TEAD3 mRNAs. The protein encoded by ACTN4, alpha-actinin-4, is a member of the spectrin superfamily[247], it is expressed in non-muscle cells, and is involved in cellular motility and adhesion[248,249]. On the other hand, the transcriptional enhanced associated domain (TEAD) conforms a family of transcription factors (TEAD1-4) expressed in most human tissues[250] regulating transcription.

Following the same approach that we used to analyze splicing of the FMNL2 and TPM1 mRNAs, we generated sets of PCR primers specific for PTBP1 regulated regions of the ACTN4 (exons 17-20) and TEAD3 (exons 2-9) pre mRNAs and analyzed overall splicing patterns in infected and uninfected Calu3 cells by RT-PCR. As seen in Figure 6A, we observed the appearance of a larger band as well as a low amount of a shorter PCR product in total RNA from SARS-CoV-2 infected cells as compared to uninfected cells for ACTN4. Interestingly, we observed at least four novel bands in the PCR products of total RNA from SARS-CoV-2 infected cells compared to uninfected cells for the TEAD3 mRNA (Figure 6B). From these data, we conclude that infection with SARS-CoV-2 likely also affects the splicing pattern of these PTBP1-regulated pre-mRNAs.

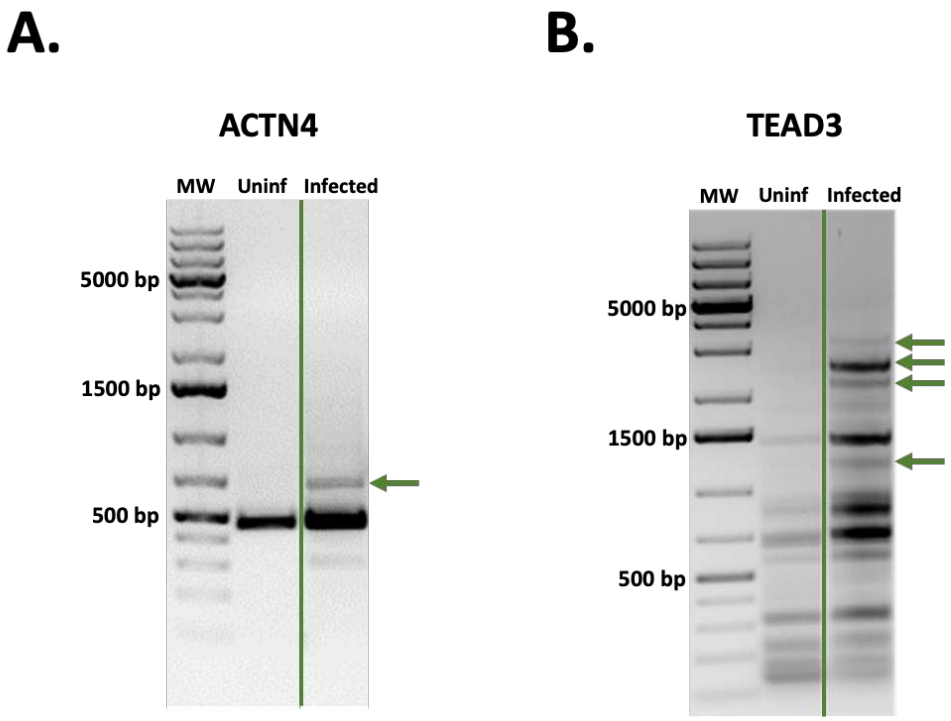

Figure 6. SARS-CoV-2 infection dysregulates the splicing patterns of PTBP1-regulated pre-mRNAs ACTN4 and TEAD3*. Panel A. Calu3 cells were mock-infected (Uninf. Lanes) or infected for 48 hrs with SARS-CoV-2 (Inf. Lanes). Total RNA was obtained and analyzed by RT-PCR using primers specific for exons 17 and 20 of the ACTN4 pre-mRNA. The green arrow indicates a potentially mis-spliced band of interest. Molecular weight markers (MW lane) are shown on the left. Panel B. Calu3 cells were mock-infected (Uninf. Lanes) or infected for 48 hrs with SARS-CoV-2 (Inf. Lanes). Total RNA was obtained and analyzed by RT-PCR using primers specific for exons 2 and 9 of the TEAD3 mRNA. The green arrows indicate potentially mis-spliced bands of interest. Molecular weight markers (MW lane) are shown on the left.*

PTBP1 is retained in the cytoplasm of SARS-CoV-2 infected cells preventing its normal function

While PTBP1 functions mainly in regulating alternative splicing, the protein has also been implicated in multiple aspects of RNA metabolism in both the nucleus and in the cytoplasm of eukaryotic cells[75]. Consistent with this, PTBP1 is known to shuttle along with mRNAs out of the nucleus to the cytoplasm –and then be imported back into

the nuclear compartment[79]. Based on our *in vitro* observations reported using biochemical reconstitution assays and virally infected cells (Figures 3-6 above), we hypothesize that the abundant SARS-CoV-2 RNA leader region likely binds PTBP1 in the cytoplasm and may prohibit its return to the nucleus, consequently resulting in the observed dysregulation of the splicing of PTBP1-regulated pre-mRNAs seen in Figures 4-6. Thus, we hypothesize that we may observe an accumulation of PTBP1 in the cytoplasm of infected cells due to the influence of the PTBP1-SARS-CoV-2 leader interaction. To directly address our hypothesis, we extracted cytoplasmic and nuclear fractions from mock-infected or SARS-CoV-2 infected HeLa cells at 12, 24, and 48 hours post infection (hpi), followed by the detection of PTBP1 presence using our validated anti-PTBP1 antibody. As seen in Figure 7A and B, we detected a progressive redistribution of PTBP1 from the nucleus to the cytoplasm over the time course of infection. Notably, the relative levels of PTBP1 in the nucleus and cytoplasm did not vary during the time course in uninfected cells. Therefore, we conclude that PTBP1 progressively redistributes from the nucleus to the cytoplasm in SARS-CoV-2 infected cells, and that this redistribution is consistent with its interaction with the SARS-CoV-2 leader RNA. This redistribution of PTBP1 from the nucleus to the cytoplasm was observed decades ago with other betacoronavirus infections[88], suggesting that it may be conserved aspect of coronavirus-host interactions.

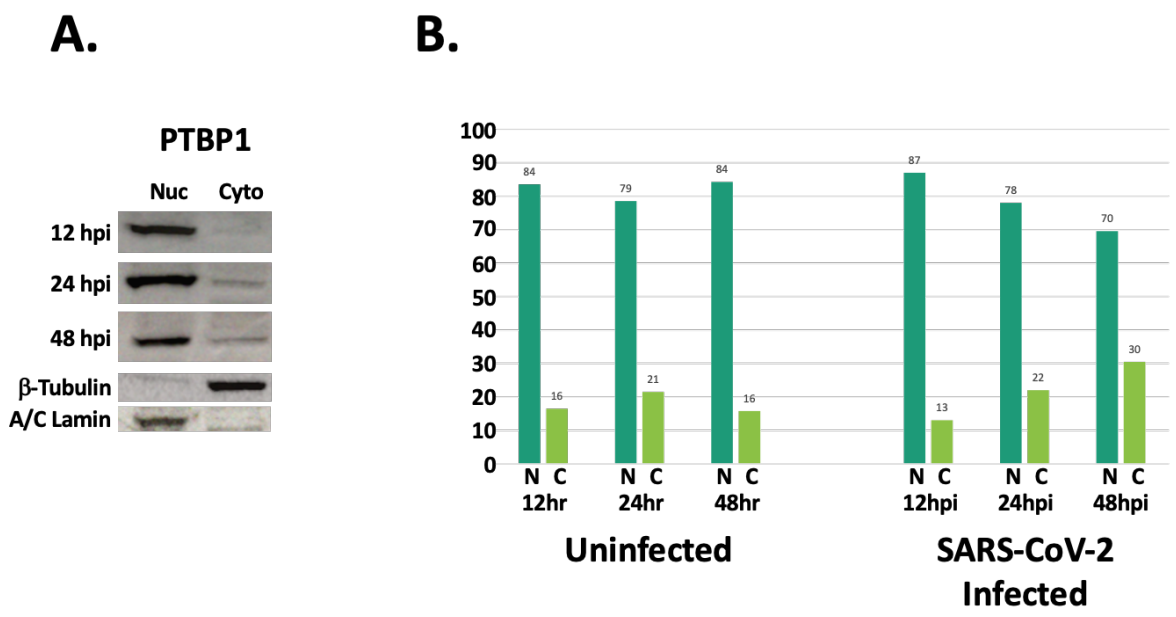

Figure 7. PTBP1 becomes increasingly cytoplasmic during SARS-CoV-2 infection. *Panel A. HeLa cells were infected with SARS-CoV-2 and cytoplasmic and nuclear fractions were obtained at the indicated time points post infection. The presence of PTBP1 in the fractions were analyzed by western blotting. We observed an increment of PTBP1 in the cytoplasmic fraction through the infection, the collection time are indicated to the left, β-Tubulin and A/C Lamin as cytoplasmic and nuclear markers respectively. Panel B: quantification of western blot from panel A, compared to the presence of PTBP1 in the cytoplasm and nucleus of uninfected cells.*

Knocking down PTBP1 and SARS-CoV-2 infection both influence the expression of TPM1 in a similar fashion

Our results on the interaction of PTBP1 with the SARS-CoV-2 leader RNA (Figure 3C) and the mis-splicing of PTBP1-regulated genes observed in Figures 4-6 are consistent with our hypothesis that PTBP1 is sequestered in infected cells and prevented from carrying out its normal function. Therefore, we wished to obtain additional data to suggest that PTBP1 function is disrupted in SARS-CoV-2 infected cells. To address this, we used small interfering RNAs (siRNAs) to knockdown PTBP1 expression (Figure 8A) and analyzed the impact of low functional levels of PTBP1 on

the cell. Curiously, TPM1 was expressed at very low levels in uninfected HeLa or 293T cells as seen by semi-quantitative RT-PCR assays (Figure 8B). However, when PTBP1 expression was knocked down using siRNA, the expression of TPM1 in both cell lines was activated (Figure 8B). Interestingly, as seen in Figure 9, TPM1 expression was also activated when HeLa or 293T cells were infected with SARS-CoV-2. TPM1 expression was also dramatically increased by SARS-CoV-2 infection of Calu3 cells which naturally produce higher baseline levels of the mRNA in uninfected cells. Therefore, we conclude that SARS-CoV-2 infection mimics PTBP1 knockdown by inducing the expression of TPM1 in three independent cell lines. These data provide additional evidence indicating PTBP1 activity is likely impaired during SARS-CoV-2 infection.

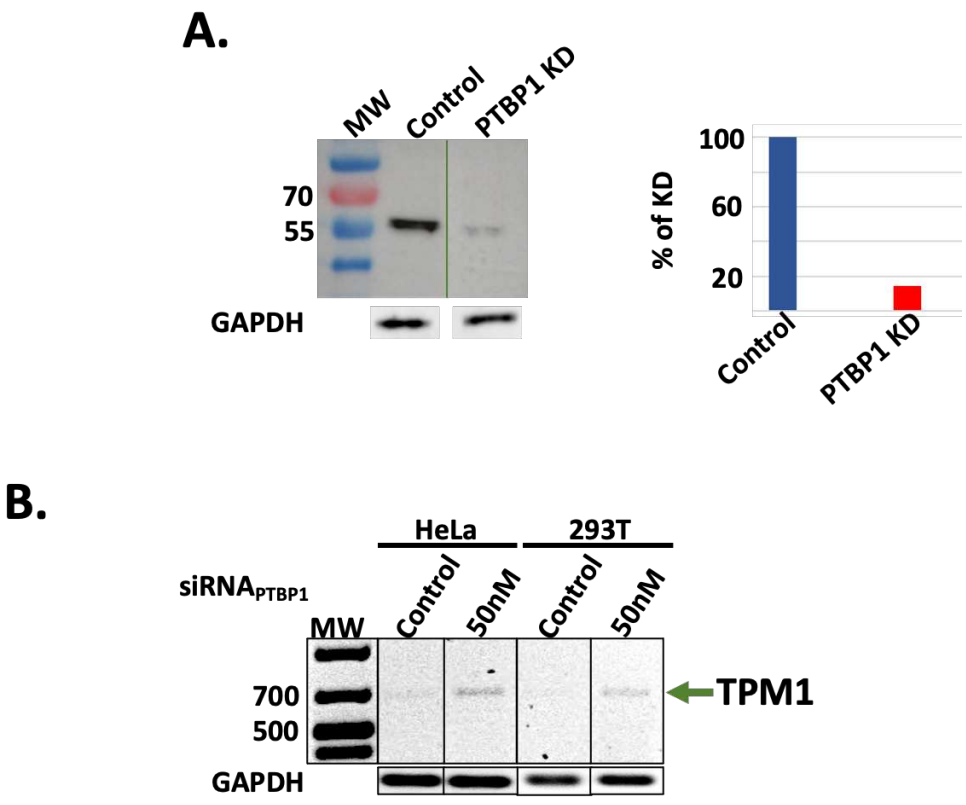

Figure 8. PTBP1 knockdown in HeLa and 293T cells influences TPM1 gene expression. *Panel A. The gel on the left is a western blot using anti-PTBP1 antibodies on total protein obtained from wild type (Control lane) or PTBP1 siRNA knock down (PTBP1 kD lane) cells; the quantification of this gel is shown on the right. Panel B. HeLa or 293T cells were transfected with the indicated amount of siRNA to knock down PTBP1 expression. Total RNA was obtained and analyzed by RT-PCR using TPM1-specific primers that amplified exons 2-9. RT-PCR products were analyzed on a 1% agarose gel. Molecular weight (MW) markers are shown on the on the left. GAPDH levels were determined by RT-PCR as a control for equivalent levels of starting RNA and are shown in the lanes below the main gel.*

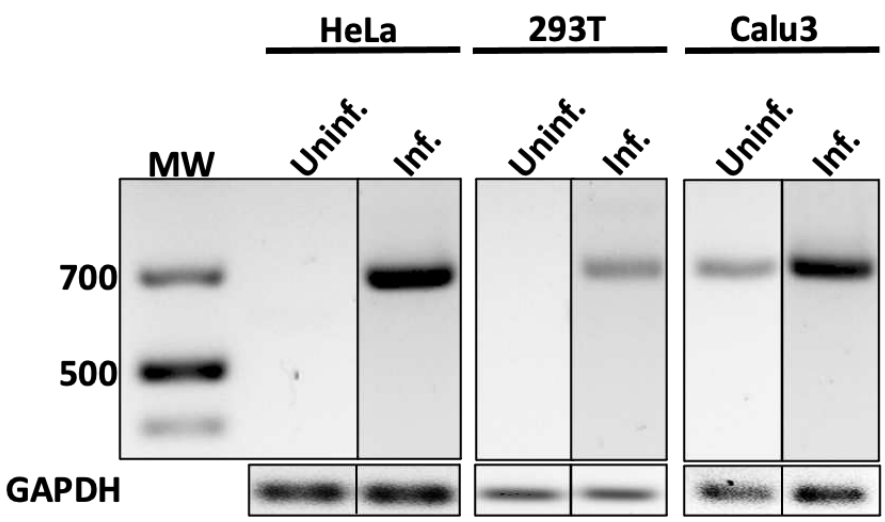

Figure 9. SARS-CoV-2 infection influences TPM1 gene expression in HeLa, 293T, and Calu3 cells, mimicking the results obtained when PTBP1 expression is knocked down. *The expression of TPM1 was evaluated in HeLa, 293T, or Calu3 cells following mock infection (Uninf. lane) or infection with SARS-CoV-2 at MOI 3 (Inf. lane) for 48 hours. Total RNA was obtained and analyzed by RT-PCR using TPM1-specific primers that amplified exons 2-9. RT-PCR products were analyzed on a 1% agarose gel. Molecular weight (MW) markers are shown in the lane on the left. GAPDH levels were determined by RT-PCR as a control for equivalent levels of starting RNA and are shown in the lanes below the main gel.*

SARS-CoV-2 uses the cellular PCIF1 to methylate the 5' terminal fragments of its RNA

Cellular mRNAs present different nucleotide modifications that regulate their fate in the cell[251]. Two common nucleotide modifications in mRNAs are an internal N^6-methyladenosine (m^6A)[252] and an N^6,2'-O-dimethyladenosine (m^6A_m) found at the cap proximal first encoded nucleotide[174]. All cellular mRNAs that have adenosine as first encoded nucleotide contain an N6 methylation mediated by PCIF1 (Phosphorylated CTD Interacting Factor 1)[229]. SARS-CoV-2 mRNAs also begin with an adenosine at the first position[3], but no RNA virus to date appears to encode an identifiable m^6A modifying enzyme[25]. Interestingly, methylations at the first nucleotide can play a major role in

differentiating ‘self’ versus ‘non-self’ mRNAs in the host cell [253] [192]. We hypothesize; therefore, that SARS-CoV-2 may have uncovered a way to usurp the cellular machinery to incorporate the N6 methylation portion of the m^6A_m modification in the 5’ terminal region of its mRNAs to make them look as ‘self’ as possible to establish a highly productive infection. The goal of our study is to lay a foundation for gaining novel insights into a growing area of viral RNA epigenetics and identify a potential avenue for broad anti-coronaviral therapeutic intervention at a very early step in virus gene expression/host interaction via disruption of viral m^6A_m formation.

m^6A modifications are present in SARS-CoV-2 transcripts

Our first goal was to determine if m^6A modifications occurred at all on SARS-CoV-2 RNAs. We infected African green monkey kidney cells (Vero) with SARS-CoV-2 virus and obtained total RNA over a time course of the infection. RNAs containing an m^6A modification were immunoprecipitated using an anti-m^6A antibody[254–256]. As seen in Figure 10, SARS-CoV-2 mRNAs clearly contain m^6A modified adenosines as viral RNAs were precipitated using the anti-m^6A antibody but not by control IgG antisera. Therefore, we conclude that SARS-CoV-2 RNAs can be added to the growing list of viral transcripts that are m^6A modified during infections[208].

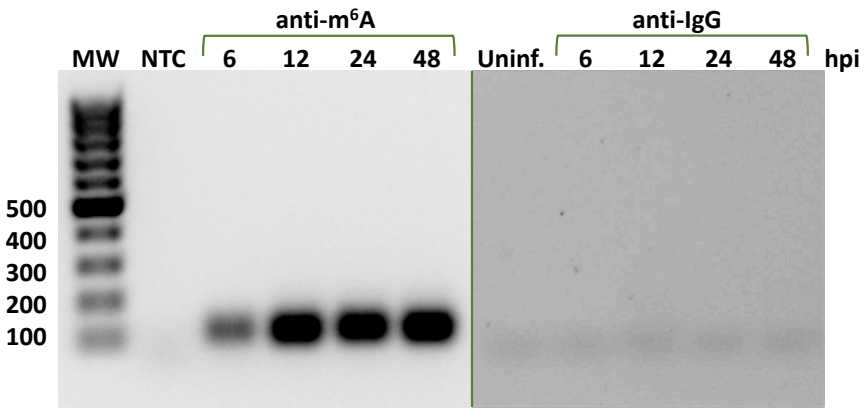

Figure 10. Adenosines of SARS-CoV-2 transcripts are methylated at the N^6 position (m^6A). *Vero cells were infected with SARS-CoV-2 at MOI 5. Total RNA was obtained at 6, 12, 24, and 48 hours post infection (hpi), and immunoprecipitated with anti-m^6A or anti-IgG antibodies as indicated at the top of the gel. The immunoprecipitation products were analyzed by RT-PCR using SARS-CoV-2 specific primers that amplified the viral 5' leader sequence. Results after electrophoresis of the RT-PCR products on a 1% agarose gel are shown with molecular weight (MW) markers loaded on the left. NTC lanes indicate PCR reactions performed with a 'No Template Control' and the Uninf. lane refers to reactions run using total RNA from uninfected Vero cells.*

An m^6A modification is present in the cap-proximal region of SARS-CoV-2 transcripts

Knowing that (1) the SARS-CoV-2 transcripts present m^6A modification and (2) that we can effectively detect it, our next step was to determine if the viral RNAs contain an m^6A modification on the cap proximal adenosine. To achieve this goal, we opted to use an RNA fragmentation, dual-immunoprecipitation approach that is outlined in Figure 11. Total RNA was obtained at different times post infection from SARS-CoV-2 infected Vero cells and fragmented to ~200 base pieces using the NEBNext magnesium RNA fragmentation module. Next, two successive rounds of immunoprecipitation were performed to first isolate 5' capped terminal RNA fragments using the anti-m^7G cap antibody and then to specifically isolate m^6A modified capped 5' RNA fragments using a

monoclonal anti-m^6A antibody. Finally, RT-PCR was used to detect RNA fragments containing the 5' SARS-CoV-2 leader sequence. As seen in Figure 12A, capped SARS-CoV-2 viral RNA fragments were specifically isolated using anti-m^7G antibodies as compared to the use of control IgG antibodies. As seen Figure 12B, m^6A-containing SARS-CoV-2 RNA fragments were specifically isolated from the pool of capped RNA fragments, indicating that the m^6A modification is indeed present on the 5' terminal fragments of SARS-CoV-2. Finally, as shown in Figure 13, we assessed the level of m^6A-containing capped terminal SARS-CoV-2 RNA fragments over the time course of infection using either semi-quantitative RT-PCR (Figure 13A) or quantitative digital droplet RT-PCR (Figure 13B). Collectively, these data clearly demonstrate that 5' terminal capped RNA fragments from SARS-CoV-2 RNAs do contain an m^6A modification, consistent with our hypothesis that the 5' terminal A residue of SARS-CoV-2 transcripts contains the m^6A_m modification.

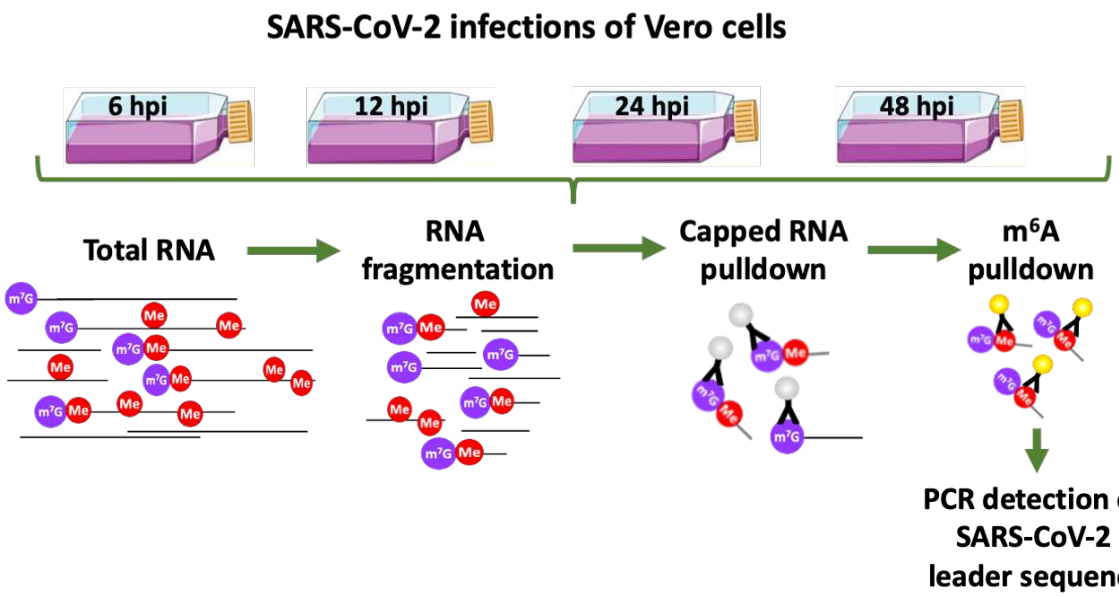

Figure 11. Workflow for a cap/m^{6}A double pulldown using fragmented RNA. *First, we infected Vero cells with SARS-CoV-2 for the times indicated. Next, we obtained total RNA from the cells using TRIzol® and fragmented them using the NEBNext magnesium RNA fragmentation module to obtain RNA fragments of ~200 bases. Next, we performed consecutive immunoprecipitations of the fragmented RNAs using anti-m^{7}G antibodies to isolate 5' capped RNA fragments and then with anti-m^{6}A antibodies to ultimately obtain ~200 base RNA fragments that were both capped and m^{6}A modified. Finally, the products of this double pulldown were analyzed by RT-PCR using SARS-CoV-2 specific primers that amplified the viral 5' leader sequence.*

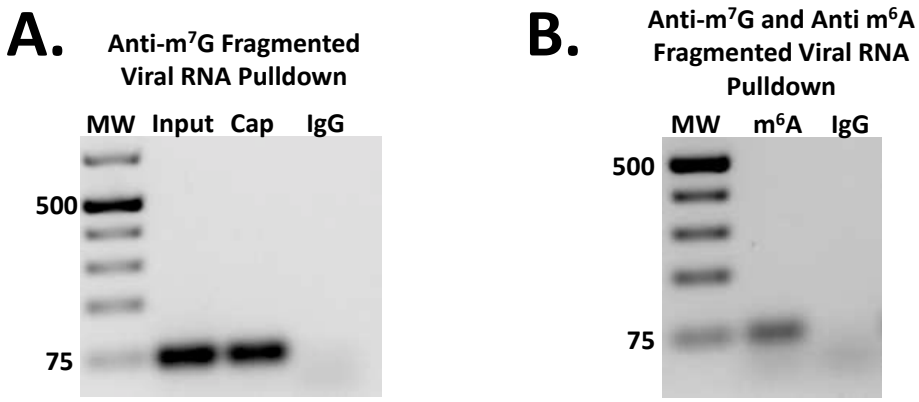

Figure 12. Capped 5' terminal fragments of SARS-CoV-2 RNAs contain an m^{6}A modification. *Panel A: Fragmented RNA obtained as described above (Input lane) was immunoprecipitated using anti-m^{7}G antibody (cap lane) or anti-IgG antibody (IgG lane) and analyzed by RT-PCR using primers specific for the 5' leader region of SARS-CoV-2 RNAs. Panel B: anti-m^{7}G antibody precipitated fragmented RNA prepared as described in the left panel was immunoprecipitated using anti-m^{6}A antibody (m^{6}A lane) or a control anti-IgG antibody (IgG lane) to isolate capped RNA fragments that also contain an m^{6}A modification. Immunoprecipitated products were analyzed by RT-PCR using primers specific for the 5' leader region of SARS-CoV-2 RNA and products were analyzed on a 1% agarose gel. Molecular weight markers (MW lanes) on shown in the left lane of each gel.*

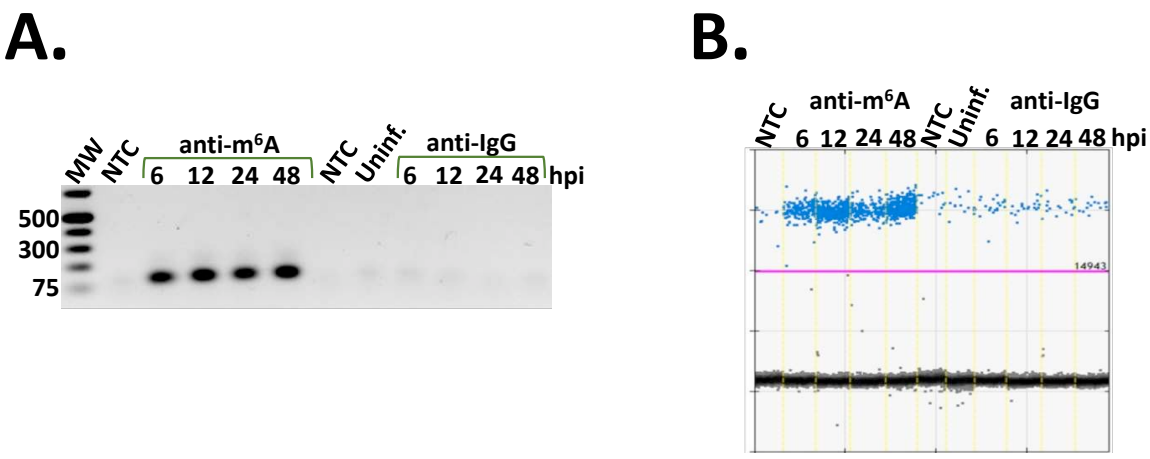

Figure 13. SARS-CoV-2 RNAs contain an m^{6}A modification in cap-proximal fragments. *Vero cells were infected with SARS-CoV-2 for the indicated time. Total RNA was collected, fragmented and consecutively immunoprecipitated with a control IgG antibody (anti-IgG lanes) or anti-m^{7}G antibodies and anti-m^{6}A antibodies (anti-m^{6}A lanes) as described in Figure 3 to isolate capped and m^{6}A modified RNA fragments. Products were analyzed by RT-PCR using primers specific for the 5' leader region of SARS-CoV-2 and analyzed by electrophoresis on a 1% agarose gel (Panel A) or by digital-droplet PCR (panel B). NTC represent reactions using a no-template control and Uninf. lanes indicate PCR reactions run using total RNA from uninfected Vero cells. Molecular weight markers (MW lane) are shown at the left in panel A. The magenta bar in Panel B represents an arbitrary threshold that was set so that any droplet above this line would be considered positive.*

Capping and m^{6}A modification of 5' terminal fragments are regulated during SARS-CoV-2 infections

If capping and m^{6}A modification are playing a key role throughout a SARS-CoV-2 infection, these RNA processing events may be regulated to allow the virus maximum flexibility in adapting to the changing environment inside of the infected cell. Therefore, we reasoned that if we could demonstrate regulated m^{6}A modification of 5' capped terminal fragments throughout a time course of SARS-CoV-2 infection, this would provide added insight into the importance of this modification to the biology of the virus-host interaction. To assess the regulation of 5' terminal capped fragment RNA m^{6}A

methylation on viral RNAs, we performed a time course of SARS-CoV-2 infection in Vero cells and isolated total RNA. As seen in Figure 14A, 5' leader-containing RNA increased as expected throughout 48 hours post infection. Interestingly, as seen in Figure 14B, the percentage of that leader RNA that was 5' capped varied throughout the infection. While nearly all the viral RNAs were capped at 12 hpi, the percentage of viral RNAs that were capped at other times post infection was significantly reduced. At 6 hpi as well as later times post infection (24 and 48 hpi), the percentage of viral RNAs that were capped hovered around 50%. Thus, we conclude that capping is a regulated process on SARS-CoV-2 viral RNAs during infection, with maximal efficiency around 12 hpi when the virus is establishing itself in the cell and beginning to usurp cellular processes. At other times post infection, the virus may choose not to cap a portion of its RNA transcripts so that they won't be targeted to the ribosome and get translated, allowing them perhaps to participate as non-coding RNAs and influence other aspects of virus/cell biology. Thus, regulated viral RNA capping may increase the versatility and functions of SARS-CoV-2 RNAs throughout infection.

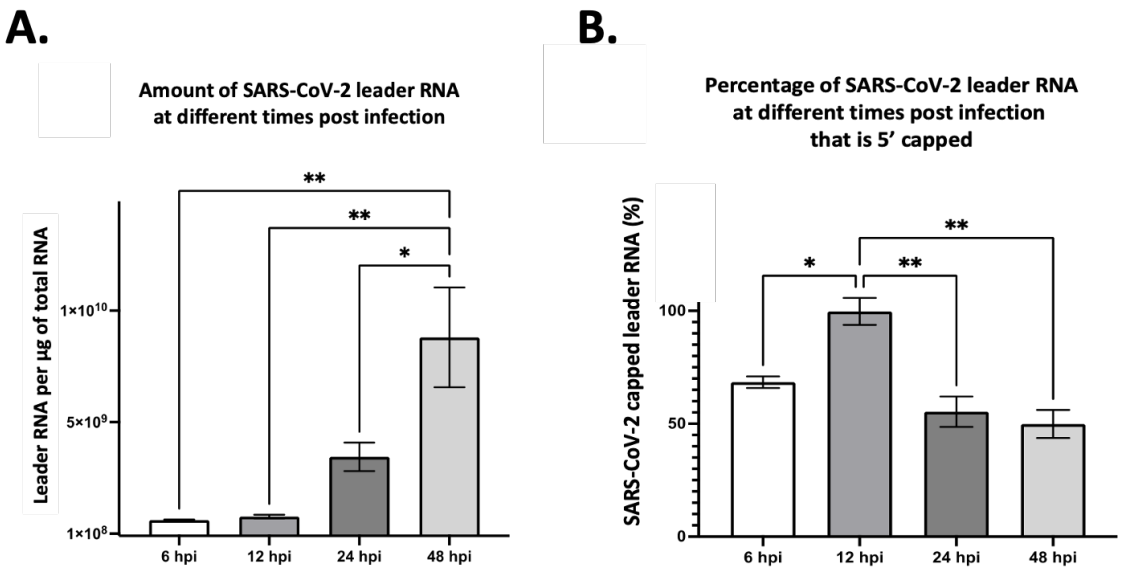

Figure 14. The relative amount of capping of SARS-CoV-2 mRNAs is regulated during infection. *Panel A: Vero cells were infected with SARS-CoV-2, total RNA was obtained at the indicated time points, fragmented as discussed above in Figure 9, and the absolute amount of leader RNA per µg of starting total RNA was calculated by digital droplet RT-PCR using primers specific for the SARS-CoV-2 5' leader RNA. Panel B: Vero cells were infected with SARS-CoV-2, total RNA was obtained at the time points indicated and fragmented/immunoprecipitated with anti-m^7G antibodies. The amount of capped leader RNA relative to the amount of total leader RNA per ug of starting material was calculated by digital droplet RT-PCR using primers specific for the SARS-CoV-2 5' leader RNA. Results are shown as the mean ± S.D. determined from three independent infections. Significance was determined using two-way ANOVA analysis with * = $p<0.05$ and ** = $p<0.005$.*

Next, we determined if the relative amount of capped 5' terminal viral RNA fragments that was modified with m^6A was also regulated. As seen in Figure 15, m^6A modification, like capping efficiency of SARS-CoV-2, also peaked at 12 hpi. At other times post infection, the relative amount of m^6A modification on these capped fragments was reduced 5-fold or more from this peak at 12 hpi. Therefore, m^6A modification of the 5' region of SARS-CoV-2 RNAs is also regulated and corresponds with the production of high levels of translatable transcripts during infection. Collectively, these data suggest that 5' end modification of SARS-CoV-2 transcripts undergoes dynamic

regulation/coordination during infection, indicating that it may play a very important role in the interplay between the virus and the host cell.

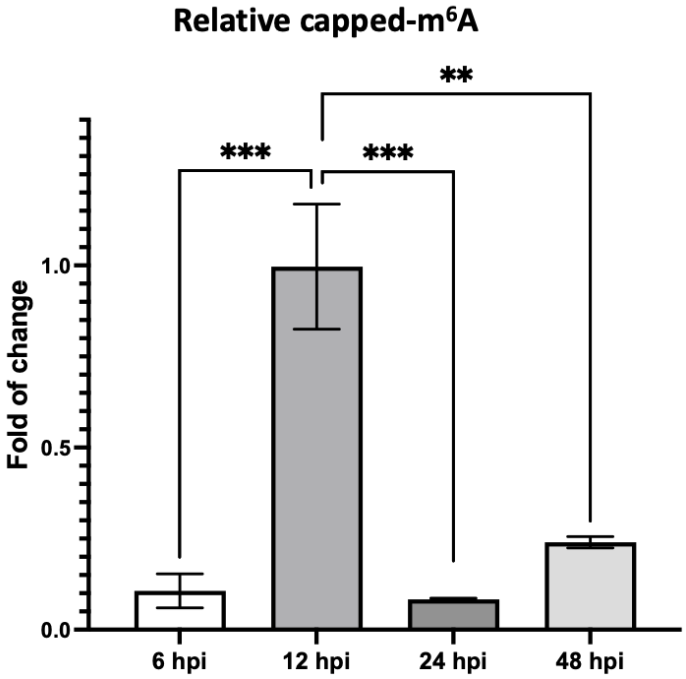

Figure 15. The amount of m^{6}A on capped 5' terminal fragments of SARS-COV-2 mRNAs is regulated during infection. *Vero cells were infected with SARS-CoV-2 for the indicated times and total RNA was isolated, fragmented and subjected to consecutive immunoprecipitations using anti-m^{7}G and anti-m^{6}A antibodies as described in Figure 9. SARS-CoV-2 leader RNAs that contained both modifications were determined by digital droplet RT-PCR using primers specific for the SARS-CoV-2 5' leader RNA region. Results are shown as the mean ± S.D. determined from three independent infections with the mean of the 12 hpi time point set to 1.0. Significance was determined using a two-way ANOVA analysis with **= p<0.005 and ***=p<0.0005.*

PCIF1 knockout reduces m^{6}A levels on SARS-CoV-2 mRNAs

PCIF1 is the cellular enzyme involved in N6 methylation at the first adenosine residue proximal to the m^{7}G cap to generate the m^{6}A$_m$ moiety[25, 229]. Since there appears to be no viral proteins capable of performing this RNA modification, we hypothesize that SARS-CoV-2 usurps this cellular enzyme to provide an m^{6}A modification on the 5' terminal adenosine on its mRNAs. Consistent with this hypothesis, the Whelan

laboratory recently demonstrated that PCIF1 can modify the 5' terminal adenosine residue of several negative sense RNA viruses[204,229,257]. To test this hypothesis, we assessed the level of m^6A in 5' terminal viral RNA fragments in SARS-CoV-2 infected wild type and PCIF1-KO HeLa cells. As seen in representative data in Figure 16, the level of methylation at position N6 of the adenosine on the 5' terminal fragment of SARS-CoV-2 transcripts substantially decreased to about 10% of its normal level in absence of PCIF1 in HeLa cells. We conclude, therefore, that m^6A modification at 5' terminal capped viral RNA fragments depends on the presence of the cellular methyltransferase, PCIF1.

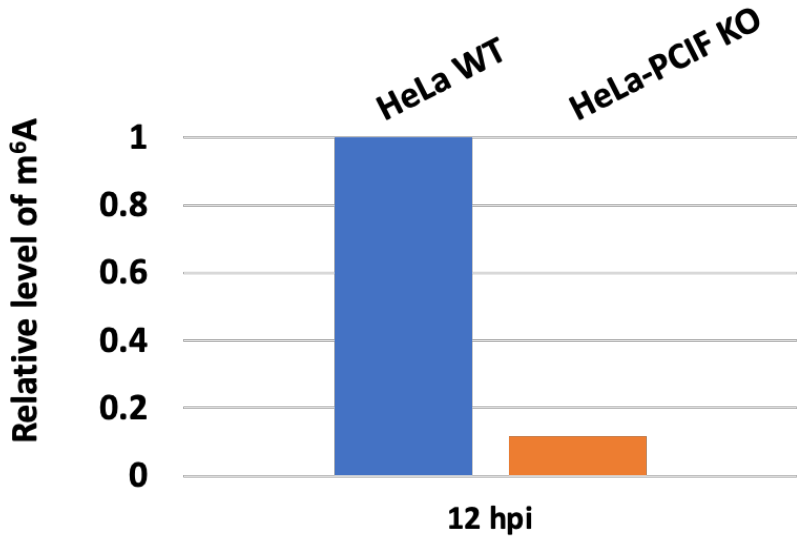

Figure 16. The absence of PCIF1 substantially decreases the level of m^6A modification of the 5' terminal fragments of SARS-CoV-2 RNAs*. HeLa-WT and HeLa-PCIF1 KO cells were infected with SARS-CoV-2 at MOI 3 for the indicated time and total RNA was isolated, fragmented and subjected to consecutive immunoprecipitations using anti-m^7G and anti-m^6A antibodies as described in Figure 9. The levels of SARS-CoV-2 leader RNAs that contained both modifications were determined by digital droplet RT-PCR using primers specific for the SARS-CoV-2 5' leader RNA region.*

The cellular enzyme responsible for the m^{6}A modification of 5' terminal adenosines influences the efficiency of SARS-CoV-2 and other plus sense RNA virus infections

To begin to assess whether PCIF1 can impact positive sense RNA virus infections, we infected wild type or PCIF1 knockout 293T cells with Zika virus and assessed the production of extracellular virus at different times post infection. We opted to use Zika virus (ZIKV) instead of SARS-CoV-2 in these initial studies due to logistical issues associated with BSL3 utilization for SARS-CoV-2 studies. As seen in the representative data in Figure 17, in this initial experiment we observed a dramatic reduction in infectious virus produced at each time point in PCIF1 knockout cells compared to wild type 293T cells. Therefore, we conclude from these preliminary data that PCIF1 appears to have a large impact on a plus-stranded RNA virus (ZIKV) in a similar fashion as it does on negative sense RNA viruses[28] when assayed in a cell line with a competent interferon response. We are currently planning to assess the effect of the PCIF1 KO on SARS-CoV-2 infections.

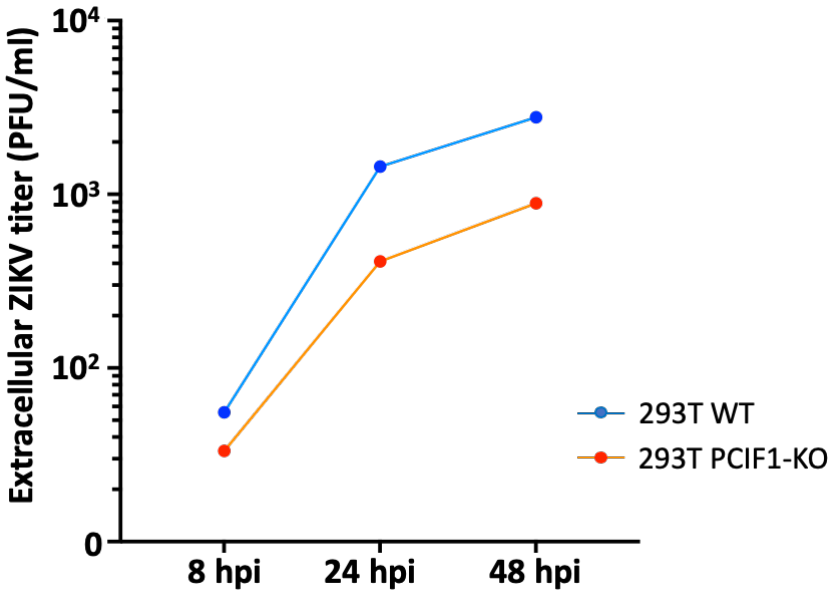

Figure 17. Zika virus production is reduced in the absence of the cellular enzyme that generates m^{6}A at the 5' end of transcripts that initiate with a terminal adenosine. *Wild type 293T cells (WT) or a CRISPR-generated PCIF1-knock out line (PCIF1-KO) of 293T cells were infected with Zika virus (ZIKV) for the indicated times. Extracellular virus was isolated and titered. Results shown are preliminary data from one experiment.*

DISCUSSION

In the first part of this study, we demonstrate that the alternative splicing of four PTBP1-regulated genes is altered in SARS-CoV-2 infected cells, most likely because of the interaction between the PTBP1 protein and the SARS-CoV-2 leader RNA. Our findings using a subcellular fraction of mock and viral infected cells suggest a model where the alteration of cellular splicing is associated with the sequestration of PTBP1 in the cytoplasm by viral RNAs (Figure 18). Consistent with this model, SARS-CoV-2 infected cells give a gene expression phenotype of target genes similar to a PTBP1 knockdown, further suggesting an impairment of PTBP1 function during viral infection.

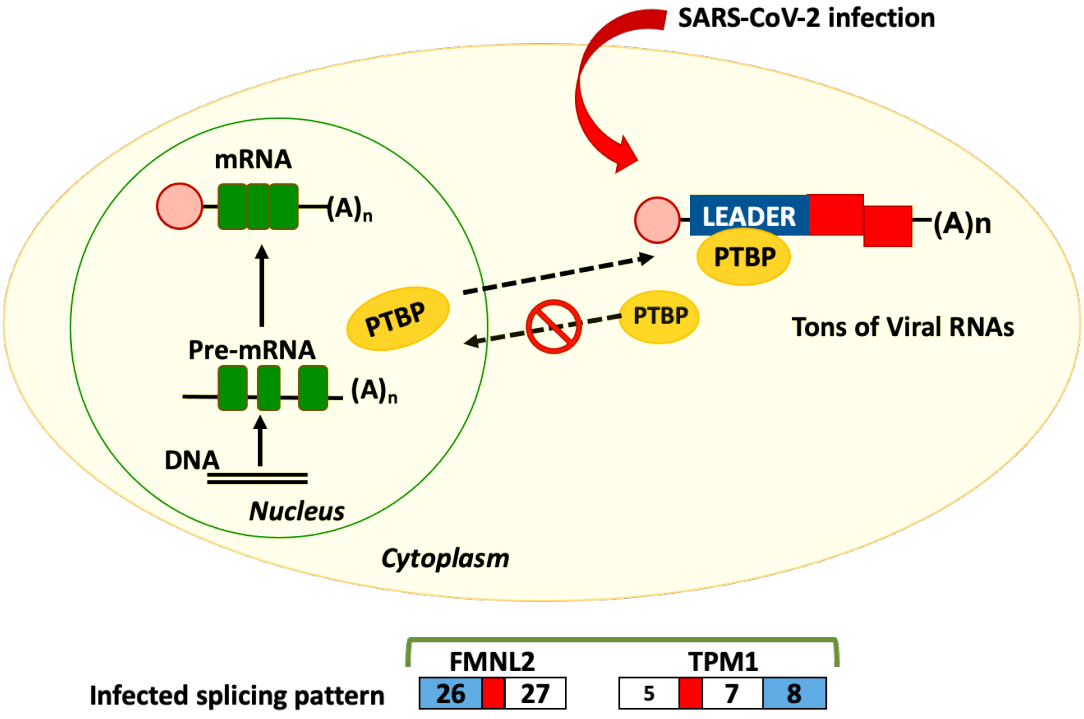

Figure 18. Mechanistic working model of how SARS-CoV-2 leader RNA can sequester host splicing factor PTBP in the cytoplasm and alter the normal splicing of host cell pre-mRNA.

In the second half of this dissertation, we demonstrated that SARS-CoV-2 usurps a specific cellular m^6A 'writer' to decorate its mRNA with post-transcriptional modifications. Importantly, our data indicate the first encoded nucleotide in viral mRNAs, the 5' proximal adenosine, is likely methylated at both the N6 position of the purine base as well as the 2'-O position of the ribose moiety, generating m^6A_m. Knockdown studies indicated that SARS-CoV-2 usurps the cellular PCIF1 enzyme to generate m^6A_m on viral RNAs. Curiously, both the 5' capping and m^6A_m modifications on SARS-CoV-2 mRNAs are regulated during the infection course – with ~ 50% of transcripts getting cap at most times post infection and a burst of modification occurring at 12 hpi. While we could not perform the experiment for technical reasons with SARS-CoV-2, PCIF1 knockdown did result in a dramatic decrease on viral yields for another positive sense RNA virus (whose mRNAs also have adenosine as the first transcribed residue) – Zika virus. Collectively, the two studies reported in this dissertation identified novel mechanism by which SARS-CoV-2 interferes with host cell processes, potentially contributing to viral pathology.

Are there perhaps additional cellular RNA binding proteins whose interaction with SARS-CoV-2 RNAs may influence the RNA biology of the cell?

This study focused exclusively on the interaction of the cellular PTBP1 protein with the SARS-CoV-2 leader RNA region due to previous studies that demonstrated the interaction of PTBP1 with RNAs from other coronaviruses that indicated that the cellular protein binding to this region of viral transcripts[87]. To begin to answer this question, we performed a motif enrichment analysis using the SARS-CoV-2 RNA leader sequence

using the RNA binding protein database (RBPDB). This analysis revealed an interesting subset of cellular RBPs might interact with the SARS-CoV-2 leader RNA (Figure 19). Intriguingly, many of these candidate factors, like the PTBP1 protein addressed in this study, were also involved in the regulation of alternative splicing – four of which are highlighted below. RNA binding motif protein, X-linked (RBMX, Uni
Prot ID P38159, or hnRNP-G) is involved in the regulation of alternative splicing of several pre-mRNAs. Zinc finger Ran-binding domain-containing protein 2 (ZRANB2, UniProt ID O95218) interferes with the constitutive 5' splice site selection. Splicing factor arginine/serine-rich 13A (SFRS13A, UniProt ID O75494) is involved in repressing the splicing of pre-mRNAs. Finally, KH domain containing, RNA binding, signal transduction associated 3 (KHDRBS3, UniProt ID O75525) influences splicie site selection and exon inclusion.

	Score	Relative Score	RBP Name	Start	End	Matching sequence	UniProt ID	Function
1	10.3039	100%	ZRANB2	22	27	AGGUAA	O95218	Splice factor required for alternative splicing of TRA2B/SFRS10 transcripts. May interfere with constitutive 5'-splice site selection.
2	7.2294	100%	Pum2	52	55	UGUA	Q80U58	Sequence-specific RNA-binding protein that acts as a post-transcriptional repressor by binding the 3'-UTR of mRNA targets.
3	7.1545	84%	PABPC1	27	33	ACAAACC	P11940	Binds the poly(A) tail of mRNA, including that of its own transcript, and regulates processes of mRNA metabolism such as pre-mRNA splicing and mRNA stability (PubMed:11051545, PubMed:17212783, PubMed:25480299).
4	6.8772	75%	Psi	36	46	CCAACUUUCGA	FBgn0014870	Drosophila: P-element somatic inhibitor (Psi) encodes a protein that has dual roles in RNA processing and transcriptional regulation. It is required for activating Myc transcription.
5	5.3788	63%	PTBP1	55	69	AGAUCUGUUCUCUAA	P26599	Plays a role in pre-mRNA splicing and in the regulation of alternative splicing events. Activates exon skipping of its own pre-mRNA during muscle cell differentiation. Binds to the polypyrimidine tract of introns. May promote RNA looping when bound to two separate polypyrimidine tracts in the same pre-mRNA. May promote the binding of U2 snRNP to pre-mRNA. Cooperates with RAVER1 to modulate switching between mutually exclusive exons during maturation of the TPM1 pre-mRNA. Represses the splicing of MAPT/Tau exon 10 (PubMed:15009664).
6	5.2683	100%	RBMX	20	23	CCAG	P38159	RNA-binding protein that plays several role in the regulation of pre- and post-transcriptional processes. Implicated in tissue-specific regulation of gene transcription and alternative splicing of several pre-mRNAs.
3	5.1459	61%	PABPC1	31	37	ACCAACC	P11940	Binds the poly(A) tail of mRNA, including that of its own transcript, and regulates processes of mRNA metabolism such as pre-mRNA splicing and mRNA stability (PubMed:11051545, PubMed:17212783, PubMed:25480299).
7	4.4036	100%	ELAVL1	8	11	GUUU	Q15717	RNA-binding protein that binds to the 3'-UTR region of mRNAs and increases their stability (PubMed:14517288, PubMed:18285462, PubMed:31358969).
8	4.2938	84%	SFRS13A	4	10	AAAGGUU	O75494	Splicing factor that in its dephosphorylated form acts as a general repressor of pre-mRNA splicing (PubMed:11684676, PubMed:12419250, PubMed:14765198).
9	4.2845	67%	QKI	34	43	AACCAACUUU	Q96PU8	RNA-binding protein that plays a central role in myelinization (PubMed:16641098).
10	4.0940	88%	KHDRBS3	65	70	UCUAAA	O75525	RNA-binding protein that plays a role in the regulation of alternative splicing and influences mRNA splice site selection and exon inclusion.
10	4.0924	87%	KHDRBS3	1	6	AUUAAA		
10	3.3665	72%	KHDRBS3	23	28	GGUAAC		
7	2.7829	63%	ELAVL1	1	4	AUUA	Q15717	RNA-binding protein that binds to the 3'-UTR region of mRNAs and increases their stability (PubMed:14517288, PubMed:18285462, PubMed:31358969).
7	2.7224	61%	ELAVL1	40	43	CUUU		

***Figure 19**. Candidate cellular RNA binding proteins that interact with the 5' proximal region of SARS-CoV-2 mRNAs as identified by RBPDB analysis.*

Proteins involved in other aspects of post-transcriptional gene regulation were also identified in this search as potential interactors with the SARS-CoV-2 leader RNA. The most notable of these are PABPC1, Pum2 and ELAVL1, cellular RNA binding proteins that are known to be involved in mRNA stability, translation and metabolism.

The presence of these binding sites for additional cellular RNA binding proteins in the leader sequence of SARS-CoV-2 may indicate additional mechanisms for the interplay and interference of the virus with additional splicing substrates and other aspects of post-transcriptional gene regulation. Leader RNA interactions with these additional factors can be readily tested by pulldown experiments using factor-specific antibodies and extracts from virus infectied cells. Functional assays like those described

above to impact the effect of viral infection on protein function, in conjunction with gene knockout or knockdown approach would provide insight into the biological relevance of these protein-leader RNA interactions.

In summary, the impact of viral RNAs binding and sequestering cellular RNA binding protein on the RNA biology of the cell remains an understudied area that we feel is vital to explore to understand a clearer picture of virus-host interactions at the molecular level. These protein-RNA interactions could assist with efficient viral replication, and/or they can contribute to cytopathology and overall pathogenesis. Given the large impact of post-transcriptional gene regulation on cellular gene expression and responses to environmental stresses and stimulations, understanding the impact of dysregulated RNA binding protein functions in infected cells remains an important area for future investigations.

A plethora of ways that SARS-CoV-2 may dysregulate cellular RNA splicing

While leader RNA interactions with PTBP1 is an attractive mechanism that SARS-CoV-2 uses to dysregulate aspects of RNA splicing in infected cells, it is important to point out that it is not the only one. Some viral nonstructural proteins have recently been shown to interact with other aspects of the RNA splicing machinery. nsp16[31], for example, interacts with and sequesters the core splicesome snRNPs U1 and U2 and data indicate that nsp16 can interfere with normal splicing in the cell[31]. Thus, a reduction overall splicing efficiency is occurring during SARS-CoV-2 infection – in addition to the targeted dysregulation of PTBP1 alternative splicing established in this dissertation. Clearly SARS-CoV-2 has evolved multiple ways to limit splicing efficacy in

the infected cell – consistent with the idea that debilitating this post-transcriptional gene expression target is an important aspect of virus host interactions.

Leader RNA structure, as well as its primary sequence, may provide a binding platform for proteins

While the RNA protein interaction analysis provided above relies on primary sequence information, it is also possibly important to point out that the SARS-CoV-2 leader RNA also contains secondary structures that may play a key role in its biology. Interestingly, models of coronavirus leader regions have indicated that the first 70 bases from the 5' end contains two stem loop structures that appear to be conserved structural elements throughout the betacoronaviruses[258]. Stem loop 1 in SARS-CoV-2, for example, is located from positon 7-33 and represents a hairpin with a 4 base loop with a bulge around its midpoint. Stem loop 2 is located from positions 45 to 59 – and structural probing data is consistent with the 5 base loop of that structure participating in a pseudoknot with sequences upstream[58]. There are four additional stem loop structures from there to the start codon of the nsp1 gene – including an upstream open reading frame along with a large 145 nucleotide branched loop that includes that key AUG codon. Collectively these structural elements can serve as binding platforms for a variety of additional cellular factors that remain to be identified in future studies. Furthermore, these interactions may be highly functionally relevant to coronavirus biology. The 5' UTR, for example, plays a key role in translation regulation and the escape of virus-specific transcripts from nsp1-mediated shut off[259]. Thus, the work in this dissertation not only provides a foundation for leader RNA-host protein interactions

but may also represent the tip of the iceberg in RBP communication with this important regulatory region of viral transcripts.

The potential impact of SARS-CoV-2 induced dysregulation of PTBP1 alternative splicing targets

Formin-Like 2 (FMNL2) transcription is highly regulated since the gene can produce 4 different mRNAs and several alternative spliced variants. FMNL2 (https://omim.org/entry/616285) is involved in morphogenesis, cytokinesis and cell polarity[260]; however, the role and impact of alternative splice versions of the gene have not been studied yet. Among the spliced variants that have been characterized, one reported splice variant retains an intron with a stop codon, thus likely representing a non-coding transcript. Interestingly, in our study the intron retention observed in SARS-CoV-2 infected cells was at a different location, between exons 26 and 27. There are two splice variants of FMNL2 that have been described in the literature that differ in the inclusion or exclusion of exon 26, thus this is a hot spot for alternative splicing decisions in this gene[261]. We can speculate that perhaps SARS-CoV-2 infection and PTBP1 sequestration causing difficulties in making clear splice site choice decisions in the area of exon 26, resulting in the partial intron retention that we observed.

Looking at the potential biological role of the FMNL2 splice variant that we observe in SARS-CoV-2 infected cells, it is clear that the intron retention described in Fig. 4 will alter the normal function of the protein. FMNL2 protein contains 6 domains: GTPase binding domain (GBD), FH3, FH1 and FH2 (formin homology domains), a WH2

domain (WASP homology 2) and a Diaphonous Autoinhibitory Domain (DAD) followed by a polybasic region important for the autoinhibition regulation. These domains are important to regulate the dynamics of actin filaments. In normal conditions, the protein is inhibited by folding into a structure that blocks these key binding domains from their potential targets. This autoinhibition results from an intramolecular interaction between the DAD domain and the GBD domain of FMNL2 protein. Strikingly, the retained intron reported in our study falls within this autoregulatory region, disrupting the reading frame of the C-terminal region. This piece of intron retained between exons 26 and 27 separates the DAD domain and the polybasic region containing a critical Serine residue (Ser1072) important for FMNL2 activation[262]. This frameshift also introduced a stop codon, producing a truncated version of the protein. The characterization of a L136P mutation has been reported in the FMNL2 gene of a patient with chronic inflammatory bowel disease [263]. This mutation, like the alternative splicing dysregulation caused by SARS-CoV-2 infection, blocks the autoregulatory domain of FMNL2 leading to a gain of function change in FMNL2, leading to the protein malfunction/misregulation. It will be curious in future experiments to examine FMNL2 protein function in SARS-CoV-2 infected cells and assess their contribution to cytopathology.

TPM1 is a complicated gene containing several isoforms and a complex (and sometimes conflicting) nomenclature in the literature[264]. The gene structure contains 15 exons, five of which - exons 3, 4, 5, 7, and 8 – are constitutively included in the mature mRNA. Thus, different TPM1 isoforms are present by alternative splicing of exons 1a, 1b, 2a, 2b, 6a, 6b, 9a, 9b, 9c, and 9d (https://omim.org/entry/191010). We based our assessment of TPM1 splicing in Fig. 5 using the reference form of TPM1 (Transcript:

ENST00000358278.7 TPM1-206) expressed at the cytoskeleton in non-muscle cells. The PCR primers used for our analysis amplified this reference transcript from exon 2b through exon 9d - the version of TPM1 that we observed in uninfected Calu3 cells used in our experiments. Interestingly, as seen in Fig. 5 cDNA amplified from SARS-CoV-2 infected cells showed the replacement of TPM1 transcripts carriying exon 6a with mis-spliced transcript that lacked exon 6a with what we originally identified as a portion of a retained intron. Retrospective analysis of the sequences with updated TPM1 gene maps now demonstrate that the retained intron was actually exon 6b (with 100% homology). Therefore, SARS-CoV-2 infection / PTBP1 sequestration causes an altered splicing product of TPM1 that was not expressed in uninfected cells. This exon swapping can readily alter TPM1 protein function – which can be assessed in future studies.

Why would PTBP1 sequestration by SARS-CoV-2 RNAs lead to cryptic intron or exon inclusion and exon skipping?

Alternative splicing of both FMNL2 and TPM1 is regulated by the same splicing factor, PTBP1. Consequently, any alteration in functional PTBP1 levels – as we hypothesize is the case in SARS-CoV-2 infected cells - might be reflected in the splicing products of these genes (Figs. 4 and 5). In the case of TPM1 mutually exclusive exon 6a (E6a) and exon 6b (E6b), previous studies (Llorian et al.2010; Bielli et al.2018) in cancer cells showed that high levels of PTBP1 favor the inclusion of exon 6a in the TPM1 gene. Conversely, E6b is included in the transcript when PTBP1 levels are reduced in knockdown experiments. Along the same lines, FMNL2 mRNAs showed

increased frequency of the intron retention after PTBP1/nPTBP1 double knockdowns[245]. Our analysis of the sequences surrounding both E6a and E6b in TPM1[265,266] indicated that E6a has a PTBP1/MBNL binding site next to the U2 snRNP site upstream of the exon while E6b has an ESE and is flanked by two PTBP1 binding sites in the intronic region surrounding the exon. We hypothesize that at normal levels of PTBP1, E6a would not be blocked by PTBP1 due to the the recruitment of splicing factors at an ISE that will promote exon definition and splicing at the 3'SS and 5'SS of the exon. At the same time, PTBP1 binding sites surrounding E6b will block the recruitment of splicing factors leading to the exclusion of this exon due to the lack of an ISE downstream the exon. A reduction of PTBP1 levels, as seen in SARS-CoV-2 infection, may cause a reduction in the competition for the binding sites in the 3'SS and 5'SS of E6b leading to the successful inclusion of this portion in the final spliced transcript. MBNL, on the other hand, would outcompete PTBP1 for the binding site upstream E6a and block U2 snRNP recruitment. At the same time, recruitment of the spliceosome on E6b will also block the ISE of E6a, inhibiting the promotion of exon definition on E6a. Consequently, lower levels of PTBP1 will lead to E6b inclusion and E6a exclusion, as we observe in Fig.5. This provides a rational mechanistic explanation for our data and further directly implicates PTBP1 sequestration as the underlying mechanism for the dysregulated splicing that we observe in SARS-CoV-2 infected cells.

Why might SARS-CoV-2 RNA amplify 'non-specifically' with two different sets of PCR primers?

Interestingly, PCR amplification with either FMNL2 or TPM1 mRNA-specific primers of SARS-CoV-2 infected samples collected from different cell lines showed additional bands of higher molecular weights with no alignment with the human genome. However, the sequences aligned perfectly to regions of SARS-CoV-2 RNA. Sequences amplified with FMNL2 primers aligned with a specific region of the virus located in the 5' end of the Spike gene. Meanwhile, TPM1 primers amplified a different region of the virus; located in the coding region of the Nucleocapsid gene. Interestingly, the amplified regions were always the same regardless of the infected cell line (Calu3, Vero, or 293T) with the exception of HeLa that never produced the 1500 base pair bands. Careful re-analysis of the primers *in silico* did not give any indication of full or partial homology with any region of the viral genome. Additionally, when we tested the primers against pieces of SARS-CoV-2 genome cloned in plasmids, the same PCR products were generated from the S gene with the FMNL2 primers and the N gene with the TPM1 primers. Unfortunately, we have no clear explanation for these amplifications - but do note that they appear to be non-random in nature. This could reflect the natural propensity of coronavirus sequences to be 'slippery' in nature and recombine[267].

Sequestration of shuttling RBPs in the cytoplasm during SARS-CoV-2 infections

PTBP1 is not only a key regulator of alternative splicing, but also shuttles mRNAs from the nucleus to the cytoplasm[79]. In addition, PTBP1 has been implicated in every step of mRNA metabolism. Therefore, PTBP1 is often exported with mRNAs into the cytoplasm of the cell. Our *in vitro* experiments support the hypothesis that the abundant SARS-CoV-2 RNA leader sequences on viral cytoplasmic transcripts capture PTBP1,

forcing the protein to remain in the cytoplasm changing the overall balance between nuclear and cytoplasmic PTBP1 (Fig. 7). Our results here agreed with previous evidence on the redistribution of PTBP1 with other betacoronavirus infections[88]; thus, indicating that PTBP1 cytoplasmic retention is a conserved feature of the interaction coronaviruses with host cells.

Biological relevance of cap proximal modifications: m^6A

The cap structure protects the mRNA from 5'-3' exonucleolytic degradation, increasing the transcript's stability, promoting translation. In addition, Cap1 structures help identify self from aberrant or foreign RNA via the innate immune system[226]. Internal RNA modifications, like N6-methylation of adenosines (m^6A), help influence mRNA localization, splicing, and translation[268]. Particularly interesting to us is the m^6A modification present at the cap-proximal of mRNAs, referred to as m^6A_m. SARS-CoV-2 replicates in the cytoplasm of the host cell and its genome contains adenosine as the first transcribed nucleotide, and presumably this nucleotide should be modified as m^6A_m to mimic the host mRNA.

The dynamics we observed when we pulled down cap-proximal fragments using anti-cap antibodies from SARS-CoV-2 infected cells was very interesting. Samples analyzed at 6, 12, 24 and 48 hpi showed that while the infection increased exponentially; the capping of the viral genomic RNA did not follow the same trend. Surprisingly, our results showed that only about 50% of the viral RNA was capped; except for the 12 hpi that showed 90% or more of the viral RNAs were capped. This unexpected result leads us to conclude that the capping event on viral RNAs in SARS-CoV-2 infections is higly

regulated. Curiously, the biological consequences of maintaining this 50% capping rate at other times post infection are unclear. One possible explanation for regulated capping in SARS-CoV-2 infections is to maximize translationally competent viral mRNAs at a time of infection when they are most needed to take control of the cell. Before and after such a wave, the virus might use its transcripts to moonlight as long noncoding RNAs (lncRNAs) to perform yet to be determined functions in the infected cells. The role of cellular and viral lncRNAs during infection is an understudied area. The results described above indicate that it may be a very productive area to pursue that could open up novel aspects of viral-host interactions at the RNA level.

SARS-CoV-2 is not the only virus that has been described to date that makes a considerable amount of uncapped mRNAs during infection

During the early stages of infection, alphaviruses, positive-sense RNA viruses like Sindbis virus (SINV), produce a subpopulation of uncapped genomic RNA[128,269]. The subpopulation of uncapped genomic RNAs of SINV have shorter half-lives than SINV-capped genomic RNAs and appear to mainly generate non-infectious particles as one might expect. However, alphaviral uncapped genomic RNA production are still important to establish and maintain the infection[269]. Two mechanisms have been proposed. First, viral RNA populations containing subpopulations of uncapped RNA interface with the type I IFN response for the benefit of viral infection. Second, leaving a percentage of its RNA uncapped may also lead to its degradation by cellular “RNA quality control” circulating in the cytoplasm, which may overload the RNA turnover machinery due to the high levels of RNA degradation. Interestingly, the production of uncapped viral

RNAs increased the severity of the disease[270]. The presence of noncapped viral particles correlated with activating a type I IFN response, indicating that the activation of the immune response is important for viral dissemination within the host. Finally, one cannot of course rule out the possibility that the function of uncapped viral RNAs is to regulate the host cell environment to enhance viral infection in other fashions.

Use of an RNA fragmentation approach to delimit cap proximal m^{6}A modifications

The m^{6}A modification is an abundant RNA methylation found in cellular as well as viral RNAs and plays a variety of roles in mRNA metabolism. Since it was already described that m^{6}A is present through the body of viral RNAs we opted instead in this study to analyze the specific and rather unique RNA methylation that occurs at the cap proximal nucleotide. To do this, we used an RNA fragmentation approach that to our knowledge has not been reported to date. To approach this, we produced fragments of about 200 nucleotides long using a non-enzymatic buffer. By fragmenting the RNA to this size and using leader RNA-specific primers, we ensure that the fragments that we are analyzing contain only the first 200 nts of the virus. If the m^{6}A modification exists in this region it will be pulled down using the anti-m^{6}A antibody and we assume that this represents a cap-proximal modification due to (1) the relative paucity of m^{6}A modifications in the 5' UTR of mRNAs and, most importantly, (2) the level of modification of this fragment was greatly reduced by PCIF1 knock out (Fig. 16). Therefore, we feel confident that our assay is detecting m^{6}A$_m$. Further confirmation of

this could be performed by mass spectrometry analysis of viral RNAs or thin layer chromatography[208].

Why would viruses regulate m^{6}A on the cap proximal nucleotide?

Viral life cycles are often coordinated by precise mechanisms that act on their RNA. The m^{6}A modification works on the virus likely contributes to both viral gene expression/replication as well as a means to avoid or interface with the innate immune response in the infected cell host. Internal m^{6}A modifications is a feature that SARS-CoV-2 shares with many other viruses, including as HIV and ZIKV[51]. Cellular Pattern Recognition Receptors (PRRs), like TLRs and RIG-I-like receptors, can bind and recognize as 'non-self' viral RNA[271], triggering signaling that induces an IFN antiviral response. *In vitro* studies performed by adding m^{6}A to transcribed RNAs prevents PRR recognition[272,273], indicating that viruses could use this strategy to avoid the innate immune responses. Another modification on the cap of viral RNA, 2′-O methylation[120], is well-established to help viruses (e.g., WNV and VSV) to avoid the detection by IFIT1, which inhibits the translation of viral RNAs lacking this 2'-O methylation[227,228]. To date, there is no evidence that viruses can encode their methyltransferase to add m^{6}A to the cap proximal nucleotide. Our study provides evidence that SARS-CoV-2 usurps the host methyltransferase PCIF1 to decorate their 5' cap proximal base to likely avoid the detection by host PRRs like has been recently established for negative-sense RNA viruses (e.g., VSV)[257].

How cellular mRNAs obtain their (m^6A_m) modification?

One of more the abundant mRNA modifications is N^6,2'-O-dimethyladenosine (m^6A_m). Eukaryotic mRNAs have a 7-methylguanosine cap (m^7G) at the 5'end linked to the mRNA body by a 5'-5' triphosphate bond. If the first nucleotide after the m^7G cap is an adenosine, it can be sequentially methylated on the ribose sugar (A_m) and then on the at its N6 position (m^6A_m). The Phosphorylated CTD Interacting Factor 1 (PCIF1) catalizes the addition of m^6A methylation only on 2'-O-methylated adenines (A_m) located at 5' ends of mRNAs to generate m^6A_m, but not internal m^6A methylation[229]. If a transcript that initiates with an adenosine lacks this modification, a reduction in cap-dependent translation is observed compared to transcripts with the double methylation m^6A_m, suggesting that the presence of this modification is important for gene regulation.

CONCLUSIONS

Through the experiments presented herein, we have demonstrated several important findings. First, PTBP1, a regulator of cellular mRNA alternative splicing, binds to the SARS-CoV-2 viral RNA leader sequence. This interaction impacts the splicing of several genes regulated by PTBP1. We suggest a mechanism by which SARS-CoV-2 sequesters PTBP1 in the cytoplasm preventing PTBP1 re-localization to the nucleus, thus affecting cellular mRNA splicing patterns during SARS-CoV-2 infection. Secondly, we provide evidence that SARS-CoV-2 can usurp the cellular enzyme, PCIF1, to place a methyl group on the first adenosine of viral mRNAs to generate a m^6A_m moiety. This double methylation may help the viral mRNA avoid host innate immune recognition. Furthermore, we demonstrated that SARS-CoV-2 RNA capping and m^6A_m modifications are significantly regulated throughout infection, with maximum efficiency at 12 hpi consistent with the establishment of viral gene expression in infected cells. Collectively, our findings provide new insights on the complexity of the interactions established between SARS-CoV-2 and the RNA biology of the cell during the infection. From a broader perspective, the data presented here identify novel avenues for the development of anti-coronavirus drugs to treat current and potential emerging coronavirus diseases.

REFERENCES

1. Zhou Z, Qiu Y, Ge X. The taxonomy, host range and pathogenicity of coronaviruses and other viruses in the Nidovirales order. *Animal Dis*. 2021;1(1):5. doi:10.1186/s44149-021-00005-9

2. Payne S. Viruses. *Viruses*. Published online 2017:149-158. doi:10.1016/b978-0-12-803109-4.00017-9

3. Kim D, Lee JY, Yang JS, Kim JW, Kim VN, Chang H. The Architecture of SARS-CoV-2 Transcriptome. *Cell*. 2020;181(4):914-921.e10. doi:10.1016/j.cell.2020.04.011

4. Gorbalenya AE, Enjuanes L, Ziebuhr J, Snijder EJ. Nidovirales: Evolving the largest RNA virus genome. *Virus Res*. 2006;117(1):17-37. doi:10.1016/j.virusres.2006.01.017

5. Maldonado LL, Bertelli AM, Kamenetzky L. Molecular features similarities between SARS-CoV-2, SARS, MERS and key human genes could favour the viral infections and trigger collateral effects. *Sci Rep-uk*. 2021;11(1):4108. doi:10.1038/s41598-021-83595-1

6. Maranon DG, Anderson JR, Maranon AG, Wilusz J. The interface between coronaviruses and host cell RNA biology: Novel potential insights for future therapeutic intervention. *Wiley Interdiscip Rev Rna*. Published online 2020:e1614. doi:10.1002/wrna.1614

7. Wang LF, Shi Z, Zhang S, Field HE, Daszak P, Eaton BT. Review of Bats and SARS - Volume 12, Number 12—December 2006 - Emerging Infectious Diseases journal - CDC. *Emerg Infect Dis*. 2006;12(12):1834-1840. doi:10.3201/eid1212.060401

8. Clark MA. Bovine coronavirus. *Brit Vet J*. 1993;149(1):51-70. doi:10.1016/s0007-1935(05)80210-6

9. Liu DX, Liang JQ, Fung TS. Encyclopedia of Virology. *Encycl Virology*. 2021;(Advances in Virus Research 2018):428-440. doi:10.1016/b978-0-12-809633-8.21501-x

10. Falsey AR, Walsh EE. Novel coronavirus and severe acute respiratory syndrome. *Lancet*. 2003;361(9366):1312-1313. doi:10.1016/s0140-6736(03)13084-x

11. Hoek L van der, Pyrc K, Jebbink MF, et al. Identification of a new human coronavirus. *Nat Med*. 2004;10(4):368-373. doi:10.1038/nm1024

12. Woo PCY, Lau SKP, Chu C ming, et al. Characterization and Complete Genome Sequence of a Novel Coronavirus, Coronavirus HKU1, from Patients with Pneumonia. *J Virol*. 2005;79(2):884-895. doi:10.1128/jvi.79.2.884-895.2005

13. M. ZA, Sander van B, M. BT, D.M.E. OA, A.M. FR. Isolation of a Novel Coronavirus from a Man with Pneumonia in Saudi Arabia. *New Engl J Med*. 2012;367(19):1814-1820. doi:10.1056/nejmoa1211721

14. Zhu N, Zhang D, Wang W, et al. A Novel Coronavirus from Patients with Pneumonia in China, 2019. *New Engl J Med*. 2020;382(8):727-733. doi:10.1056/nejmoa2001017

15. Corman VM, Muth D, Niemeyer D, Drosten C. Hosts and Sources of Endemic Human Coronaviruses. *Adv Virus Res*. 2018;100:163-188. doi:10.1016/bs.aivir.2018.01.001

16. Wang LF, Eaton BT. Wildlife and Emerging Zoonotic Diseases: The Biology, Circumstances and Consequences of Cross-Species Transmission. *Curr Top Microbiol*. 2007;315:325-344. doi:10.1007/978-3-540-70962-6_13

17. Cui J, Eden JS, Holmes EC, Wang LF. Adaptive evolution of bat dipeptidyl peptidase 4 (dpp4): implications for the origin and emergence of Middle East respiratory syndrome coronavirus. *Virol J*. 2013;10(1):304. doi:10.1186/1743-422x-10-304

18. Kan B, Wang M, Jing H, et al. Molecular Evolution Analysis and Geographic Investigation of Severe Acute Respiratory Syndrome Coronavirus-Like Virus in Palm Civets at an Animal Market and on Farms. *J Virol*. 2005;79(18):11892-11900. doi:10.1128/jvi.79.18.11892-11900.2005

19. Zhao J, Cui W, Tian B ping. The Potential Intermediate Hosts for SARS-CoV-2. *Front Microbiol*. 2020;11:580137. doi:10.3389/fmicb.2020.580137

20. Holmes EC, Goldstein SA, Rasmussen AL, et al. The origins of SARS-CoV-2: A critical review. *Cell*. 2021;184(19):4848-4856. doi:10.1016/j.cell.2021.08.017

21. Garry RF. The evidence remains clear: SARS-CoV-2 emerged via the wildlife trade. *Proc National Acad Sci*. 2022;119(47):e2214427119. doi:10.1073/pnas.2214427119

22. Ruiz-Aravena M, McKee C, Gamble A, et al. Ecology, evolution and spillover of coronaviruses from bats. *Nat Rev Microbiol*. 2022;20(5):299-314. doi:10.1038/s41579-021-00652-2

23. Pambuccian SE. The COVID-19 pandemic: implications for the cytology laboratory. *J Am Soc Cytopathol*. 2020;9(3):202-211. doi:10.1016/j.jasc.2020.03.001

24. Greenhalgh T, Jimenez JL, Prather KA, Tufekci Z, Fisman D, Schooley R. Ten scientific reasons in support of airborne transmission of SARS-CoV-2. *Lancet*. 2021;397(10285):1603-1605. doi:10.1016/s0140-6736(21)00869-2

25. Guan WJ, Ni ZY, Hu Y, et al. Clinical Characteristics of Coronavirus Disease 2019 in China. *New Engl J Med*. 2020;382(18):1708-1720. doi:10.1056/nejmoa2002032

26. Vetter P, Vu DL, L'Huillier AG, Schibler M, Kaiser L, Jacquerioz F. Clinical features of covid-19. *Bmj*. 2020;369:m1470. doi:10.1136/bmj.m1470

27. Du L, He Y, Zhou Y, Liu S, Zheng BJ, Jiang S. The spike protein of SARS-CoV--a target for vaccine and therapeutic development. *Nat Rev Microbiol*. 2009;7(3):226-236. doi:10.1038/nrmicro2090

28. Akca UK, Kesici S, Ozsurekci Y, et al. Kawasaki-like disease in children with COVID-19. *Rheumatol Int*. 2020;40(12):2105-2115. doi:10.1007/s00296-020-04701-6

29. Sardu C, Gambardella J, Morelli MB, Wang X, Marfella R, Santulli G. Hypertension, Thrombosis, Kidney Failure, and Diabetes: Is COVID-19 an Endothelial Disease? A Comprehensive Evaluation of Clinical and Basic Evidence. *J Clin Medicine*. 2020;9(5):1417. doi:10.3390/jcm9051417

30. Davis HE, McCorkell L, Vogel JM, Topol EJ. Long COVID: major findings, mechanisms and recommendations. *Nat Rev Microbiol*. 2023;21(3):133-146. doi:10.1038/s41579-022-00846-2

31. Banerjee AK, Blanco MR, Bruce EA, et al. SARS-CoV-2 Disrupts Splicing, Translation, and Protein Trafficking to Suppress Host Defenses. *Cell*. 2020;183(5):1325-1339.e21. doi:10.1016/j.cell.2020.10.004

32. Siu YL, Teoh KT, Lo J, et al. The M, E, and N Structural Proteins of the Severe Acute Respiratory Syndrome Coronavirus Are Required for Efficient Assembly, Trafficking, and Release of Virus-Like Particles. *J Virol*. 2008;82(22):11318-11330. doi:10.1128/jvi.01052-08

33. Hikmet F, Méar L, Edvinsson Å, Micke P, Uhlén M, Lindskog C. The protein expression profile of ACE2 in human tissues. *Mol Syst Biol*. 2020;16(7):e9610. doi:10.15252/msb.20209610

34. Li W, Moore MJ, Vasilieva N, et al. Angiotensin-converting enzyme 2 is a functional receptor for the SARS coronavirus. *Nature*. 2003;426(6965):450-454. doi:10.1038/nature02145

35. V'kovski P, Kratzel A, Steiner S, Stalder H, Thiel V. Coronavirus biology and replication: implications for SARS-CoV-2. *Nat Rev Microbiol*. 2021;19(3):155-170. doi:10.1038/s41579-020-00468-6

36. Hoffmann M, Kleine-Weber H, Schroeder S, et al. SARS-CoV-2 Cell Entry Depends on ACE2 and TMPRSS2 and Is Blocked by a Clinically Proven Protease Inhibitor. *Cell*. 2020;181(2):271-280.e8. doi:10.1016/j.cell.2020.02.052

37. Matsuyama S, Nagata N, Shirato K, Kawase M, Takeda M, Taguchi F. Efficient Activation of the Severe Acute Respiratory Syndrome Coronavirus Spike Protein by the Transmembrane Protease TMPRSS2. *J Virol*. 2010;84(24):12658-12664. doi:10.1128/jvi.01542-10

38. Gierer S, Bertram S, Kaup F, et al. The Spike Protein of the Emerging Betacoronavirus EMC Uses a Novel Coronavirus Receptor for Entry, Can Be Activated by TMPRSS2, and Is Targeted by Neutralizing Antibodies. *J Virol*. 2013;87(10):5502-5511. doi:10.1128/jvi.00128-13

39. Li F, Han M, Dai P, et al. Distinct mechanisms for TMPRSS2 expression explain organ-specific inhibition of SARS-CoV-2 infection by enzalutamide. *Nat Commun*. 2021;12(1):866. doi:10.1038/s41467-021-21171-x

40. Jackson CB, Farzan M, Chen B, Choe H. Mechanisms of SARS-CoV-2 entry into cells. *Nat Rev Mol Cell Bio*. 2022;23(1):3-20. doi:10.1038/s41580-021-00418-x

41. Shi ST, Lai MMC. Current Topics in Microbiology and Immunology. *Curr Top Microbiol*. 2005;287:95-131. doi:10.1007/3-540-26765-4_4

42. Mariano G, Farthing RJ, Lale-Farjat SLM, Bergeron JRC. Structural Characterization of SARS-CoV-2: Where We Are, and Where We Need to Be. *Frontiers Mol Biosci*. 2020;7:605236. doi:10.3389/fmolb.2020.605236

43. Finkel Y, Mizrahi O, Nachshon A, et al. The coding capacity of SARS-CoV-2. *Nature*. 2021;589(7840):125-130. doi:10.1038/s41586-020-2739-1

44. Low ZY, Zabidi NZ, Yip AJW, Puniyamurti A, Chow VTK, Lal SK. SARS-CoV-2 Non-Structural Proteins and Their Roles in Host Immune Evasion. *Viruses*. 2022;14(9):1991. doi:10.3390/v14091991

45. Bao L, Deng W, Huang B, et al. The pathogenicity of SARS-CoV-2 in hACE2 transgenic mice. *Nature*. 2020;583(7818):830-833. doi:10.1038/s41586-020-2312-y

46. Lamers MM, Beumer J, Vaart J van der, et al. SARS-CoV-2 productively infects human gut enterocytes. *Science*. 2020;369(6499):50-54. doi:10.1126/science.abc1669

47. Finkel Y, Gluck A, Nachshon A, et al. SARS-CoV-2 uses a multipronged strategy to impede host protein synthesis. *Nature*. 2021;594(7862):240-245. doi:10.1038/s41586-021-03610-3

48. Wang C, Chen L, Chen Y, et al. Abnormal global alternative RNA splicing in COVID-19 patients. *Plos Genet*. 2022;18(4):e1010137. doi:10.1371/journal.pgen.1010137

49. Zaffagni M, Harris JM, Patop IL, Pamudurti NR, Nguyen S, Kadener S. SARS-CoV-2 Nsp14 mediates the effects of viral infection on the host cell transcriptome. *Elife*. 2022;11:e71945. doi:10.7554/elife.71945

50. Srivastava R, Daulatabad SV, Srivastava M, Janga SC. Role of SARS-CoV-2 in Altering the RNA-Binding Protein and miRNA-Directed Post-Transcriptional Regulatory Networks in Humans. *Int J Mol Sci*. 2020;21(19):7090. doi:10.3390/ijms21197090

51. Liu J, Xu YP, Li K, et al. The m6A methylome of SARS-CoV-2 in host cells. *Cell Res*. 2021;31(4):404-414. doi:10.1038/s41422-020-00465-7

52. Li N, Hui H, Bray B, et al. METTL3 regulates viral m6A RNA modification and host cell innate immune responses during SARS-CoV-2 infection. *Cell Reports*. 2021;35(6):109091. doi:10.1016/j.celrep.2021.109091

53. Wang Q, Wu J, Wang H, et al. Structural Basis for RNA Replication by the SARS-CoV-2 Polymerase. *Cell*. 2020;182(2):417-428.e13. doi:10.1016/j.cell.2020.05.034

54. Brian DA, Baric RS. Coronavirus Replication and Reverse Genetics. *Curr Top Microbiol*. 2005;287:1-30. doi:10.1007/3-540-26765-4_1

55. Liu H, Iketani S, Zask A, et al. Development of optimized drug-like small molecule inhibitors of the SARS-CoV-2 3CL protease for treatment of COVID-19. *Nat Commun*. 2022;13(1):1891. doi:10.1038/s41467-022-29413-2

56. Rangan R, Zheludev IN, Hagey RJ, et al. RNA genome conservation and secondary structure in SARS-CoV-2 and SARS-related viruses: a first look. *Rna*. 2020;26(8):rna.076141.120. doi:10.1261/rna.076141.120

57. Sola I, Almazán F, Zúñiga S, Enjuanes L. Continuous and Discontinuous RNA Synthesis in Coronaviruses. *Ann Rev Virol*. 2015;2(1):265-288. doi:10.1146/annurev-virology-100114-055218

58. Miao Z, Tidu A, Eriani G, Martin F. Secondary structure of the SARS-CoV-2 5'-UTR. *Rna Biol*. 2021;18(4):447-456. doi:10.1080/15476286.2020.1814556

59. Madhugiri R, Fricke M, Marz M, Ziebuhr J. RNA structure analysis of alphacoronavirus terminal genome regions. *Virus Res*. 2014;194:76-89. doi:10.1016/j.virusres.2014.10.001

60. Zhao J, Qiu J, Aryal S, Hackett JL, Wang J. The RNA Architecture of the SARS-CoV-2 3′-Untranslated Region. *Viruses*. 2020;12(12):1473. doi:10.3390/v12121473

61. Hegde S, Tang Z, Zhao J, Wang J. Inhibition of SARS-CoV-2 by Targeting Conserved Viral RNA Structures and Sequences. *Front Chem*. 2021;9:802766. doi:10.3389/fchem.2021.802766

62. Kelly JA, Olson AN, Neupane K, et al. Structural and functional conservation of the programmed −1 ribosomal frameshift signal of SARS coronavirus 2 (SARS-CoV-2). *J Biol Chem*. 2020;295(31):10741-10748. doi:10.1074/jbc.ac120.013449

63. Jensen S, Thomsen AR. Sensing of RNA Viruses: a Review of Innate Immune Receptors Involved in Recognizing RNA Virus Invasion. *J Virol*. 2012;86(6):2900-2910. doi:10.1128/jvi.05738-11

64. Wilkins C, Gale M. Recognition of viruses by cytoplasmic sensors. *Curr Opin Immunol*. 2010;22(1):41-47. doi:10.1016/j.coi.2009.12.003

65. Stetson DB, Medzhitov R. Type I Interferons in Host Defense. *Immunity*. 2006;25(3):373-381. doi:10.1016/j.immuni.2006.08.007

66. Schreiber A, Liedmann S, Brunotte L, Anhlan D, Ehrhardt C, Ludwig S. Type I interferon antagonistic properties of influenza B virus polymerase proteins. *Cell Microbiol*. 2020;22(2):e13143. doi:10.1111/cmi.13143

67. Mann JT, Riley BA, Baker SF. All differential on the splicing front: Host alternative splicing alters the landscape of virus-host conflict. *Semin Cell Dev Biol*. Published online 2023. doi:10.1016/j.semcdb.2023.01.013

68. Hentze MW, Castello A, Schwarzl T, Preiss T. A brave new world of RNA-binding proteins. *Nat Rev Mol Cell Bio*. 2018;19(5):327-341. doi:10.1038/nrm.2017.130

69. Brinegar AE, Cooper TA. Roles for RNA-binding proteins in development and disease. *Brain Res*. 2016;1647:1-8. doi:10.1016/j.brainres.2016.02.050

70. Low YH, Asi Y, Foti SC, Lashley T. Heterogeneous Nuclear Ribonucleoproteins: Implications in Neurological Diseases. *Mol Neurobiol*. 2021;58(2):631-646. doi:10.1007/s12035-020-02137-4

71. Lu Y, Wang X, Gu Q, et al. Heterogeneous nuclear ribonucleoprotein A/B: an emerging group of cancer biomarkers and therapeutic targets. *Cell Death Discov*. 2022;8(1):337. doi:10.1038/s41420-022-01129-8

72. Wang J, Sun D, Wang M, et al. Multiple functions of heterogeneous nuclear ribonucleoproteins in the positive single-stranded RNA virus life cycle. *Front Immunol*. 2022;13:989298. doi:10.3389/fimmu.2022.989298

73. Dreyfuss G, Matunis MJ, Pinol-Roma S, Burd CG. hnRNP Proteins and the Biogenesis of mRNA. *Annu Rev Biochem*. 1993;62(1):289-321. doi:10.1146/annurev.bi.62.070193.001445

74. Han SP, Tang YH, Smith R. Functional diversity of the hnRNPs: past, present and perspectives. *Biochem J*. 2010;430(3):379-392. doi:10.1042/bj20100396

75. Sawicka K, Bushell M, Spriggs KA, Willis AE. Polypyrimidine-tract-binding protein: a multifunctional RNA-binding protein. *Biochem Soc T*. 2008;36(4):641-647. doi:10.1042/bst0360641

76. Dai S, Wang C, Zhang C, et al. PTB: Not just a polypyrimidine tract-binding protein. *J Cell Physiol*. 2022;237(5):2357-2373. doi:10.1002/jcp.30716

77. García-Blanco MA, Jamison SF, Sharp PA. Identification and purification of a 62,000-dalton protein that binds specifically to the polypyrimidine tract of introns. *Gene Dev*. 1989;3(12a):1874-1886. doi:10.1101/gad.3.12a.1874

78. Lou H, Gagel RF, Berget SM. An intron enhancer recognized by splicing factors activates polyadenylation. *Gene Dev*. 1996;10(2):208-219. doi:10.1101/gad.10.2.208

79. Kamath RV, Leary DJ, Huang S. Nucleocytoplasmic Shuttling of Polypyrimidine Tract-binding Protein Is Uncoupled from RNA Export. *Mol Biol Cell*. 2001;12(12):3808-3820. doi:10.1091/mbc.12.12.3808

80. Fritz SE, Ranganathan S, Wang CD, Hogg JR. The RNA-binding protein PTBP1 promotes ATPase-dependent dissociation of the RNA helicase UPF1 to protect transcripts from nonsense-mediated mRNA decay. *J Biol Chem*. 2020;295(33):11613-11625. doi:10.1074/jbc.ra120.013824

81. Witherell GW, Gil A, Wimmer E. Interaction of polypyrimidine tract binding protein with the encephalomyocarditis virus mRNA internal ribosomal entry site. *Biochemistry-us*. 1993;32(32):8268-8275. doi:10.1021/bi00083a030

82. Li H, Guo Y, Qi W, Liao M. N6-methyladenosine modification of viral RNA and its role during the recognition process of RIG-I-like receptors. *Front Immunol*. 2022;13:1031200. doi:10.3389/fimmu.2022.1031200

83. Garcia-Moreno M, Noerenberg M, Ni S, et al. System-wide Profiling of RNA-Binding Proteins Uncovers Key Regulators of Virus Infection. *Mol Cell*. 2019;74(1):196-211.e11. doi:10.1016/j.molcel.2019.01.017

84. Rousseau C, Meignin C. Viral sensing by RNA helicases. *Virologie*. 2020;24(6):36-52. doi:10.1684/vir.2020.0872

85. Girardi E, Pfeffer S, Baumert TF, Majzoub K. Roadblocks and fast tracks: How RNA binding proteins affect the viral RNA journey in the cell. *Semin Cell Dev Biol*. 2020;111:86-100. doi:10.1016/j.semcdb.2020.08.006

86. Luo H, Chen Q, Chen J, Chen K, Shen X, Jiang H. The nucleocapsid protein of SARS coronavirus has a high binding affinity to the human cellular heterogeneous nuclear ribonucleoprotein A1. *Febs Lett*. 2005;579(12):2623-2628. doi:10.1016/j.febslet.2005.03.080

87. Sola I, Mateos-Gomez PA, Almazan F, Zuñiga S, Enjuanes L. RNA-RNA and RNA-protein interactions in coronavirus replication and transcription. *Rna Biol*. 2011;8(2):237-248. doi:10.4161/rna.8.2.14991

88. Sola I, Galán C, Mateos-Gómez PA, et al. The Polypyrimidine Tract-Binding Protein Affects Coronavirus RNA Accumulation Levels and Relocalizes Viral RNAs to Novel Cytoplasmic Domains Different from Replication-Transcription Sites. *J Virol*. 2011;85(10):5136-5149. doi:10.1128/jvi.00195-11

89. Mukherjee N, Corcoran DL, Nusbaum JD, et al. Integrative Regulatory Mapping Indicates that the RNA-Binding Protein HuR Couples Pre-mRNA Processing and mRNA Stability. *Mol Cell*. 2011;43(3):327-339. doi:10.1016/j.molcel.2011.06.007

90. Zhang XHF, Heller KA, Hefter I, Leslie CS, Chasin LA. Sequence Information for the Splicing of Human Pre-mRNA Identified by Support Vector Machine Classification. *Genome Res*. 2003;13(12):2637-2650. doi:10.1101/gr.1679003

91. Chen M, Manley JL. Mechanisms of alternative splicing regulation: insights from molecular and genomics approaches. *Nat Rev Mol Cell Bio*. 2009;10(11):741-754. doi:10.1038/nrm2777

92. Shepard PJ, Hertel KJ. The SR protein family. *Genome Biol*. 2009;10(10):242. doi:10.1186/gb-2009-10-10-242

93. Martinez-Contreras R, Cloutier P, Shkreta L, Fisette JF, Revil T, Chabot B. Alternative Splicing in the Postgenomic Era. *Adv Exp Med Biol*. 2007;623:123-147. doi:10.1007/978-0-387-77374-2_8

94. Scotti MM, Swanson MS. RNA mis-splicing in disease. *Nat Rev Genet*. 2016;17(1):19-32. doi:10.1038/nrg.2015.3

95. Rio DC. Splicing of pre-mRNA: mechanism, regulation and role in development. *Curr Opin Genet Dev*. 1993;3(4):574-584. doi:10.1016/0959-437x(93)90093-5

96. Borišek J, Casalino L, Saltalamacchia A, Mays SG, Malcovati L, Magistrato A. Atomic-Level Mechanism of Pre-mRNA Splicing in Health and Disease. *Accounts Chem Res*. 2021;54(1):144-154. doi:10.1021/acs.accounts.0c00578

97. Papasaikas P, Tejedor JR, Vigevani L, Valcárcel J. Functional Splicing Network Reveals Extensive Regulatory Potential of the Core Spliceosomal Machinery. *Mol Cell*. 2015;57(1):7-22. doi:10.1016/j.molcel.2014.10.030

98. Xu B, Meng Y, Jin Y. RNA structures in alternative splicing and back-splicing. *Wiley Interdiscip Rev Rna*. 2021;12(1):e1626. doi:10.1002/wrna.1626

99. Malard F, Mackereth CD, Campagne S. Principles and correction of 5'-splice site selection. *Rna Biol*. 2022;19(1):943-960. doi:10.1080/15476286.2022.2100971

100. Brooks AN, Aspden JL, Podgornaia AI, Rio DC, Brenner SE. Identification and experimental validation of splicing regulatory elements in Drosophila melanogaster reveals functionally conserved splicing enhancers in metazoans. *Rna*. 2011;17(10):1884-1894. doi:10.1261/rna.2696311

101. Keren H, Lev-Maor G, Ast G. Alternative splicing and evolution: diversification, exon definition and function. *Nat Rev Genet*. 2010;11(5):345-355. doi:10.1038/nrg2776

102. Baralle FE, Giudice J. Alternative splicing as a regulator of development and tissue identity. *Nat Rev Mol Cell Bio*. 2017;18(7):437-451. doi:10.1038/nrm.2017.27

103. Bhadra M, Howell P, Dutta S, Heintz C, Mair WB. Alternative splicing in aging and longevity. *Hum Genet*. 2020;139(3):357-369. doi:10.1007/s00439-019-02094-6

104. Ule J, Blencowe BJ. Alternative Splicing Regulatory Networks: Functions, Mechanisms, and Evolution. *Mol Cell*. 2019;76(2):329-345. doi:10.1016/j.molcel.2019.09.017

105. Rooke N, Markovtsov V, Cagavi E, Black DL. Roles for SR Proteins and hnRNP A1 in the Regulation of c -src Exon N1. *Mol Cell Biol*. 2003;23(6):1874-1884. doi:10.1128/mcb.23.6.1874-1884.2003

106. House AE, Lynch KW. An exonic splicing silencer represses spliceosome assembly after ATP-dependent exon recognition. *Nat Struct Mol Biol*. 2006;13(10):937-944. doi:10.1038/nsmb1149

107. Motta-Mena LB, Partch CL, Gardner KH. The Three Rs of Transcription: Recruit, Retain, and Recycle. *Mol Cell*. 2010;40(6):855-858. doi:10.1016/j.molcel.2010.12.010

108. Modafferi EF, Black DL. A complex intronic splicing enhancer from the c-src pre-mRNA activates inclusion of a heterologous exon. *Mol Cell Biol*. 1997;17(11):6537-6545. doi:10.1128/mcb.17.11.6537

109. Long JC, Caceres JF. The SR protein family of splicing factors: master regulators of gene expression. *Biochem J*. 2008;417(1):15-27. doi:10.1042/bj20081501

110. Inoue D, Bradley RK, Abdel-Wahab O. Spliceosomal gene mutations in myelodysplasia: molecular links to clonal abnormalities of hematopoiesis. *Gene Dev*. 2016;30(9):989-1001. doi:10.1101/gad.278424.116

111. Yoshida K, Ogawa S. Splicing factor mutations and cancer. *Wiley Interdiscip Rev Rna*. 2014;5(4):445-459. doi:10.1002/wrna.1222

112. Maio FAD, Risso G, Iglesias NG, et al. The Dengue Virus NS5 Protein Intrudes in the Cellular Spliceosome and Modulates Splicing. *Plos Pathog*. 2016;12(8):e1005841. doi:10.1371/journal.ppat.1005841

113. Lu Y, Qian XY, Krug RM. The influenza virus NS1 protein: a novel inhibitor of pre-mRNA splicing. *Gene Dev*. 1994;8(15):1817-1828. doi:10.1101/gad.8.15.1817

114. Zhang X, Aida Y. HIV-1 Vpr: A Novel Role in Regulating RNA Splicing. *Curr Hiv Res*. 2009;7(2):163-168. doi:10.2174/157016209787581517

115. Michalski D, Ontiveros JG, Russo J, et al. Zika virus noncoding sfRNAs sequester multiple host-derived RNA-binding proteins and modulate mRNA decay and splicing during infection. *J Biol Chem*. 2019;294(44):16282-16296. doi:10.1074/jbc.ra119.009129

116. Shatkin AJ, Manley JL. The ends of the affair: Capping and polyadenylation. *Nat Struct Biol*. 2000;7(10):838-842. doi:10.1038/79583

117. Moteki S, Price D. Functional Coupling of Capping and Transcription of mRNA. *Mol Cell*. 2002;10(3):599-609. doi:10.1016/s1097-2765(02)00660-3

118. Ghosh A, Lima CD. Enzymology of RNA cap synthesis. *Wiley Interdiscip Rev Rna*. 2010;1(1):152-172. doi:10.1002/wrna.19

119. Decroly E, Debarnot C, Ferron F, et al. Crystal Structure and Functional Analysis of the SARS-Coronavirus RNA Cap 2′-O-Methyltransferase nsp10/nsp16 Complex. *Plos Pathog*. 2011;7(5):e1002059. doi:10.1371/journal.ppat.1002059

120. Daffis S, Szretter KJ, Schriewer J, et al. 2'-O methylation of the viral mRNA cap evades host restriction by IFIT family members. *Nature*. 2010;468(7322):452-456. doi:10.1038/nature09489

121. Devarkar SC, Wang C, Miller MT, et al. Structural basis for m7G recognition and 2′-O-methyl discrimination in capped RNAs by the innate immune receptor RIG-I. *Proc National Acad Sci*. 2016;113(3):596-601. doi:10.1073/pnas.1515152113

122. Darnell JE. Transcription Units for mRNA Production in Eukaryotic Cells and Their DNA Viruses11This work is supported by grants from the National Institutes of Health

(CA 16006-05) and the American Cancer Society (NP 213G). *Prog Nucleic Acid Re*. 1979;22:327-353. doi:10.1016/s0079-6603(08)60803-x

123. Schibler U, Perry RP. The 5′-termini of heterogeneous nuclear RNA: a comparison among molecules of different sizes and ages. *Nucleic Acids Res*. 1977;4(12):4133-4150. doi:10.1093/nar/4.12.4133

124. Ramanathan A, Robb GB, Chan SH. mRNA capping: biological functions and applications. *Nucleic Acids Res*. 2016;44(16):7511-7526. doi:10.1093/nar/gkw551

125. Vlugt CD, Sikora D, Pelchat M. Insight into Influenza: A Virus Cap-Snatching. *Viruses*. 2018;10(11):641. doi:10.3390/v10110641

126. Saeedi BJ, Geiss BJ. Regulation of flavivirus RNA synthesis and capping. *Wiley Interdiscip Rev Rna*. 2013;4(6):723-735. doi:10.1002/wrna.1191

127. Park GJ, Osinski A, Hernandez G, et al. The mechanism of RNA capping by SARS-CoV-2. *Nature*. 2022;609(7928):793-800. doi:10.1038/s41586-022-05185-z

128. LaPointe AT, Moreno-Contreras J, Sokoloski KJ. Increasing the Capping Efficiency of the Sindbis Virus nsP1 Protein Negatively Affects Viral Infection. *Mbio*. 2018;9(6):e02342-18. doi:10.1128/mbio.02342-18

129. LaPointe AT, Landers VD, Westcott CE, Sokoloski KJ. Production of Noncapped Genomic RNAs Is Critical to Sindbis Virus Disease and Pathogenicity. *Mbio*. 2020;11(6):e02675-20. doi:10.1128/mbio.02675-20

130. Moreno-Contreras J, Sánchez-Tacuba L, Arias CF, López S. Mature Rotavirus Particles Contain Equivalent Amounts of 7meGpppG-Capped and Noncapped Viral Positive-Sense RNAs. *J Virol*. 2022;96(17):e01151-22. doi:10.1128/jvi.01151-22

131. Kouwaki T, Nishimura T, Wang G, Oshiumi H. RIG-I-Like Receptor-Mediated Recognition of Viral Genomic RNA of Severe Acute Respiratory Syndrome Coronavirus-2 and Viral Escape From the Host Innate Immune Responses. *Front Immunol*. 2021;12:700926. doi:10.3389/fimmu.2021.700926

132. Onomoto K, Onoguchi K, Yoneyama M. Regulation of RIG-I-like receptor-mediated signaling: interaction between host and viral factors. *Cell Mol Immunol*. 2021;18(3):539-555. doi:10.1038/s41423-020-00602-7

133. Platanias LC. Mechanisms of type-I- and type-II-interferon-mediated signalling. *Nat Rev Immunol*. 2005;5(5):375-386. doi:10.1038/nri1604

134. Schoggins JW. Interferon-Stimulated Genes: What Do They All Do? *Ann Rev Virol*. 2019;6(1):1-18. doi:10.1146/annurev-virology-092818-015756

135. Pfaender S, Mar KB, Michailidis E, et al. LY6E impairs coronavirus fusion and confers immune control of viral disease. *Nat Microbiol*. 2020;5(11):1330-1339. doi:10.1038/s41564-020-0769-y

136. Zhao X, Chen D, Li X, et al. Interferon Control of Human Coronavirus Infection and Viral Evasion: Mechanistic Insights and Implications for Antiviral Drug and Vaccine Development. *J Mol Biol*. 2022;434(6):167438. doi:10.1016/j.jmb.2021.167438

137. Martin-Sancho L, Lewinski MK, Pache L, et al. Functional landscape of SARS-CoV-2 cellular restriction. *Mol Cell*. 2021;81(12):2656-2668.e8. doi:10.1016/j.molcel.2021.04.008

138. Bastard P, Rosen LB, Zhang Q, et al. Autoantibodies against type I IFNs in patients with life-threatening COVID-19. *Science*. 2020;370(6515):eabd4585. doi:10.1126/science.abd4585

139. Kim YM, Shin EC. Type I and III interferon responses in SARS-CoV-2 infection. *Exp Mol Medicine*. 2021;53(5):750-760. doi:10.1038/s12276-021-00592-0

140. Chiale C, Greene TT, Zuniga EI. Interferon induction, evasion, and paradoxical roles during SARS-CoV-2 infection*. *Immunol Rev*. 2022;309(1):12-24. doi:10.1111/imr.13113

141. Beyer DK, Forero A. Mechanisms of Antiviral Immune Evasion of SARS-CoV-2. *J Mol Biol*. 2022;434(6):167265. doi:10.1016/j.jmb.2021.167265

142. Shin D, Mukherjee R, Grewe D, et al. Papain-like protease regulates SARS-CoV-2 viral spread and innate immunity. *Nature*. 2020;587(7835):657-662. doi:10.1038/s41586-020-2601-5

143. Liu G, Lee JH, Parker ZM, et al. ISG15-dependent activation of the sensor MDA5 is antagonized by the SARS-CoV-2 papain-like protease to evade host innate immunity. *Nat Microbiol*. 2021;6(4):467-478. doi:10.1038/s41564-021-00884-1

144. Konno Y, Kimura I, Uriu K, et al. SARS-CoV-2 ORF3b Is a Potent Interferon Antagonist Whose Activity Is Increased by a Naturally Occurring Elongation Variant. *Cell Reports*. 2020;32(12):108185. doi:10.1016/j.celrep.2020.108185

145. Zheng Y, Zhuang MW, Han L, et al. Severe acute respiratory syndrome coronavirus 2 (SARS-CoV-2) membrane (M) protein inhibits type I and III interferon production by targeting RIG-I/MDA-5 signaling. *Signal Transduct Target Ther*. 2020;5(1):299. doi:10.1038/s41392-020-00438-7

146. Han L, Zhuang M, Deng J, et al. SARS-CoV-2 ORF9b antagonizes type I and III interferons by targeting multiple components of the RIG-I/MDA-5–MAVS, TLR3–TRIF,

and cGAS–STING signaling pathways. *J Med Virol*. 2021;93(9):5376-5389. doi:10.1002/jmv.27050

147. Miyamoto Y, Itoh Y, Suzuki T, et al. SARS-CoV-2 ORF6 disrupts nucleocytoplasmic trafficking to advance viral replication. *Commun Biology*. 2022;5(1):483. doi:10.1038/s42003-022-03427-4

148. Liu H, Bai Y, Zhang X, et al. SARS-CoV-2 N Protein Antagonizes Stress Granule Assembly and IFN Production by Interacting with G3BPs to Facilitate Viral Replication. *J Virol*. 2022;96(12):e00412-22. doi:10.1128/jvi.00412-22

149. Schubert K, Karousis ED, Jomaa A, et al. SARS-CoV-2 Nsp1 binds the ribosomal mRNA channel to inhibit translation. *Nat Struct Mol Biol*. 2020;27(10):959-966. doi:10.1038/s41594-020-0511-8

150. Hsu JCC, Laurent-Rolle M, Pawlak JB, Wilen CB, Cresswell P. Translational shutdown and evasion of the innate immune response by SARS-CoV-2 NSP14 protein. *Proc National Acad Sci*. 2021;118(24):e2101161118. doi:10.1073/pnas.2101161118

151. Fisher T, Gluck A, Narayanan K, et al. Parsing the role of NSP1 in SARS-CoV-2 infection. *Cell Reports*. 2022;39(11):110954. doi:10.1016/j.celrep.2022.110954

152. Wang S, Dai T, Qin Z, et al. Targeting liquid–liquid phase separation of SARS-CoV-2 nucleocapsid protein promotes innate antiviral immunity by elevating MAVS activity. *Nat Cell Biol*. 2021;23(7):718-732. doi:10.1038/s41556-021-00710-0

153. Wu W, Cheng Y, Zhou H, Sun C, Zhang S. The SARS-CoV-2 nucleocapsid protein: its role in the viral life cycle, structure and functions, and use as a potential target in the development of vaccines and diagnostics. *Virol J*. 2023;20(1):6. doi:10.1186/s12985-023-01968-6

154. Zhao LY, Song J, Liu Y, Song CX, Yi C. Mapping the epigenetic modifications of DNA and RNA. *Protein Cell*. 2020;11(11):792-808. doi:10.1007/s13238-020-00733-7

155. Gilbert WV, Bell TA, Schaening C. Messenger RNA modifications: Form, distribution, and function. *Science*. 2016;352(6292):1408-1412. doi:10.1126/science.aad8711

156. Boccaletto P, Magnus M, Almeida C, et al. RNArchitecture: a database and a classification system of RNA families, with a focus on structural information. *Nucleic Acids Res*. 2017;46(Database issue):gkx966. doi:10.1093/nar/gkx966

157. Dominissini D, Moshitch-Moshkovitz S, Schwartz S, et al. Topology of the human and mouse m6A RNA methylomes revealed by m6A-seq. *Nature*. 2012;485(7397):201-206. doi:10.1038/nature11112

158. Meyer KD, Saletore Y, Zumbo P, Elemento O, Mason CE, Jaffrey SR. Comprehensive Analysis of mRNA Methylation Reveals Enrichment in 3′ UTRs and near Stop Codons. *Cell*. 2012;149(7):1635-1646. doi:10.1016/j.cell.2012.05.003

159. Desrosiers R, Friderici K, Rottman F. Identification of Methylated Nucleosides in Messenger RNA from Novikoff Hepatoma Cells. *Proc National Acad Sci*. 1974;71(10):3971-3975. doi:10.1073/pnas.71.10.3971

160. Perry RP, Kelley DE. Existence of methylated messenger RNA in mouse L cells. *Cell*. 1974;1(1):37-42. doi:10.1016/0092-8674(74)90153-6

161. Bringmann P, Lührmann R. Antibodies specific for N 6-methyladenosine react with intact snRNPs U2 and U4/U6. *Febs Lett*. 1987;213(2):309-315. doi:10.1016/0014-5793(87)81512-0

162. Williams GD, Gokhale NS, Horner SM. Regulation of Viral Infection by the RNA Modification N6-methyladenosine. *Ann Rev Virol*. 2019;6(1):1-19. doi:10.1146/annurev-virology-092818-015559

163. Ke S, Pandya-Jones A, Saito Y, et al. m6A mRNA modifications are deposited in nascent pre-mRNA and are not required for splicing but do specify cytoplasmic turnover. *Gene Dev*. 2017;31(10):990-1006. doi:10.1101/gad.301036.117

164. Frye M, Blanco S. Post-transcriptional modifications in development and stem cells. *Development*. 2016;143(21):3871-3881. doi:10.1242/dev.136556

165. Roundtree IA, Evans ME, Pan T, He C. Dynamic RNA Modifications in Gene Expression Regulation. *Cell*. 2017;169(7):1187-1200. doi:10.1016/j.cell.2017.05.045

166. Fu Y, Dominissini D, Rechavi G, He C. Gene expression regulation mediated through reversible m6A RNA methylation. *Nat Rev Genet*. 2014;15(5):293-306. doi:10.1038/nrg3724

167. Song J, Yi C. Reading Chemical Modifications in the Transcriptome. *J Mol Biol*. 2020;432(6):1824-1839. doi:10.1016/j.jmb.2019.10.006

168. Rosa-Mercado NA, Withers JB, Steitz JA. Settling the m6A debate: methylation of mature mRNA is not dynamic but accelerates turnover. *Gene Dev*. 2017;31(10):957-958. doi:10.1101/gad.302695.117

169. Shi H, Wei J, He C. Where, When, and How: Context-Dependent Functions of RNA Methylation Writers, Readers, and Erasers. *Mol Cell*. 2019;74(4):640-650. doi:10.1016/j.molcel.2019.04.025

170. Bokar JA, Shambaugh ME, Polayes D, Matera AG, Rottman FM. Purification and cDNA cloning of the AdoMet-binding subunit of the human mRNA (N6-adenosine)-methyltransferase. *Rna New York N Y*. 1997;3(11):1233-1247.

171. Wang P, Doxtader KA, Nam Y. Structural Basis for Cooperative Function of Mettl3 and Mettl14 Methyltransferases. *Mol Cell*. 2016;63(2):306-317. doi:10.1016/j.molcel.2016.05.041

172. Zaccara S, Ries RJ, Jaffrey SR. Reading, writing and erasing mRNA methylation. *Nat Rev Mol Cell Bio*. 2019;20(10):608-624. doi:10.1038/s41580-019-0168-5

173. Morales DG, Reyes JL. A birds'-eye view of the activity and specificity of the mRNA m6A methyltransferase complex. *Wiley Interdiscip Rev Rna*. 2021;12(1):e1618. doi:10.1002/wrna.1618

174. Oerum S, Meynier V, Catala M, Tisné C. A comprehensive review of m6A/m6Am RNA methyltransferase structures. *Nucleic Acids Res*. 2021;49(13):gkab378-. doi:10.1093/nar/gkab378

175. Ping XL, Sun BF, Wang L, et al. Mammalian WTAP is a regulatory subunit of the RNA N6-methyladenosine methyltransferase. *Cell Res*. 2014;24(2):177-189. doi:10.1038/cr.2014.3

176. Yue Y, Liu J, Cui X, et al. VIRMA mediates preferential m6A mRNA methylation in 3′UTR and near stop codon and associates with alternative polyadenylation. *Cell Discov*. 2018;4(1):10. doi:10.1038/s41421-018-0019-0

177. Patil DP, Chen CK, Pickering BF, et al. m6A RNA methylation promotes XIST-mediated transcriptional repression. *Nature*. 2016;537(7620):369-373. doi:10.1038/nature19342

178. Knuckles P, Lence T, Haussmann IU, et al. Zc3h13/Flacc is required for adenosine methylation by bridging the mRNA-binding factor Rbm15/Spenito to the m6A machinery component Wtap/Fl(2)d. *Gene Dev*. 2018;32(5-6):415-429. doi:10.1101/gad.309146.117

179. Balacco DL, Soller M. The m6A Writer: Rise of a Machine for Growing Tasks. *Biochemistry-us*. 2019;58(5):363-378. doi:10.1021/acs.biochem.8b01166

180. Satterwhite ER, Mansfield KD. RNA methyltransferase METTL16: Targets and function. *Wiley Interdiscip Rev Rna*. 2022;13(2):e1681. doi:10.1002/wrna.1681

181. Gerken T, Girard CA, Tung YCL, et al. The Obesity-Associated FTO Gene Encodes a 2-Oxoglutarate-Dependent Nucleic Acid Demethylase. *Science*. 2007;318(5855):1469-1472. doi:10.1126/science.1151710

182. Jia G, Yang CG, Yang S, et al. Oxidative demethylation of 3-methylthymine and 3-methyluracil in single-stranded DNA and RNA by mouse and human FTO. *Febs Lett*. 2008;582(23-24):3313-3319. doi:10.1016/j.febslet.2008.08.019

183. Jia G, Fu Y, Zhao X, et al. N6-Methyladenosine in nuclear RNA is a major substrate of the obesity-associated FTO. *Nat Chem Biol*. 2011;7(12):885-887. doi:10.1038/nchembio.687

184. Zheng G, Dahl JA, Niu Y, et al. ALKBH5 Is a Mammalian RNA Demethylase that Impacts RNA Metabolism and Mouse Fertility. *Mol Cell*. 2013;49(1):18-29. doi:10.1016/j.molcel.2012.10.015

185. Han Z, Xu Z, Yu Y, et al. ALKBH5-mediated m6A mRNA methylation governs human embryonic stem cell cardiac commitment. *Mol Ther - Nucleic Acids*. 2021;26:22-33. doi:10.1016/j.omtn.2021.05.019

186. Qu J, Yan H, Hou Y, et al. RNA demethylase ALKBH5 in cancer: from mechanisms to therapeutic potential. *J Hematol Oncol*. 2022;15(1):8. doi:10.1186/s13045-022-01224-4

187. Liu X, Wang Z, Yang Q, et al. RNA Demethylase ALKBH5 Prevents Lung Cancer Progression by Regulating EMT and Stemness via Regulating p53. *Frontiers Oncol*. 2022;12:858694. doi:10.3389/fonc.2022.858694

188. Cruz BMDL, Markus R, Malla S, et al. Modifying the m6A brain methylome by ALKBH5-mediated demethylation: a new contender for synaptic tagging. *Mol Psychiatr*. 2021;26(12):7141-7153. doi:10.1038/s41380-021-01282-z

189. Zheng Q, Hou J, Zhou Y, Li Z, Cao X. The RNA helicase DDX46 inhibits innate immunity by entrapping m6A-demethylated antiviral transcripts in the nucleus. *Nat Immunol*. 2017;18(10):1094-1103. doi:10.1038/ni.3830

190. Zhou KI, Pan T. An additional class of m6A readers. *Nat Cell Biol*. 2018;20(3):230-232. doi:10.1038/s41556-018-0046-y

191. Xu C, Liu K, Ahmed H, Loppnau P, Schapira M, Min J. Structural Basis for the Discriminative Recognition of N 6-Methyladenosine RNA by the Human YT521-B Homology Domain Family of Proteins*. *J Biol Chem*. 2015;290(41):24902-24913. doi:10.1074/jbc.m115.680389

192. Liu J, Li K, Cai J, et al. Landscape and Regulation of m6A and m6Am Methylome across Human and Mouse Tissues. *Mol Cell*. 2020;77(2):426-440.e6. doi:10.1016/j.molcel.2019.09.032

193. Kasowitz SD, Ma J, Anderson SJ, et al. Nuclear m6A reader YTHDC1 regulates alternative polyadenylation and splicing during mouse oocyte development. *Plos Genet*. 2018;14(5):e1007412. doi:10.1371/journal.pgen.1007412

194. Hartmann AM, Nayler O, Schwaiger FW, Obermeier A, Stamm S. The Interaction and Colocalization of Sam68 with the Splicing-associated Factor YT521-B in Nuclear Dots Is Regulated by the Src Family Kinase p59fyn. *Mol Biol Cell*. 1999;10(11):3909-3926. doi:10.1091/mbc.10.11.3909

195. Imai Y, Matsuo N, Ogawa S, Tohyama M, Takagi T. Cloning of a gene, YT521, for a novel RNA splicing-related protein induced by hypoxia/reoxygenation. *Mol Brain Res*. 1998;53(1-2):33-40. doi:10.1016/s0169-328x(97)00262-3

196. Xiao W, Adhikari S, Dahal U, et al. Nuclear m6A Reader YTHDC1 Regulates mRNA Splicing. *Mol Cell*. 2016;61(4):507-519. doi:10.1016/j.molcel.2016.01.012

197. Wang X, Lu Z, Gomez A, et al. N6-methyladenosine-dependent regulation of messenger RNA stability. *Nature*. 2014;505(7481):117-120. doi:10.1038/nature12730

198. Du H, Zhao Y, He J, et al. YTHDF2 destabilizes m6A-containing RNA through direct recruitment of the CCR4–NOT deadenylase complex. *Nat Commun*. 2016;7(1):12626. doi:10.1038/ncomms12626

199. Shi H, Wang X, Lu Z, et al. YTHDF3 facilitates translation and decay of N6-methyladenosine-modified RNA. *Cell Res*. 2017;27(3):315-328. doi:10.1038/cr.2017.15

200. Hsu PJ, Zhu Y, Ma H, et al. Ythdc2 is an N6-methyladenosine binding protein that regulates mammalian spermatogenesis. *Cell Res*. 2017;27(9):1115-1127. doi:10.1038/cr.2017.99

201. Wang J yan, Lu A qing. The biological function of m6A reader YTHDF2 and its role in human disease. *Cancer Cell Int*. 2021;21(1):109. doi:10.1186/s12935-021-01807-0

202. Cayir A. RNA modifications as emerging therapeutic targets. *Wiley Interdiscip Rev Rna*. 2022;13(4):e1702. doi:10.1002/wrna.1702

203. Sun H, Li K, Zhang X, et al. m6Am-seq reveals the dynamic m6Am methylation in the human transcriptome. *Nat Commun*. 2021;12(1):4778. doi:10.1038/s41467-021-25105-5

204. Boulias K, Toczydłowska-Socha D, Hawley BR, et al. Identification of the m6Am Methyltransferase PCIF1 Reveals the Location and Functions of m6Am in the Transcriptome. *Mol Cell*. 2019;75(3):631-643.e8. doi:10.1016/j.molcel.2019.06.006

205. WEI CM, GERSHOWITZ A, Moss B. N6, O2′-dimethyladenosine a novel methylated ribonucleoside next to the 5′ terminal of animal cell and virus mRNAs. *Nature*. 1975;257(5523):251-253. doi:10.1038/257251a0

206. Akichika S, Hirano S, Shichino Y, et al. Cap-specific terminal N6-methylation of RNA by an RNA polymerase II–associated methyltransferase. *Science*. 2019;363(6423). doi:10.1126/science.aav0080

207. Sun H, Zhang M, Li K, Bai D, Yi C. Cap-specific, terminal N6-methylation by a mammalian m6Am methyltransferase. *Cell Res*. 2019;29(1):80-82. doi:10.1038/s41422-018-0117-4

208. Tartell MA, Boulias K, Hoffmann GB, Bloyet LM, Greer EL, Whelan SPJ. Methylation of viral mRNA cap structures by PCIF1 attenuates the antiviral activity of interferon-β. *Proc National Acad Sci*. 2021;118(29):e2025769118. doi:10.1073/pnas.2025769118

209. Pandey RR, Delfino E, Homolka D, et al. The Mammalian Cap-Specific m6Am RNA Methyltransferase PCIF1 Regulates Transcript Levels in Mouse Tissues. *Cell Reports*. 2020;32(7):108038. doi:10.1016/j.celrep.2020.108038

210. Mauer J, Luo X, Blanjoie A, et al. Reversible methylation of m6Am in the 5′ cap controls mRNA stability. *Nature*. 2017;541(7637):371-375. doi:10.1038/nature21022

211. Sommer S, Salditt-Georgieff M, Bachenheimer S, et al. The methylation of adenovirus-specific nuclear and cytoplasmic RNA. *Nucleic Acids Res*. 1976;3(3):749-766. doi:10.1093/nar/3.3.749

212. Lavi S, Shatkin AJ. Methylated simian virus 40-specific RNA from nuclei and cytoplasm of infected BSC-1 cells. *Proc National Acad Sci*. 1975;72(6):2012-2016. doi:10.1073/pnas.72.6.2012

213. Dimock K, Stoltzfus CM. Sequence specificity of internal methylation in B77 avian sarcoma virus RNA subunits. *Biochemistry-us*. 1977;16(3):471-478. doi:10.1021/bi00622a021

214. Kane SE, Beemon K. Precise localization of m6A in Rous sarcoma virus RNA reveals clustering of methylation sites: implications for RNA processing. *Mol Cell Biol*. 1985;5(9):2298-2306. doi:10.1128/mcb.5.9.2298-2306.1985

215. Gokhale NS, McIntyre ABR, McFadden MJ, et al. N6-Methyladenosine in Flaviviridae Viral RNA Genomes Regulates Infection. *Cell Host Microbe*. 2016;20(5):654-665. doi:10.1016/j.chom.2016.09.015

216. Lichinchi G, Zhao BS, Wu Y, et al. Dynamics of Human and Viral RNA Methylation during Zika Virus Infection. *Cell Host Microbe*. 2016;20(5):666-673. doi:10.1016/j.chom.2016.10.002

217. Liu Y, Li K, Xu Y, et al. Characterization of m6A modifications in the contemporary Zika virus genome and host cellular transcripts. *J Med Virol*. 2022;94(9):4309-4318. doi:10.1002/jmv.27869

218. Barranco C. Viral infection linked to m6A alterations in host mRNAs. *Nat Rev Mol Cell Bio*. 2020;21(2):64-65. doi:10.1038/s41580-019-0202-7

219. Chen Y, Guo D. Molecular mechanisms of coronavirus RNA capping and methylation. *Virol Sin*. 2016;31(1):3-11. doi:10.1007/s12250-016-3726-4

220. Abbas YM, Laudenbach BT, Martínez-Montero S, et al. Structure of human IFIT1 with capped RNA reveals adaptable mRNA binding and mechanisms for sensing N1 and N2 ribose 2′-O methylations. *Proc National Acad Sci*. 2017;114(11):E2106-E2115. doi:10.1073/pnas.1612444114

221. Charley PA, Wilusz CJ, Wilusz J. Identification of phlebovirus and arenavirus RNA sequences that stall and repress the exoribonuclease XRN1. *J Biol Chem*. 2018;293(1):285-295. doi:10.1074/jbc.m117.805796

222. Moon SL, Blackinton JG, Anderson JR, et al. XRN1 stalling in the 5' UTR of Hepatitis C virus and Bovine Viral Diarrhea virus is associated with dysregulated host mRNA stability. *Plos Pathog*. 2015;11(3):e1004708. doi:10.1371/journal.ppat.1004708

223. Barnhart MD, Moon SL, Emch AW, Wilusz CJ, Wilusz J. Changes in Cellular mRNA Stability, Splicing, and Polyadenylation through HuR Protein Sequestration by a Cytoplasmic RNA Virus. *Cell Reports*. 2013;5(4):909-917. doi:10.1016/j.celrep.2013.10.012

224. Palusa S, Ndaluka C, Bowen RA, Wilusz CJ, Wilusz J. The 3′ Untranslated Region of the Rabies Virus Glycoprotein mRNA Specifically Interacts with Cellular PCBP2 Protein and Promotes Transcript Stability. *Plos One*. 2012;7(3):e33561. doi:10.1371/journal.pone.0033561

225. Sokoloski KJ, Dickson AM, Chaskey EL, Garneau NL, Wilusz CJ, Wilusz J. Sindbis Virus Usurps the Cellular HuR Protein to Stabilize Its Transcripts and Promote Productive Infections in Mammalian and Mosquito Cells. *Cell Host Microbe*. 2010;8(2):196-207. doi:10.1016/j.chom.2010.07.003

226. Leung DW, Amarasinghe GK. When your cap matters: structural insights into self vs non-self recognition of 5′ RNA by immunomodulatory host proteins. *Curr Opin Struc Biol*. 2016;36:133-141. doi:10.1016/j.sbi.2016.02.001

227. Hyde JL, Diamond MS. Innate immune restriction and antagonism of viral RNA lacking 2′-O methylation. *Virology*. 2015;479:66-74. doi:10.1016/j.virol.2015.01.019

228. Johnson B, VanBlargan LA, Xu W, et al. Human IFIT3 Modulates IFIT1 RNA Binding Specificity and Protein Stability. *Immunity*. 2018;48(3):487-499.e5. doi:10.1016/j.immuni.2018.01.014

229. Sendinc E. PCIF1 Catalyzes m6Am mRNA Methylation to Regulate Gene Expression. *Molecular cell*. doi:https://doi.org/10.1016/j.molcel.2019.05.030

230. Paz I, Kosti I, Ares M, Cline M, Mandel-Gutfreund Y. RBPmap: a web server for mapping binding sites of RNA-binding proteins. *Nucleic Acids Res*. 2014;42(W1):W361-W367. doi:10.1093/nar/gku406

231. Wilusz J, Shenk T. A 64 kd nuclear protein binds to RNA segments that include the AAUAAA polyadenylation motif. *Cell*. 1988;52(2):221-228. doi:10.1016/0092-8674(88)90510-7

232. Sokoloski KJ, Wilusz J, Wilusz CJ. Chapter 8 The Preparation and Applications of Cytoplasmic Extracts from Mammalian Cells for Studying Aspects of mRNA Decay. *Methods Enzymol*. 2008;448:139-163. doi:10.1016/s0076-6879(08)02608-6

233. Zhu W, Zhou B lun, Rong L juan, et al. Roles of PTBP1 in alternative splicing, glycolysis, and oncogensis. *J Zhejiang Univ-sc B*. 2020;21(2):122-136. doi:10.1631/jzus.b1900422

234. Greenberg DS, Soreq H. Brenner's Encyclopedia of Genetics (Second Edition). *Article Titles*. 2013;(Cell1262006):97-98. doi:10.1016/b978-0-12-374984-0.00043-7

235. Black DL. MECHANISMS OF ALTERNATIVE PRE-MESSENGER RNA SPLICING. *Biochemistry-us*. 2003;72(1):291-336. doi:10.1146/annurev.biochem.72.121801.161720

236. Izquierdo JM, Majós N, Bonnal S, et al. Regulation of Fas Alternative Splicing by Antagonistic Effects of TIA-1 and PTB on Exon Definition. *Mol Cell*. 2005;19(4):475-484. doi:10.1016/j.molcel.2005.06.015

237. Wagner EJ, Garcia-Blanco MA. Polypyrimidine Tract Binding Protein Antagonizes Exon Definition. *Mol Cell Biol*. 2001;21(10):3281-3288. doi:10.1128/mcb.21.10.3281-3288.2001

238. Deeks MJ, Hussey PJ, Davies B. Formins: intermediates in signal-transduction cascades that affect cytoskeletal reorganization. *Trends Plant Sci*. 2002;7(11):492-498. doi:10.1016/s1360-1385(02)02341-5

239. Naranatt PP, Krishnan HH, Smith MS, Chandran B. Kaposi's Sarcoma-Associated Herpesvirus Modulates Microtubule Dynamics via RhoA-GTP-Diaphanous 2 Signaling and Utilizes the Dynein Motors To Deliver Its DNA to the Nucleus. *J Virol*. 2005;79(2):1191-1206. doi:10.1128/jvi.79.2.1191-1206.2005

240. Kloc M, Uosef A, Wosik J, Kubiak JZ, Ghobrial RM. Virus interactions with the actin cytoskeleton—what we know and do not know about SARS-CoV-2. *Arch Virol*. 2022;167(3):737-749. doi:10.1007/s00705-022-05366-1

241. Ng ML, Lee JWM, Leong MLN, Ling AE, Tan HC, Ooi EE. Topographic Changes in SARS Coronavirus–infected Cells during Late Stages of Infection - Volume 10, Number 11—November 2004 - Emerging Infectious Diseases journal - CDC. *Emerg Infect Dis*. 2004;10(11):1907-1914. doi:10.3201/eid1011.040195

242. Caldas LA, Carneiro FA, Higa LM, et al. Ultrastructural analysis of SARS-CoV-2 interactions with the host cell via high resolution scanning electron microscopy. *Sci Rep-uk*. 2020;10(1):16099. doi:10.1038/s41598-020-73162-5

243. Lehmann MJ, Sherer NM, Marks CB, Pypaert M, Mothes W. Actin- and myosin-driven movement of viruses along filopodia precedes their entry into cells. *J Cell Biology*. 2005;170(2):317-325. doi:10.1083/jcb.200503059

244. Wen Z, Zhang Y, Lin Z, Shi K, Jiu Y. Cytoskeleton—a crucial key in host cell for coronavirus infection. *J Mol Cell Biol*. 2020;12(12):mjaa042-. doi:10.1093/jmcb/mjaa042

245. Llorian M, Schwartz S, Clark TA, et al. Position-dependent alternative splicing activity revealed by global profiling of alternative splicing events regulated by PTB. *Nat Struct Mol Biol*. 2010;17(9):1114-1123. doi:10.1038/nsmb.1881

246. Teekakirikul P, Ho CY, Seidman CE. Emery and Rimoin's Principles and Practice of Medical Genetics. *Appl Specif Disord Chromosomal Disord*. 2013;(J. Clin. Invest.11532005):1-38. doi:10.1016/b978-0-12-383834-6.00053-7

247. Honda K, Yamada T, Endo R, et al. Actinin-4, a Novel Actin-bundling Protein Associated with Cell Motility and Cancer Invasion. *J Cell Biology*. 1998;140(6):1383-1393. doi:10.1083/jcb.140.6.1383

248. Ehrlicher AJ, Krishnan R, Guo M, Bidan CM, Weitz DA, Pollak MR. Alpha-actinin binding kinetics modulate cellular dynamics and force generation. *Proc National Acad Sci*. 2015;112(21):6619-6624. doi:10.1073/pnas.1505652112

249. Hamill KJ, Hopkinson SB, Skalli O, Jones JCR. Actinin-4 in keratinocytes regulates motility via an effect on lamellipodia stability and matrix adhesions. *Faseb J*. 2013;27(2):546-556. doi:10.1096/fj.12-217406

250. Yasunami M, Suzuki K, Ohkubo H. A Novel Family of TEA Domain-Containing Transcription Factors with Distinct Spatiotemporal Expression Patterns. *Biochem Bioph Res Co*. 1996;228(2):365-370. doi:10.1006/bbrc.1996.1667

251. Song J, Yi C. Chemical Modifications to RNA: A New Layer of Gene Expression Regulation. *Acs Chem Biol*. 2017;12(2):316-325. doi:10.1021/acschembio.6b00960

252. Jiang X, Liu B, Nie Z, et al. The role of m6A modification in the biological functions and diseases. *Signal Transduct Target Ther*. 2021;6(1):74. doi:10.1038/s41392-020-00450-x

253. Sikorski PJ, Warminski M, Kubacka D, et al. The identity and methylation status of the first transcribed nucleotide in eukaryotic mRNA 5′ cap modulates protein expression in living cells. *Nucleic Acids Res*. 2020;48(4):1607-1626. doi:10.1093/nar/gkaa032

254. Chen M, Wei L, Law C, et al. RNA N6-methyladenosine methyltransferase-like 3 promotes liver cancer progression through YTHDF2-dependent posttranscriptional silencing of SOCS2. *Hepatology*. 2018;67(6):2254-2270. doi:10.1002/hep.29683

255. Huang H, Weng H, Sun W, et al. Recognition of RNA N6-methyladenosine by IGF2BP proteins enhances mRNA stability and translation. *Nat Cell Biol*. 2018;20(3):285-295. doi:10.1038/s41556-018-0045-z

256. Li Z, Weng H, Su R, et al. FTO Plays an Oncogenic Role in Acute Myeloid Leukemia as a N 6-Methyladenosine RNA Demethylase. *Cancer Cell*. 2017;31(1):127-141. doi:10.1016/j.ccell.2016.11.017

257. Tartell MA. Methylation of viral mRNA cap structures by PCIF1 attenuates the antiviral activity of interferon-β. *PNAS*. https://doi.org/10.1073/pnas.2025769118

258. Yang D, Leibowitz JL. The structure and functions of coronavirus genomic 3′ and 5′ ends. *Virus Res*. 2015;206:120-133. doi:10.1016/j.virusres.2015.02.025

259. Vora SM, Fontana P, Mao T, et al. Targeting stem-loop 1 of the SARS-CoV-2 5′ UTR to suppress viral translation and Nsp1 evasion. *Proc National Acad Sci*. 2022;119(9):e2117198119. doi:10.1073/pnas.2117198119

260. Kage F, Winterhoff M, Dimchev V, et al. FMNL formins boost lamellipodial force generation. *Nat Commun*. 2017;8(1):14832. doi:10.1038/ncomms14832

261. Katoh M, Katoh M. Identification and characterization of human FMNL1, FMNL2 and FMNL3 genes in silico. *Int J Oncol*. 2003;22(5):1161-1168.

262. Wang Y, Arjonen A, Pouwels J, et al. Formin-like 2 Promotes β1-Integrin Trafficking and Invasive Motility Downstream of PKCα. *Dev Cell*. 2015;34(4):475-483. doi:10.1016/j.devcel.2015.06.015

263. Trefzer R, Elpeleg O, Gabrusskaya T, et al. Characterization of a L136P mutation in Formin-like 2 (FMNL2) from a patient with chronic inflammatory bowel disease. *Plos One*. 2021;16(5):e0252428. doi:10.1371/journal.pone.0252428

264. Geeves MA, Hitchcock-DeGregori SE, Gunning PW. A systematic nomenclature for mammalian tropomyosin isoforms. *J Muscle Res Cell M*. 2015;36(2):147-153. doi:10.1007/s10974-014-9389-6

265. Holste D, Ohler U. Strategies for Identifying RNA Splicing Regulatory Motifs and Predicting Alternative Splicing Events. *Plos Comput Biol*. 2008;4(1):e21. doi:10.1371/journal.pcbi.0040021

266. Cao J, Routh AL, Kuyumcu-Martinez MN. Nanopore sequencing reveals full-length Tropomyosin 1 isoforms and their regulation by RNA-binding proteins during rat heart development. *J Cell Mol Med*. 2021;25(17):8352-8362. doi:10.1111/jcmm.16795

267. Turakhia Y, Thornlow B, Hinrichs A, et al. Pandemic-scale phylogenomics reveals the SARS-CoV-2 recombination landscape. *Nature*. 2022;609(7929):994-997. doi:10.1038/s41586-022-05189-9

268. Motorin Y, Helm M. RNA nucleotide methylation: 2021 update. *Wiley Interdiscip Rev Rna*. 2022;13(1):e1691. doi:10.1002/wrna.1691

269. Sokoloski KJ, Haist KC, Morrison TE, Mukhopadhyay S, Hardy RW. Noncapped Alphavirus Genomic RNAs and Their Role during Infection. *J Virol*. 2015;89(11):6080-6092. doi:10.1128/jvi.00553-15

270. Burrack KAS, Hawman DW, Jupille HJ, et al. Attenuating Mutations in nsP1 Reveal Tissue-Specific Mechanisms for Control of Ross River Virus Infection. *J Virol*. 2014;88(7):3719-3732. doi:10.1128/jvi.02609-13

271. McFadden MJ, Gokhale NS, Horner SM. Protect this house: cytosolic sensing of viruses. *Curr Opin Virol*. 2017;22:36-43. doi:10.1016/j.coviro.2016.11.012

272. Karikó K, Buckstein M, Ni H, Weissman D. Suppression of RNA Recognition by Toll-like Receptors: The Impact of Nucleoside Modification and the Evolutionary Origin of RNA. *Immunity*. 2005;23(2):165-175. doi:10.1016/j.immuni.2005.06.008

273. Durbin AF, Wang C, Marcotrigiano J, Gehrke L. RNAs Containing Modified Nucleotides Fail To Trigger RIG-I Conformational Changes for Innate Immune Signaling. *Mbio*. 2016;7(5):e00833-16. doi:10.1128/mbio.00833-16